Research Paper

GEOSPHERE

GEOSPHERE, v. 16, no. 6

https://doi.org/10.1130/GES02244.1

19 figures; 1 set of supplemental files

CORRESPONDENCE: edgett@msss.com

CITATION: Edgett, K.S., Banham, S.G., Bennett, K.A., Edgar, L.A., Edwards, C.S., Fairén, A.G., Fedo, C.M., Fey, D.M., Garvin, J.B., Grotzinger, J.P., Gupta, S., Henderson, M.J., House, C.H., Mangold, N., McLennan, S.M., Newsom, H.E., Rowland, S.K., Siebach, K.L., Thompson, L., VanBommel, S.J., Wiens, R.C., Williams, R.M.E., and Yingst, R.A., 2020, Extraformational sediment recycling on Mars: Geosphere, v. 16, no. 6, p. 1508–1537, https://doi.org/10.1130/GES02244.1.

Science Editor: Shanaka de Silva
Associate Editor: Lesli Wood

Received 8 February 2020
Revision received 21 July 2020
Accepted 25 August 2020

Published online 6 October 2020

GOLD OPEN ACCESS

THE GEOLOGICAL SOCIETY OF AMERICA®

This paper is published under the terms of the CC-BY-NC license.

© 2020 The Authors

Extraformational sediment recycling on Mars

Kenneth S. Edgett[1], Steven G. Banham[2], Kristen A. Bennett[3], Lauren A. Edgar[3], Christopher S. Edwards[4], Alberto G. Fairén[5,6], Christopher M. Fedo[7], Deirdra M. Fey[1], James B. Garvin[8], John P. Grotzinger[9], Sanjeev Gupta[2], Marie J. Henderson[10], Christopher H. House[11], Nicolas Mangold[12], Scott M. McLennan[13], Horton E. Newsom[14], Scott K. Rowland[15], Kirsten L. Siebach[16], Lucy Thompson[17], Scott J. VanBommel[18], Roger C. Wiens[19], Rebecca M.E. Williams[20], and R. Aileen Yingst[20]

[1]Malin Space Science Systems, P.O. Box 910148, San Diego, California 92191-0148, USA
[2]Department of Earth Science and Engineering, Imperial College London, South Kensington, London SW7 2AZ, UK
[3]U.S. Geological Survey, Astrogeology Science Center, 2255 N. Gemini Drive, Flagstaff, Arizona 86001, USA
[4]Department of Astronomy and Planetary Science, Northern Arizona University, P.O. Box 6010, Flagstaff, Arizona 86011, USA
[5]Department of Planetology and Habitability, Centro de Astrobiología (CSIC-INTA), M-108, km 4, 28850 Madrid, Spain
[6]Department of Astronomy, Cornell University, Ithaca, New York 14853, USA
[7]Department of Earth and Planetary Sciences, The University of Tennessee, 1621 Cumberland Avenue, 602 Strong Hall, Knoxville, Tennessee 37996-1410, USA
[8]National Aeronautics and Space Administration (NASA) Goddard Space Flight Center, Mail Code 600, Greenbelt, Maryland 20771, USA
[9]Division of Geological and Planetary Sciences, California Institute of Technology, Pasadena, California 91125, USA
[10]Department of Earth, Atmospheric, and Planetary Sciences, Purdue University, 550 Stadium Mall Drive, West Lafayette, Indiana 47907, USA
[11]Department of Geosciences, The Pennsylvania State University, University Park, Pennsylvania 16802, USA
[12]Laboratoire de Planétologie et Géodynamique de Nantes, CNRS UMR 6112, Université de Nantes, Université Angers, 44300 Nantes, France
[13]Department of Geosciences, Stony Brook University, Stony Brook, New York 11794-2100, USA
[14]Institute of Meteoritics and Department of Earth and Planetary Sciences, 1 University of New Mexico, MSC03-2050, Albuquerque, New Mexico 87131, USA
[15]Department of Earth Sciences, University of Hawai'i at Mānoa, Honolulu, Hawai'i 96822, USA
[16]Department of Earth, Environmental and Planetary Sciences, Rice University, MS-126, 6100 Main Street, Houston, Texas 77005, USA
[17]Department of Earth Sciences, University of New Brunswick, P.O. Box 4400, Fredericton, New Brunswick E3B 5A3, Canada
[18]Department of Earth and Planetary Sciences, Washington University in St. Louis, 1 Brookings Drive, St. Louis, Missouri 63130, USA
[19]MS C331, Los Alamos National Laboratory, Los Alamos, New Mexico 87545, USA
[20]Planetary Science Institute, 1700 East Fort Lowell, Suite 106, Tucson, Arizona 85719-2395, USA

ABSTRACT

Extraformational sediment recycling (old sedimentary rock to new sedimentary rock) is a fundamental aspect of Earth's geological record; tectonism exposes sedimentary rock, whereupon it is weathered and eroded to form new sediment that later becomes lithified. On Mars, tectonism has been minor, but two decades of orbiter instrument–based studies show that some sedimentary rocks previously buried to depths of kilometers have been exposed, by erosion, at the surface. Four locations in Gale crater, explored using the National Aeronautics and Space Administration's *Curiosity* rover, exhibit sedimentary lithoclasts in sedimentary rock: At Marias Pass, they are mudstone fragments in sandstone derived from strata below an erosional unconformity; at Bimbe, they are pebble-sized sandstone and, possibly, laminated, intraclast-bearing, chemical (calcium sulfate) sediment fragments in conglomerates; at Cooperstown, they are pebble-sized fragments of sandstone within coarse sandstone; at Dingo Gap, they are cobble-sized, stratified sandstone fragments in conglomerate derived from an immediately underlying sandstone. Mars orbiter images show lithified sediment fans at the termini of canyons that incise sedimentary rock in Gale crater; these, too, consist of recycled, extraformational sediment. The recycled sediments in Gale crater are compositionally immature, indicating the dominance of physical weathering processes during the second known cycle. The observations at Marias Pass indicate that sediment eroded and removed from craters such as Gale crater during the Martian Hesperian Period could have been recycled to form new rock elsewhere. Our results permit prediction that lithified deltaic sediments at the *Perseverance* (landing in 2021) and *Rosalind Franklin* (landing in 2023) rover field sites could contain extraformational recycled sediment.

Kenneth S. Edgett https://orcid.org/0000-0001-7197-5751

INTRODUCTION

The processes of fragment production, weathering, transport, deposition, burial, and diagenesis would have begun to create a sedimentary record almost as soon as the Martian crust formed, perhaps just ~20 m.y. (Bouvier et al., 2018) after crystallization of the solar system's first solid particles. Although battered, shocked, and redistributed by impact events (Abramov and Mojzsis, 2016), without sustained, mobile-lid (plate) tectonics (Zhang and O'Neill, 2016), the Martian crust has largely retained its ancient sedimentary archive (Grotzinger et al., 2011). This record includes rocks older than the oldest sedimentary and metasedimentary strata on Earth (cf. Condie, 2019).

As occurs on Earth (e.g., Dunne et al., 1998; Marriott and Wright, 1996; East et al., 2015; Licht et al., 2016), Martian sediments can be recycled, or even multicycled, during transport and temporary storage on their way to their ultimate depositional basins. Such penecontemporaneous recycling can

Downloaded from http://pubs.geoscienceworld.org/gsa/geosphere/article-pdf/16/6/1508/5182958/1508.pdf
by California Inst of Technology user

include creation and deposition of intraclasts, that is, fragments of indurated sediment eroded from and reworked "within the area of deposition" (Folk, 1959, p. 4). On early Mars, such short-term recycling would have been a normal consequence of the interactions between and within the planet's fluvial, lacustrine, mass movement, and eolian transport and temporary storage systems. A key example of this is recorded by the Burns formation of Meridiani Planum, where sand-sized mud pellets are interpreted to have been deflated from playas, accumulated nearby to form eolian dunes, and then lithified to create cross-bedded eolian sandstone (Grotzinger et al., 2005).

Sediments are also recycled from older sedimentary rocks (Fig. 1). On Earth, this "cannibalistic" extraformational recycling occurs after lithified sediment is returned to the surface through tectonism and concomitant weathering and erosion (e.g., Garrels and MacKenzie, 1972; Veizer and Jansen, 1979; Cox and Lowe, 1995a, 1995b). Extraformational recycling is pervasive and vital to understanding the records of sediment provenance, climate effects on source rock weathering, and the use of sedimentary archives as records of past volcanism and tectonism (e.g., Blatt, 1967; Dickinson and Gehrels, 2010; Moecher et al., 2019). Sedimentary rock fragments—and individual grains liberated from clastic sedimentary rocks—are recycled if they are not destroyed through dissolution or (on Earth) subduction. Cannibalistic multicycling of clastic sediment on Earth "accumulates the effects of several episodes of weathering, transport, and diagenesis," (Cox and Lowe, 1995b, p. 5), providing one of the pathways (see Dott, 2003) toward sediment compositional maturation.

Although tectonism has been negligible as compared to Earth, images of the Martian surface present considerable evidence that some of its sedimentary rocks were lithified at depths measured in kilometers and later exposed at the surface by erosion (Malin and Edgett, 2000, 2001; Grotzinger and Milliken, 2012; Zabrusky et al., 2012; Grotzinger et al., 2015; Bennett and Bell, 2016; Caswell and Milliken, 2017; Schieber et al., 2017; Day and Catling, 2020). Erosion was so deep in some regions that bedrock thought to have been incised by ancient fluvial systems was completely removed (Hynek and Phillips, 2001); the remaining channel sediment bodies or valley-filling materials that resisted erosion became ridges (e.g., Davis et al., 2019). Elsewhere, lithified deltaic deposits were left behind, and the conduits through which the sediments were transported were erased from the landscape (Ansan et al., 2011; DiBiase et al., 2013). Deep erosion has also exposed formerly buried impact structures, inverting the topography of some (De Hon, 1987; Pain et al., 2007; Davis et al., 2019), and revealing that fluvial systems had been superimposed across others (Malin and Edgett, 2001, figure 32; Edgett, 2016, figure 1). Whether all of this erosion and redeposition on early Mars led to recycling of extraformational sediment into new sedimentary rock seemed likely but remained an open question (McLennan and Grotzinger, 2008), until now.

The presence of just one extraformational sedimentary rock fragment in a younger sedimentary rock is direct evidence that cannibalistic sediment recycling has transpired (Zuffa, 1987). Here, we present observations from the National Aeronautics and Space Administration (NASA) Mars Science Laboratory (MSL) *Curiosity* rover field site in Gale crater (Fig. 2) that demonstrate this form of recycling has occurred on Mars.

This contribution identifies four locations in Gale crater at which sedimentary rock fragments occur within sedimentary rock. These sites are informally named Marias Pass, Bimbe, Cooperstown, and Dingo Gap (Fig. 2C). We also present the case that recycled, extraformational sediments occur elsewhere in Gale crater at places that the *Curiosity* rover has not visited. Further, we discuss the implications for the geological history recorded by sediments in Gale crater, explore implications for the fate of sediment that might have been removed from Gale crater and craters like Gale, and consider how our observations

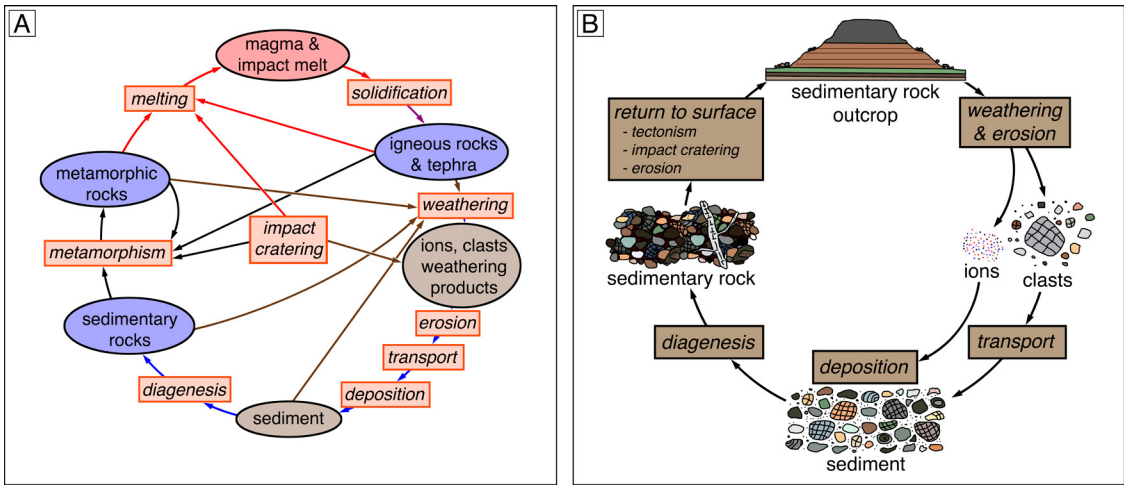

Figure 1. Rock cycle and sedimentary cycle on Mars. (A) The Martian rock cycle includes igneous, sedimentary, and metamorphic rocks (Wilson et al., 1974; McSween, 2015; McSween et al., 2015). Impact events contribute through production of clastic debris, melt, and shock metamorphic products. Metamorphic rocks also include those formed at contacts between country rock and magmatic intrusions (e.g., Flahaut et al., 2011). (B) The Martian sedimentary cycle. As shown in A, this includes rock exposure, rock breakdown, and clast production, transport, deposition, and storage that result from impact cratering.

Downloaded from http://pubs.geoscienceworld.org/gsa/geosphere/article-pdf/16/6/1508/5182958/1508.pdf
by California Inst of Technology user

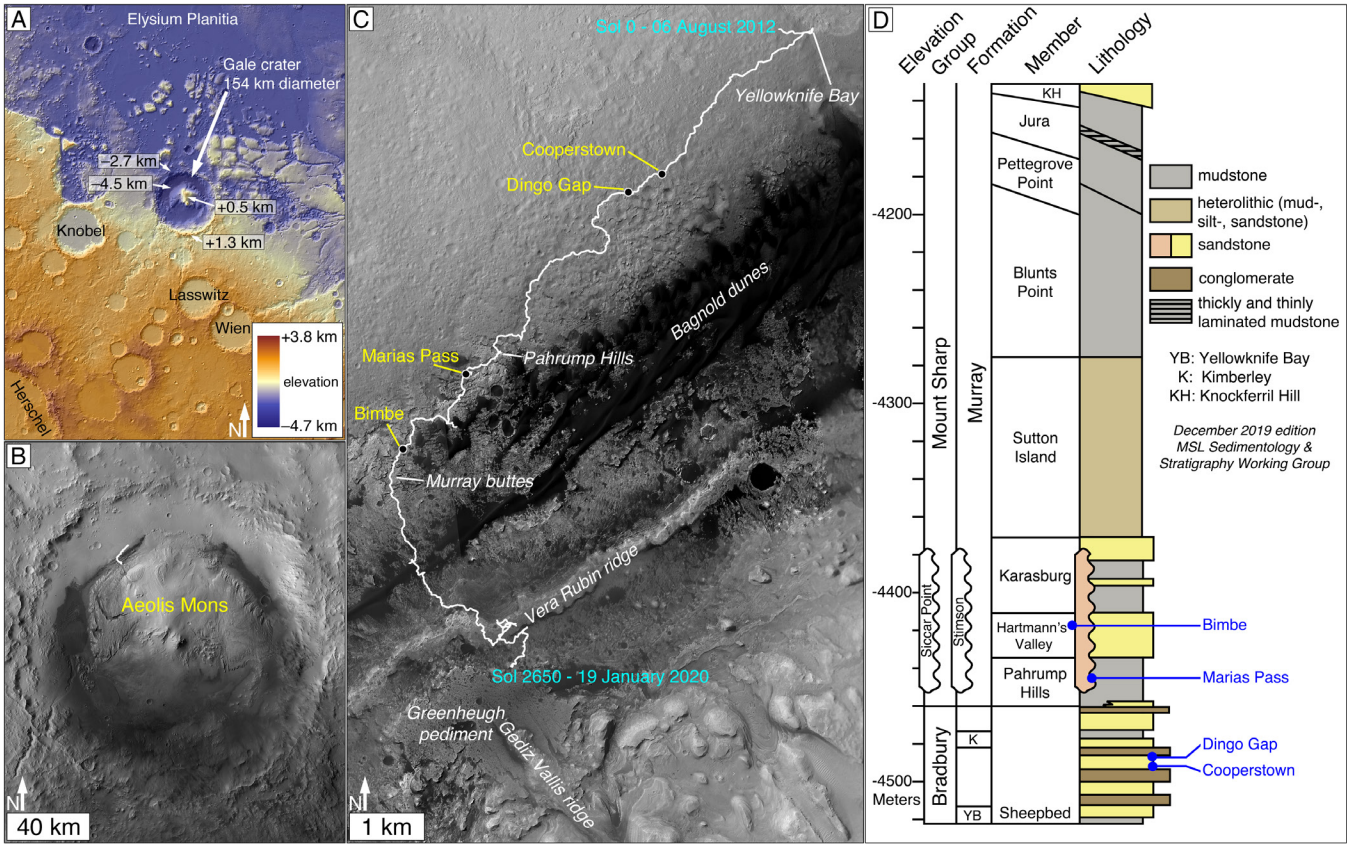

Figure 2. *Curiosity* rover field site context. (A) Regional view of Gale crater; colors indicate elevation relative to Martian datum. Gale is located at 5.4°S, 222.2°W (aerographic latitude, west-positive longitude; 5.3°S, 137.9°E areocentric latitude, east-positive longitude). (B) Gale crater and its 5-km-high interior mound, Aeolis Mons; white trace indicates rover traverse. (C) Rover traverse (white trace) between sols 0 and 2650. The four study sites are indicated in yellow. (D) Rock units encountered along the *Curiosity* rover traverse through September 2019 as a function of elevation relative to the Martian datum. Blue annotations indicate the four study sites; Bimbe is an unconsolidated accumulation of boulders, cobbles, and pebbles that is younger than the Stimson formation and superposes outcrops of the Hartmann's Valley member of the Murray formation (Wiens et al., 2020). The wavy line separating rocks of the Stimson and Murray formations, and between the Siccar Point group and Mount Sharp group, represents a subaerial paleo-erosion surface; the Stimson (Siccar Point group) rocks are younger (Watkins et al., 2016). MSL—Mars Science Laboratory. Note that, for this and subsequent figures, source images and source data products are listed in Supplement S2 (see text footnote 1).

might be applied to the interpretation of remotely sensed images of sedimentary rock occurrences elsewhere on Mars. The latter provides an opportunity to make the case that extraformational recycled sediments might occur in lithified fluvial deltas at the planned *Perseverance* (landing in 2021) and *Rosalind Franklin* (landing in 2023) rover field sites.

GEOLOGICAL SETTING

Gale crater is an ~154-km-diameter impact crater that straddles the Martian geomorphic dichotomy boundary (Mutch et al., 1976) that separates heavily cratered highlands from lightly cratered lowlands (Fig. 2). Inside Gale crater, there is a 5-km-high mountain named Aeolis Mons (informally, Mount Sharp). It consists of sedimentary rock, with a caveat that some (unidentified and maybe minor) strata could be tuff (Malin and Edgett, 2000; Anderson and Bell, 2010; Milliken et al., 2010; Thomson et al., 2011; Le Deit et al., 2013; Grotzinger et al., 2015). The lowland at the bottom of the moat that

Downloaded from http://pubs.geoscienceworld.org/gsa/geosphere/article-pdf/16/6/1508/5182958/1508.pdf
by California Inst of Technology user

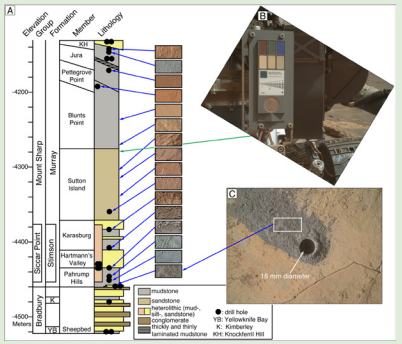

[1]Supplemental Materials. Supplement S1: Background text and figures regarding the formation of plateaus, mesas, and mounds of stratified rock within Martian impact structures. Supplement S2: List of source materials (archival data product identifiers) for Figures 1–19. Supplement S3: Text and figure explaining the methods used for the Alpha Particle X-ray Spectrometer (APXS) analysis of Funda. Supplement S4: Figure presenting a qualitative portrayal of Murray formation colors as a function of stratigraphic position. Supplement S5: Text and figures regarding the sedimentology of the Tumba-Funda and Balombo boulders and the petrology of nonsedimentary pebbles in the Tumba-Funda boulder. Supplement S6: Point cloud data product for the Funda surface relief map produced from four overlapping Mars Hand Lens Imager (MAHLI) images. Supplement S7: Figure showing additional examples of sedimentary rock fragments in the outcrop at Cooperstown. Please visit https://doi.org/10.1130/GEOS.S.12863867 to access the supplemental material, and contact editing@geosociety.org with any questions.

separates Aeolis Mons from the crater walls also exposes sedimentary rock (Williams et al., 2013; Grotzinger et al., 2014; Grant et al., 2014; Jacob, 2015; Stack et al., 2016). The original impactogenic crater floor is buried (Schwenzer et al., 2012).

Gale crater is one of the family of Martian impact structures that contain a mesa, mound, or mountain of layered rock interpreted to be composed largely of sediment (Malin and Edgett, 2000; Bennett and Bell, 2016). How such a landform can be created within an impact structure is a matter of ongoing discussion (see Supplement S1[1])—a conversation that is important to the question of extraformational sediment recycling because of the possibility that sediment exported from these craters could have been incorporated into new sedimentary rock elsewhere. The primary model is that conditions changed, over time, such that basins—net sediment sinks—eventually became net sediment sources, and they did so even after the sediments deposited in them were lithified (Supplement S1). Sediments previously buried and lithified at depths of kilometers (in Gale crater, at least 5 km for the oldest sediments) became exposed and exported from such impact basins. Exhumation of impact structures requires disaggregation of rock as well as removal of the resulting debris from the basins. The alternative is that the intracrater mesas, mounds, and mountains were built up, in place (Supplement S1). Evidence for complete (or nearly complete) fill and partial impact structure exhumation (Supplement S1) argue against the wide applicability of the built-in-place models. The presence of cross-bedded eolian strata in part of the uppermost kilometer of Aeolis Mons in Gale crater, described by Anderson et al. (2018), also indicates that Gale crater was nearly filled, because deposition, retention, and lithification of eolian dunes are more likely in a shallow basin than on a mountaintop.

Intact clastic sedimentary rock strata are exposed all along *Curiosity*'s traverse (Fig. 2C). No in-place igneous rocks have been found, consistent with orbiter image studies that have found no definitive evidence for volcanism (edifices, vents, lava flows) or igneous intrusion (surface exposures of dikes, sills, necks) inside the crater (Cabrol et al., 1999; Pelkey, et al., 2004; Anderson and Bell, 2010; Thomson et al., 2011; Le Deit et al., 2013). The rocks encountered have been interpreted as fluvial conglomerates and sandstones, deltaic and lacustrine sandstones, lacustrine mudstones, and eolian sandstones (Williams et al., 2013; Grotzinger et al., 2014, 2015; Edgar et al., 2018, 2020; Banham et al., 2018a; Stack et al., 2019). The rocks are mostly mafic, although there are also alkali-rich and silicic rocks (Sautter et al., 2014, 2015; Morris et al., 2016; Cousin et al., 2017; Mangold et al., 2017).

Figure 2D shows a summary of the rock units investigated as a function of elevation through September 2019 (rock units encountered thereafter were still in discovery, discussion, and refinement at the time of this writing). Bedding is nearly flat, with dips usually of the order of 0° to 3° (Grotzinger et al., 2015; Lewis and Turner, 2019; Stein et al., 2020). The thickest stratal package investigated during the MSL mission, thus far, is the Murray formation (Fig. 2D). It is exposed on the lowermost north slope of Aeolis Mons and consists mainly of lacustrine mudstones and fine sandstones (Grotzinger et al., 2015; Fraeman et al., 2016; Rampe et al., 2017; Gwizd et al., 2020; Rivera-Hernández et al., 2020; Edgar et al., 2020). An additional ~4.5 km section of stratified rock, unexplored by *Curiosity*, lies above the Murray formation and above the elevation range in Figure 2D (Milliken et al., 2010; Grotzinger et al., 2015). Immediately above the Murray formation, there is a package of sulfate-bearing rock (Milliken et al., 2010). Orbiter and long-range rover images show that some of the sulfate-bearing rocks are cross-bedded at meter scales; these are interpreted to be eolian sandstones (Milliken et al., 2014; Rapin et al., 2020). Other sulfate-bearing strata have been recently proposed to be fluvial in origin (Rapin et al., 2020). Above the sulfate-bearing rocks, there are two different stratal packages exhibiting meter-scale cross-bedding. The first is a light-toned, yardang-forming unit that lies above an erosional unconformity (an impact-cratered paleosurface; Malin and Edgett, 2000). Dromart et al. (2018) interpreted this unit as eolian sandstone. Above that, there lies an additional cross-bedded package interpreted by Anderson et al. (2018) to be eolian sandstone. The topmost package—exposed at the summit of Aeolis Mons—is a stratified, boulder-producing rock unit interpreted by Grotzinger and Milliken (2012) and Lewis and Aharonson (2014) to consist of fine-grained (silt- and clay-sized) eolian sediment.

Aeolis Mons, with its ~5-km-thick stratigraphy, is likely a remnant of a larger body of sediment that once filled (and possibly overtopped) Gale crater (Supplement S1 [footnote 1]; Malin and Edgett, 2000; Grotzinger et al., 2015). After most of the sedimentary rock that used to lie between the crater walls and Aeolis Mons was broken down and removed from Gale crater (Supplement S1), forming the moat that separates the mountain from the crater walls, a record of subsequent sedimentation was captured in the rocks of the Siccar Point group. These rocks include sediments deposited in Gediz Vallis (Malin and Edgett, 2000; Palucis et al., 2016; Fraeman et al., 2016) and dark-toned, erosion-resistant rocks that are today exposed in patches that unconformably drape across the older Aeolis Mons strata (Fraeman et al., 2016; Kronyak et al., 2019a). Rocks of the Stimson formation, part of the Siccar Point group, contact the Murray formation and have been explored at several locations using the *Curiosity* rover (Fig. 2D; Banham et al., 2018a, 2018b).

The contact between the Murray and Stimson formations, the basal Siccar Point unconformity, is a major erosional paleosurface that truncates >140 m of Murray formation strata (Fig. 2D; Watkins et al., 2016). Recent observations suggest that the Stimson formation could truncate >500 m of Murray formation strata (Banham et al., 2020), and, certainly, Siccar Point group rocks, as a whole, drape across more than 500 m of Mount Sharp group strata (Fraeman et al., 2016; Kronyak et al., 2019a). The paleorelief across this buried surface generally follows the slope of the modern, exposed Murray formation surface (i.e., sloping northward) but locally varies at scales of 5–25 m over the region in which Stimson formation outcrops occur (Watkins et al., 2016). The majority of Stimson formation rocks are cross-bedded eolian sandstones (Banham et al., 2018a, 2018b). Lithified below the Martian surface, the depth of burial for these sandstones is presently unconstrained (one possibility is burial beneath, at least, a terminal Gediz Vallis sediment

Downloaded from http://pubs.geoscienceworld.org/gsa/geosphere/article-pdf/16/6/1508/5182958/1508.pdf
by California Inst of Technology user

fan; Bryk et al., 2019). Evidence for burial diagenesis of the Stimson formation includes the fact that the sands are pervasively cemented with no visible (in 16–32 µm/pixel photographs) porosity (Siebach, 2016); concretions are present in some outcrops (VanBommel et al., 2017); the sandstone was fractured, and fluids that moved through these fractures caused alteration of the rock parallel to the fractures (Siebach, 2016; Yen et al., 2017); and geochemical observations of these fracture-parallel altered zones, together with the composition of sub-Stimson lithologies, suggest those fluids were under pressure and moved upward through the fractures (Frydenvang et al., 2017).

The impact event that created Gale crater is considered to have occurred around the time that Mars transitioned from its Noachian to Hesperian periods (Thomson et al., 2011; Le Deit et al., 2013). Estimates of the absolute timing of the event range from ca. 4.0 Ga (Werner, 2019) to ca. 3.8 Ga (Thomson et al., 2011; Spray et al., 2013) to ca. 3.6 Ga (Le Deit et al., 2013). Sediment deposition and lithification within Gale crater, plus the majority of erosion to form Aeolis Mons (Supplement S1 [footnote 1]), are estimated to have occurred during the Hesperian, within 150–240 (or at most, 600) m.y. after the crater formed (Thomson et al., 2011; Spray et al., 2013; Le Deit et al., 2013; Grant et al., 2014).

DATA AND METHODS

Our observations result from photogeological analysis (e.g., Ray, 1960; Fonstad and Zettler-Mann, 2020) of images acquired by cameras aboard a rover on Mars and images and altimetry data collected by instruments aboard several Mars-orbiting spacecraft. Stereopair and Structure-from-Motion (SfM; methods of Garvin et al., 2017) image analyses were performed as needed. The raw images are available from the archives of the National Aeronautics and Space Administration's Planetary Data System (NASA PDS, 2020); the one India Mars Orbiter Mission (MOM; *Mangalyaan*) image studied here came from Lakdawalla (2017). Image identifiers for each figure are listed in Supplement S2 [footnote 1].

Rover Data

The data from *Curiosity* were gathered during the first 2650 sols (06 August 2012–19 January 2020) of the MSL mission (a sol is a Martian day; duration 1.027 Earth days). Visual observations of geological features used images acquired by *Curiosity*'s color Mast Cameras (Mastcam-34, Mastcam-100; Malin et al., 2017), color Mars Hand Lens Imager (MAHLI; Edgett et al., 2012), grayscale Remote Micro-Imager (RMI; a subsystem of the Chemistry Camera, ChemCam; Le Mouélic et al., 2015), and grayscale navigation and hazard cameras (Maki et al., 2012). The rover, its remote-sensing mast (Warner et al., 2016), and its robotic arm (Robinson et al., 2013) were vital tools for positioning the instruments at each location (Fig. 2C). Data for the geochemical analysis of a target named Funda, described in Supplement S3 [footnote 1], came from *Curiosity*'s Alpha Particle X-ray Spectrometer (APXS; Gellert et al., 2015). Vasavada et al. (2014) described the informal nomenclature system used for field studies inside Gale crater; all location and target names in Gale crater are informal except for names approved by the International Astronomical Union: Gale, Aeolis Mons, and Gediz Vallis.

Orbiter Data

Data acquired by Mars-orbiting instruments provided vital context for *Curiosity's* field site and the other locations examined here. The data we studied came from the *Mars Reconnaissance Orbiter* (MRO) High Resolution Imaging Science Experiment (HiRISE; McEwen et al., 2007) and Context Camera (CTX; Malin et al., 2007); *Mars Global Surveyor* (MGS) Mars Orbiter Camera (MOC; Malin et al., 2010) and Mars Orbiter Laser Altimeter (MOLA; Smith et al., 2001); *Mars Odyssey* Thermal Emission Imaging System infrared subsystem (THEMIS-IR; Christensen et al., 2004a); the *Viking* orbiter cameras (Carr et al., 1972); and India's MOM Mars Color Camera (MCC; Arya et al., 2015). Elevations for sites inside Gale crater were determined using a topographic map produced by Parker and Calef (2016) that combines digital terrain models derived from stereopair HiRISE images with lower-spatial-resolution MOLA observations.

OBSERVATIONS AND INTERPRETATIONS

Modern Martian Environment

Present-day Martian sediments and regoliths provide guidance regarding the types of sedimentary rock fragments (lithoclasts) that can be expected to occur in the planet's rock record (Fig. 3). Examples are found in a variety of settings (e.g., Grant et al., 2006; Chojnacki et al., 2014; Thomas et al., 2020), including concretions formed in and liberated from sandstone (Christensen et al., 2004b). Contemporary sedimentary lithoclasts in Gale crater consist of fragments of mudstone (Figs. 3B and 3C), sandstone (Figs. 3A and 3D), and conglomerate (Fig. 3H). Vein mineral fragments (Figs. 3F and 3G) and concretions (Fig. 3E) have also been released from sedimentary rocks in Gale crater. Liberation of individual grains from clastic rocks is demonstrated by accumulations of pebbles below outcrops of conglomerate (Fig. 3I).

Marias Pass

Marias Pass is an erosional reentrant (Fig. 4A) that cuts across eolian sandstones of the Stimson formation (Fig. 2D) and lacustrine mudstones of the Pahrump Hills member of the Murray formation (Fig. 2D). A feature unique to Marias Pass—relative to other locations where *Curiosity*'s instruments were used to examine the major erosional unconformity that separates these two formations—is the occurrence of a lens of sandstone, above the unconformity, that differs in terms of sedimentary texture and structure from the dominant, meter-scale cross-bedded eolian sandstone of the Stimson formation (Banham et al., 2018a, 2018b).

The sandstone lens is part of the Stimson formation (Newsom et al., 2018) and is best exposed at the Clark-Missoula outcrop (Fig. 4B) at the

Downloaded from http://pubs.geoscienceworld.org/gsa/geosphere/article-pdf/16/6/1508/5182958/1508.pdf
by California Inst of Technology user

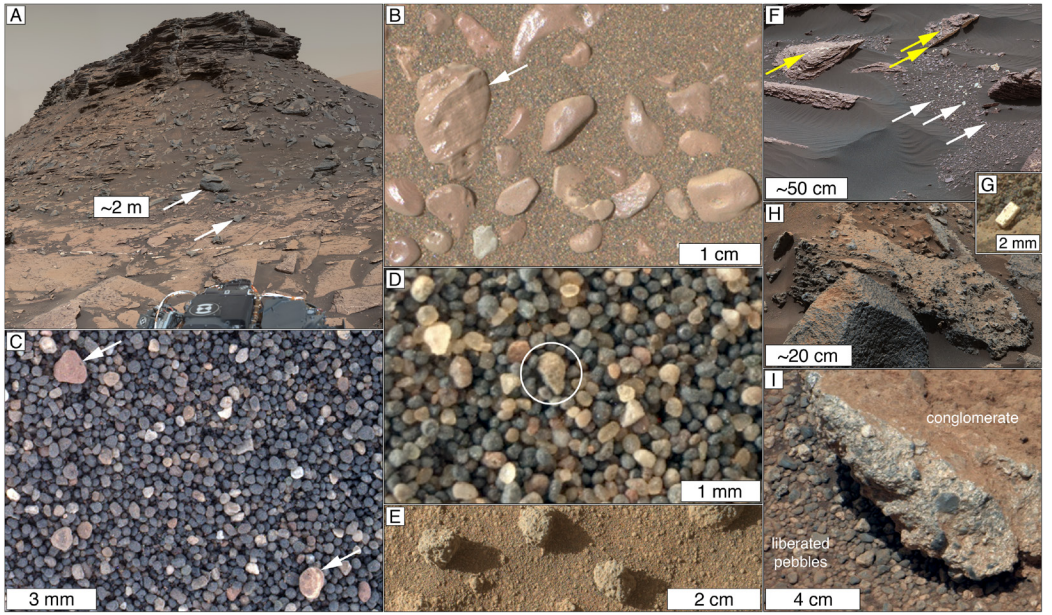

Figure 3. Sedimentary rock fragments—and fragments from veins formed in fractures in sedimentary rocks—in modern Gale crater. (A) Dark-gray, boulder- and cobble-sized sandstone fragments (e.g., arrows) shed from one of the Murray buttes. (B) Reddish mudstone pebbles; arrow indicates example mudstone laminae. (C) Reddish mudstone fragments in an eolian bed form named Trumpet (largest examples at arrows); some include white veins within them. (D) Coarse sand-sized sandstone fragment (circled), consisting of very fine sand, among the eolian sands of the Namib dune in the Bagnold dune field. (E) Examples of sand-bearing concretions liberated from eolian sandstones of the Stimson formation. (F) Pebble-sized white clasts (examples at white arrows) interpreted as vein mineral fragments; yellow arrows indicate examples of white veins in angular mudstone boulders. Note pebble-sized, reddish mudstone fragments. (G) White, cuboid vein mineral fragment, interpreted to consist of calcium sulfate, exhibiting breakage along cleavage planes. (H) Conglomeratic boulder at Bimbe surrounded and partly covered by eolian sand; boulder in left foreground is a sandstone (Wiens et al., 2020). (I) Pebbles at the left and lower center were liberated from an outcrop of conglomerate (right); target name is Link (Williams et al., 2013).

southwest end of the reentrant at Marias Pass (Fig. 4A). It consists of two facies. The lower one, the Clark facies, is an ~3-cm-thick, mafic, siliciclastic, coarse sandstone that includes distinctive larger, light-toned grains of very coarse sand to pebble size (Figs. 4B–4E; Newsom et al., 2018). The upper unit, the Lumpry facies, is an ~3–4-cm-thick, mafic, siliciclastic, coarse sandstone with interspersed medium sand, very coarse sand, and granules (Fig. 4B; Newsom et al., 2018).

The lens is interpreted to consist of grains deposited by wind in local low spots and open fractures on the paleo-erosional surface that separates the Murray formation from Stimson formation rocks at the basal Siccar Point unconformity (Newsom et al., 2018). These sediments are considered to have been emplaced penecontemporaneously with the eolian dunes of the Stimson formation (Banham et al., 2018a). In that regard, this lens records a sedimentary deposit that is similar to the sands, granules, and pebbles (some of which form lags) deposited in interdune areas of the present-day environment in Gale crater (Fig. 3F).

Some of the Clark facies sands sifted down into, and filled, open fractures on the paleo-exposed erosional surface of the Murray formation (Newsom et al., 2018). A target named Seeley (Fig. 5) was one such fracture. Other fractures in pre-Stimson Murray formation rocks had been filled by vein-forming minerals, including—but not limited to—white material (Newsom et al., 2018; Kronyak et al., 2019b). The compositional interpretation for all white veins observed along *Curiosity*'s traverse via the ChemCam Laser Induced Breakdown Spectrometer (LIBS) and APXS is that they consist of calcium sulfate (Nachon et al., 2014, 2017; VanBommel et al., 2017; L'Haridon et al., 2018).

Mudstone and Vein Mineral Fragments in Sandstone

The Clark facies sandstone at the Clark-Missoula outcrop includes 5%–10% (Fig. 4B) light-toned, very coarse sand– to pebble-sized (Figs. 4C and 4E) clasts. The Lumpry facies, above the Clark facies, does not (Fig. 4B). Some of these light-toned clasts protrude from the outcrop (Figs. 4C and 4E, white arrows), and some are recessed (Figs. 4C and 4E, yellow arrows). Some are subangular and have polygonal forms (Fig. 4E), while others are subrounded to rounded (Figs. 4C and 4E). One of the protruding clasts exhibits parallel bands of 0.5–0.6 mm thickness (Fig. 4C). In sunlight, these grains exhibit a similar color and tone as the underlying mudstone strata (Figs. 4B and 4C). The MSL team attempted to determine the composition of these clasts using *Curiosity*'s ChemCam LIBS, but, unfortunately, the laser did not impinge on any of them (Newsom et al., 2018). No other features (e.g., clasts or crystals) can be resolved to occur within them, indicating that such textural details are smaller than fine sand. In addition to these light-gray clasts, the Clark facies also includes some white or very light-gray (orange-brown in shadows), angular, granule-sized grains; two examples are visible in the right half of Figure 4E.

The Clark facies sandstone exposed at the fracture-fill target named Seeley was broken by the

Downloaded from http://pubs.geoscienceworld.org/gsa/geosphere/article-pdf/16/6/1508/5182958/1508.pdf
by California Inst of Technology user

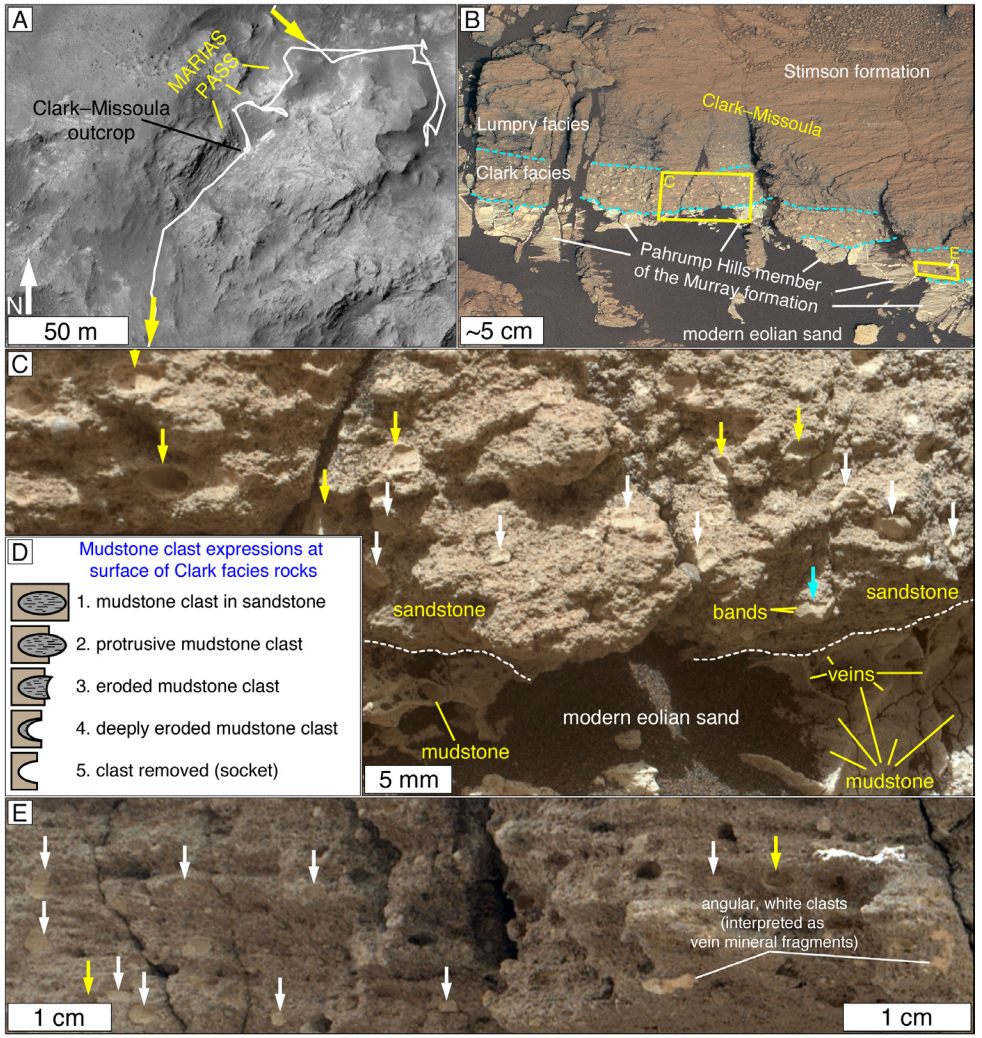

Figure 4. Mudstone and vein mineral fragments in sandstone at Marias Pass. (A) Regional view of the Marias Pass site; white trace indicates rover traverse; yellow arrows indicate traverse direction. (B) Clark-Missoula outcrop, showing a portion of a lens of coarse, dark-gray, eolian sandstone (Stimson formation) unconformably overlying light-gray and fractured (with white veins) Pahrump Hills member (Murray formation) mudstones. The light-toned granules and small pebbles in the Clark facies are interpreted to be mudstone and vein mineral fragments. The dashed blue trace below the Clark facies marks the basal Siccar Point unconformity. (C) Portion of Clark-Missoula outcrop showing that the unconformity between the sandstone and mudstone (dashed white trace) is uneven at millimeter scale and showing examples of mudstone fragments; whole fragments are indicated (white arrows); recessed (eroded) examples and sockets previously occupied by such grains are also indicated (yellow arrows). The clast indicated by a blue arrow displays bands interpreted to be depositional laminae. (D) Sketch showing interpretation of mudstone fragment weathering expressions. As the sandstone is undermined (because the subjacent mudstone is less erosion resistant), pieces of sandstone might fracture and fall away, exposing protrusive mudstone fragments as well as broken fragments and sockets as some clasts also fall away. Wind abrasion (from dark-gray sand nearby; foreground in B) can further alter exposed, protrusive mudstone fragments. (E) Portion of the Clark-Missoula outcrop showing examples of angular, white (somewhat orange in this shadowed view) clasts interpreted as vein mineral fragments. White arrows indicate intact mudstone fragments; yellow arrows indicate eroded, recessive examples or sockets.

rover wheels during a short drive (Figs. 5B and 5C). Before it was broken, Seeley was a linear, erosion-resistant ridge (~2.8 cm wide, ~10.5 cm long, ~2 cm high) that stood above the mudstone surface (Fig. 5B). After it was damaged (Fig. 5C), a white pebble was found within the gray sandstone; Figure 5D shows both pieces of this pebble (arrows). Figure 5E is a close-up view of one of the pieces, showing that it broke along multiple, orthogonal planes.

The light-gray, very coarse sand– to pebble-sized clasts in the Clark facies are interpreted to be mudstone fragments derived from Murray formation rocks (Banham et al., 2018a). The spacing between bands in one of these grains (Fig. 4C) is similar to the ~0.5 mm thickness of laminae in the Murray formation throughout the Marias Pass area (cf. Morris et al., 2016, figure 1A). The recessive clasts (Figs. 4C and 4E) might have been mudstone fragments abraded by windblown sand (dark-toned sand blankets the surface in front of the outcrop in Fig. 4B). In some cases, the recesses might be sockets from which a clast has fallen or weathered out. Because the mudstone fragments exhibit a similar

Downloaded from http://pubs.geoscienceworld.org/gsa/geosphere/article-pdf/16/6/1508/5182958/1508.pdf
by California Inst of Technology user

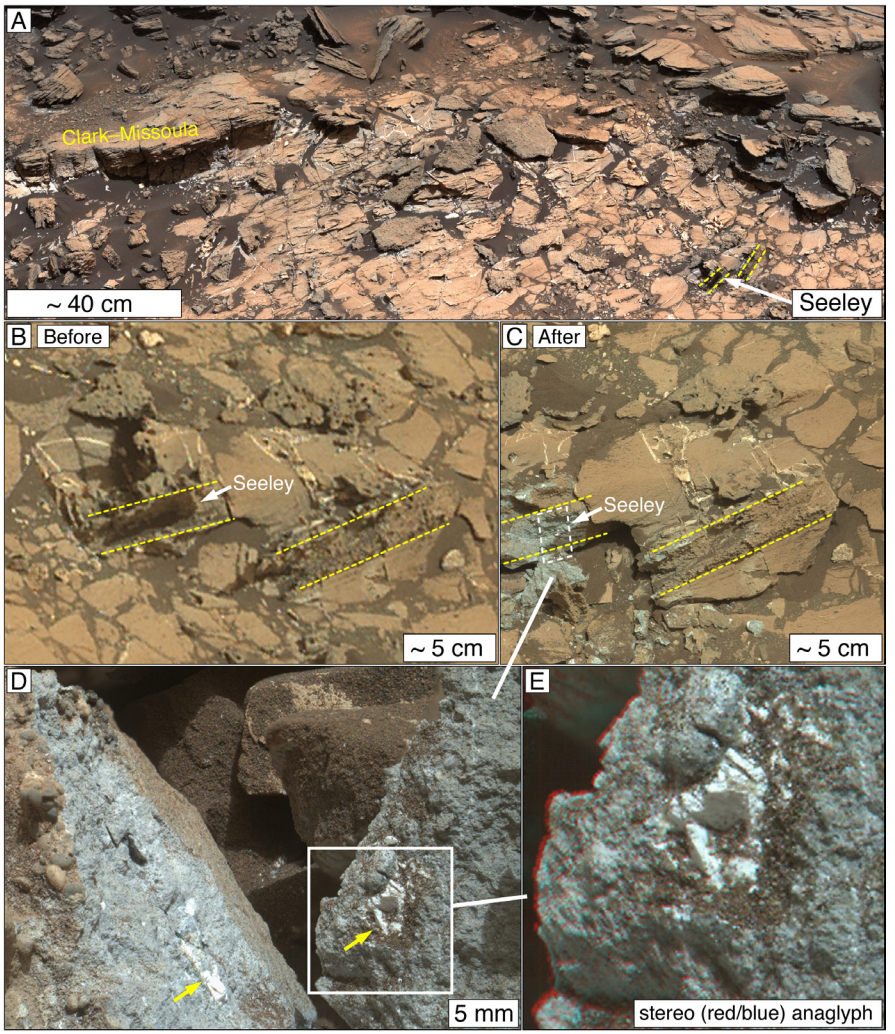

Figure 5. Vein mineral fragment in remnant of a Clark facies sandstone-filled fracture named Seeley. (A) Context view, showing Seeley in relation to the Clark-Missoula outcrop of Figure 4. (B) Mastcam view of Seeley before it was broken by *Curiosity*'s wheels. Yellow dashed lines indicate rock protruding (as fins) from two sandstone-filled, former fractures that cut into the underlying Murray formation mudstone host rock. (C) Mastcam view of Seeley after it was broken. Location of D is indicated by the dashed white box. (D) Mars Hand Lens Imager (MAHLI) view of broken sandstone, which formerly filled a fracture in Murray formation mudstone. Yellow arrows indicate pieces of a white clast that was split along the break created by the rover wheels. (E) Stereo anaglyph (please view using red/blue glasses) showing white, broken vein mineral fragment incorporated into the sandstone; note that the cleavage pattern of intersecting planes exhibits a cubic or rhombic form.

color and tone as the underlying mudstone strata (Figs. 4B and 4C), they were likely derived from that subjacent, light-gray mudstone, because most of the stratigraphically higher Murray formation rocks are not light gray (Supplement 4 [footnote 1]).

The white or very light-gray, angular granules in the Clark facies (Fig. 4E), and the broken white pebble at Seeley (Figs. 5D and 5E) are something different. We interpret these as probable fragments of white minerals (likely calcium sulfate) derived from veins that would have been exposed at the pre-Stimson Murray formation erosional surface. The breakage of the white pebble at Seeley along apparent cleavage planes resembles the planes that define the sand-sized, white cuboid observed in the modern environment in Figure 3G. Vein mineral fragments are not pieces of sedimentary rock but can, in this case, be considered extraformational clasts derived from erosion of veins that had formed in a preceding sedimentary rock unit.

Bimbe

Occurring on the lower north slope of Aeolis Mons, Bimbe (Fig. 6) is an ~16,840 m^2 unconsolidated deposit of boulders, cobbles, and windblown sand that overlies mudstones of the Hartmann's Valley member (Gwizd et al., 2020) of the Murray formation (Wiens et al., 2020). The cobbles and boulders (Figs. 6C and 6D) are mostly fragments of conglomerate and sandstone; some cobbles are locally derived mudstones (Wiens et al., 2020). Sedimentary rock fragments occur in two conglomeratic boulders examined using *Curiosity*'s instruments: Tumba-Funda (Figs. 6D, 7, and 8) and Balombo (Figs. 6D and 9). The bedrock from which these boulders were dislodged is not evident in the vicinity of Bimbe, nor was it identified in outcrops along the rover traverse (Wiens et al., 2020). The geochemical composition of a nearby conglomeratic boulder (Fig. 3H; behind boulder left of Tumba-Funda in Fig. 6D) resembles that of Stimson formation sandstones, suggesting the possibility that the pebble-bearing boulders at Bimbe could have come from an unidentified conglomeratic facies of the Stimson formation (Wiens et al., 2020).

Downloaded from http://pubs.geoscienceworld.org/gsa/geosphere/article-pdf/16/6/1508/5182958/1508.pdf
by California Inst of Technology user

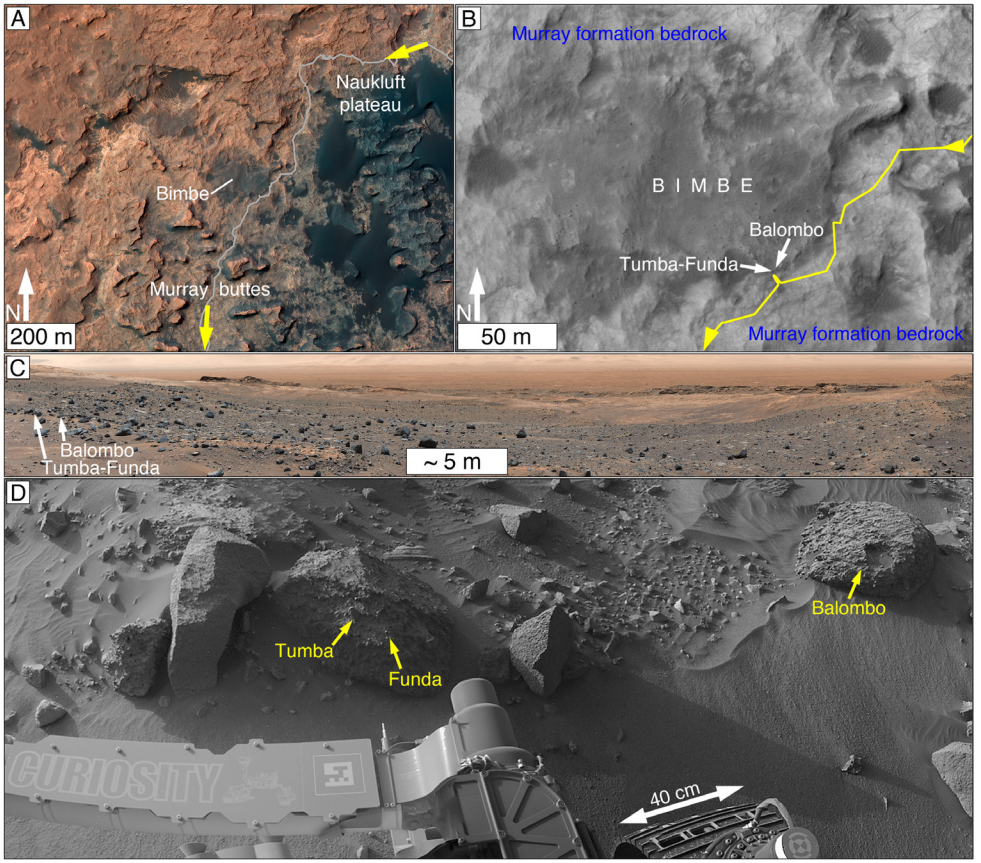

Figure 6. Context views of the boulder- and cobble-strewn accumulation named Bimbe. (A) Bimbe in regional context. *Curiosity*'s traverse is gray; yellow arrows indicate rover drive direction from northeast to south. Bedrock surrounding Bimbe consists of exposures of the Murray formation; Stimson formation eolian sandstones cap the Naukluft plateau and Murray buttes; the darkest gray features are modern eolian sand dunes. (B) Local context view of Bimbe showing the locations of boulders Tumba-Funda and Balombo; rover traverse is in yellow (arrowheads indicate drive direction). (C) Panoramic view of Bimbe, as viewed from the east; locations of Tumba-Funda and Balombo are indicated. (D) Rover navigation camera view of the Tumba-Funda and Balombo boulders; rover wheel for scale.

The Tumba-Funda and Balombo conglomerates are interpreted to consist of fluvial sediment (Supplement S5 [footnote 1]). The boulders contain pebbles of at least two different varieties: sedimentary rock fragments (examples described below) and clasts derived from igneous rocks, impact melt rocks, or both (see Supplement S5). Tumba-Funda also contains white, recessive, pebble-sized features (Fig. 8), including the target named Funda (Figs. 8 and 10); the Balombo boulder does not (Fig. 9). If the white features are clasts, then the two boulders might not consist of contemporaneous sediment; if the white features are diagenetic, then the two boulders were not subjected to quite the same diagenetic events or fluids. Thus, although the two boulders are ~1.6 m apart, they might have come from different rock units.

Sandstone Pebbles in Conglomerate

The Tumba-Funda boulder includes a gray pebble called Tumba (Fig. 7). It is composed of well-sorted (visual estimation), very fine sand– to fine sand–sized particles (Figs. 7A and 7C). The pebble also contains scattered, larger grains, nearly 1 mm across (Fig. 7A). No bedding was observed. The sand grains are too small to be certain about their internal texture (e.g., polymineralic or monomineralic). A vein cuts across Tumba (Figs. 7A and 7C) and does not extend into the matrix of the boulder. The boulder also displays a layered pebble (Fig. 7D) for which there are insufficient data for detailed study. No compositional data (APXS or ChemCam LIBS) were acquired for either pebble.

A ChemCam RMI image of a portion of the Balombo boulder (Fig. 9B) shows that it contains a pebble that has a bumpy texture at the scale of coarse sand (500–1000 μm). The ChemCam LIBS was used to investigate boulder surfaces a few centimeters away (red crosshairs in Fig. 9B), but no compositional data were acquired for this specific pebble.

The pebble called Tumba (Fig. 7A) and the unnamed one at Balombo (Fig. 9B) are both interpreted to be extraformational sandstone fragments. The Tumba parent sandstone was fractured, and a vein-forming mineral or minerals occupied the fracture. Later, after eroding from its source outcrop, the pebble survived transport, deposition, and the diagenesis that caused lithification of the conglomerate in which it occurs, all without splitting apart along the fracture.

Calcium Sulfate Pebbles in Conglomerate

Funda is one of several pebble-sized, recessively weathered, white features in the Tumba-Funda boulder (Figs. 8C and 10; Supplement S3 [footnote 1]). In the orientation shown in Figure 10, the top two thirds of Funda are banded. Stereo-pair images (Fig. 10B) show that the bands are a series of treads and risers (i.e., stair steps), with alternating dark-light-dark banding exposed on each riser. A sub-millimeter-scale surface relief map of

Downloaded from http://pubs.geoscienceworld.org/gsa/geosphere/article-pdf/16/6/1508/5182958/1508.pdf
by California Inst of Technology user

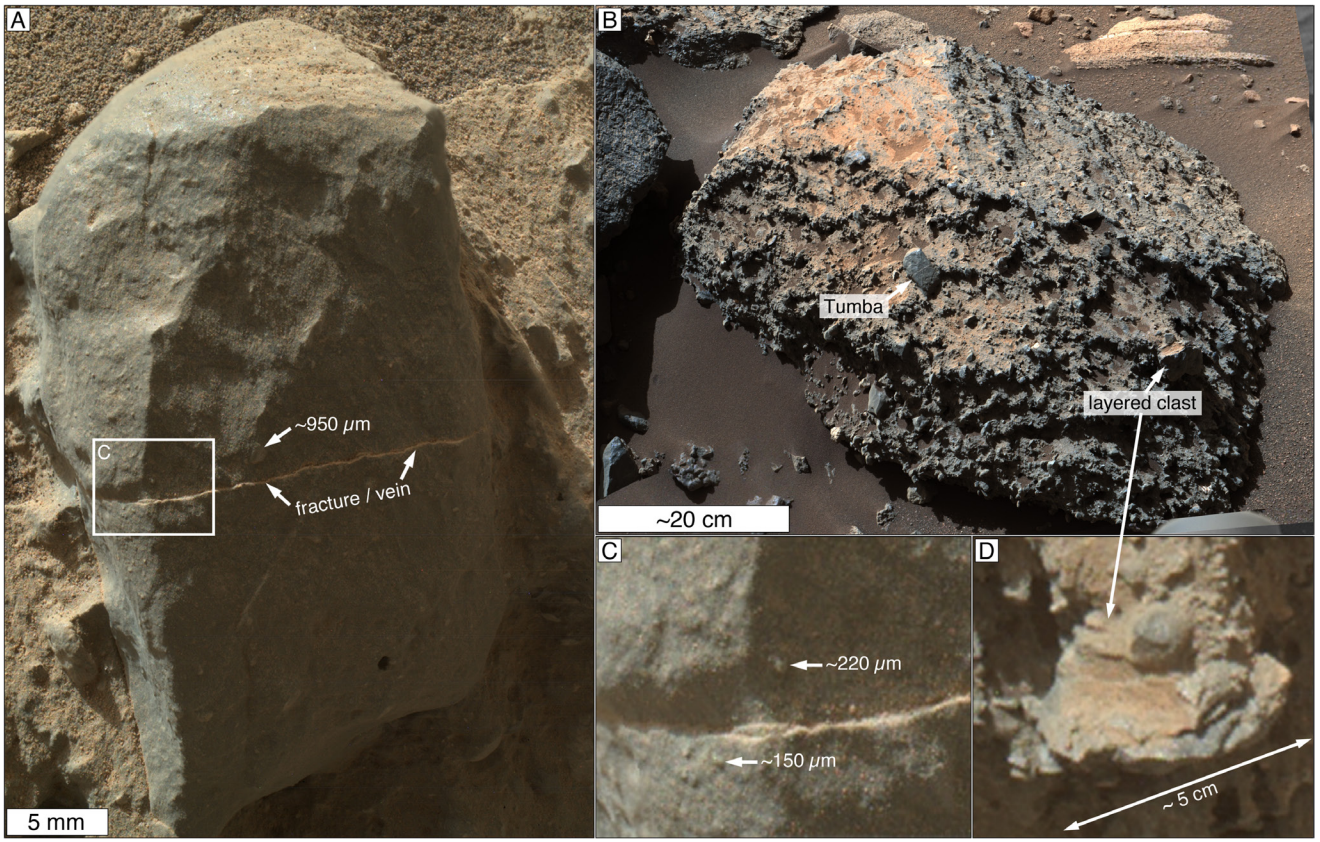

Figure 7. Tumba and layered clast in conglomeratic boulder named Tumba-Funda. (A) Sandstone pebble named Tumba; locations of fracture and vein and one of its largest grains are indicated. Box shows location of C. (B) Context view of layered pebble in D and Tumba sandstone pebble in A. (C) Expanded view of a portion of Tumba; larger grain sizes are indicated. (D) Layered pebble in the Tumba-Funda boulder, likely a sedimentary lithoclast.

Funda (Fig. 10D), constructed from four overlapping MAHLI images, indicates that the tread-and-riser offsets are 100–130 μm (±15%; Fig. 10E). The tread-and-riser pattern is abruptly truncated between the upper two thirds and lower one third of Funda's surface (Fig. 10C). The lower third contains three elliptical, medium sand–sized objects (green in Fig. 10C); these have rounded edges and a color similar to the rest of Funda. The lower third also exhibits many smaller elliptical and angular features of differing color and tone, ranging from white to a yellowish brown (yellow in Fig. 10C); these are ~90–140 μm across. A few such features also occur in the upper two thirds of Funda (examples also in yellow in Fig. 10C).

Analysis of APXS data showed that Funda is composed of calcium sulfate (Supplement S3). The mineral phase cannot be determined from the observations (which provide only chemical, not mineral, compositional information). However, three forms of calcium sulfate have been detected by X-ray diffraction of drill-extracted powders from rocks elsewhere along *Curiosity*'s traverse: gypsum, bassanite, and anhydrite (Vaniman et al., 2018). Funda can be interpreted as either a void-filling mineral, a vein mineral fragment, or a sedimentary rock fragment. The latter two hypotheses require that Funda, and similar recessive white features (Fig. 8), are pebbles that were transported and deposited with the siliciclastic pebbles and sands that compose the Tumba-Funda boulder.

Calcium sulfate–bearing void fills occur in rocks elsewhere in Gale crater, particularly in mudstones of the Sheepbed member of the Yellowknife Bay formation (Fig. 2D; Stack et al., 2014; Schieber et al., 2017). In the Sheepbed member, void fills

Downloaded from http://pubs.geoscienceworld.org/gsa/geosphere/article-pdf/16/6/1508/5182958/1508.pdf
by California Inst of Technology user

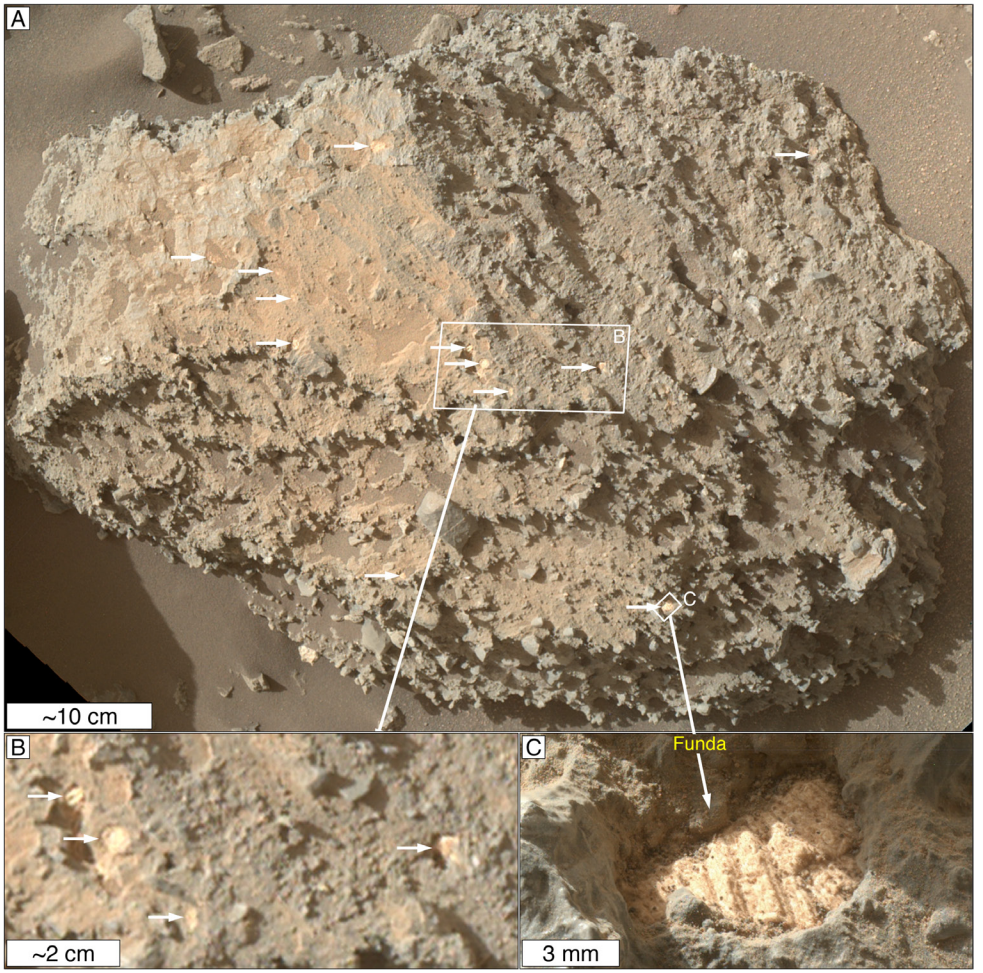

Figure 8. Recessed white features in Tumba-Funda boulder. (A) Mars Hand Lens Imager (MAHLI) view looking downward on the boulder; arrows indicate pebble-sized, recessed white features. (B) Expanded view showing some of the recessive white features (arrows). (C) Close-up view of the recessive white feature named Funda.

are connected to veins formed in hairline fractures through which flowed the fluid that carried the ions of the void-filling precipitates (Grotzinger et al., 2014). No veins were observed in the Tumba-Funda boulder, and the hypothesis offers no explanation for the banding and tread-and-riser morphology, nor the rounded and angular sand-sized objects within Funda. Thus, the void-fill hypothesis is the least likely interpretation. As noted above, the vein fragment hypothesis fits well with the observations of white granule- and pebble-sized clasts in the Clark facies sandstone at Marias Pass (Figs. 4E, 5D, and 5E). However, the step-and-riser banding and sand-sized rounded features in Funda (Fig. 10) are unlike vein textures previously observed in Gale crater (cf. Schieber et al., 2017; L'Haridon, 2018; Kronyak et al., 2019b).

The banding and stair-stepped morphology of Funda are instead interpreted here as indicators of bedding (laminae). In this view, the truncation that divides bands from the lower one third of Funda in Figure 10 marks an intraformational erosional surface, and the well-rounded and angular sand-sized objects within Funda are sand-sized intraclasts. If Funda and the other recessive white features in the Tumba-Funda boulder are indeed chemical sediment lithoclasts, then they are unlike any rock thus far encountered along *Curiosity*'s traverse. Sulfate-bearing rocks, not yet reached by the rover, occur higher up section in Aeolis Mons stratigraphy; however, these are interpreted (albeit at scales of meters per pixel) to be magnesium sulfates (Milliken et al., 2010, 2014; Fraeman et al., 2016). Assuming they are transported pebbles of calcium sulfate composition, Funda and the other white, recessive features in the Tumba-Funda boulder appear to be subrounded (the modern erosional surface not withstanding). These grains were apparently durable enough to survive fluvial transport along with siliciclastic pebbles and sands, although the distance of transport is unknown. To have survived transport until the time of deposition, the calcium sulfate clasts could have been added to the stream not far from the depositional site.

Cooperstown

The Rensselaer unit of the Bradbury group at the Cooperstown site is an ~20-cm-thick, bench-forming, dark-gray sandstone that overlies an unnamed recessive, lighter-gray sandstone (Fig. 11; Supplement S7 [footnote 1]; Le Deit et al., 2016; Stack et al., 2016). The Rensselaer unit consists of coarse to very coarse sand with scattered, protruding granules and pebbles; it is so well consolidated that, in the highest-spatial-resolution MAHLI images, grain boundaries are difficult to distinguish from dark-gray cement. Both the resistant and underlying recessive sandstones are considered to be fluvial or alluvial sediments (Stack et al., 2016).

Downloaded from http://pubs.geoscienceworld.org/gsa/geosphere/article-pdf/16/6/1508/5182958/1508.pdf
by California Inst of Technology user

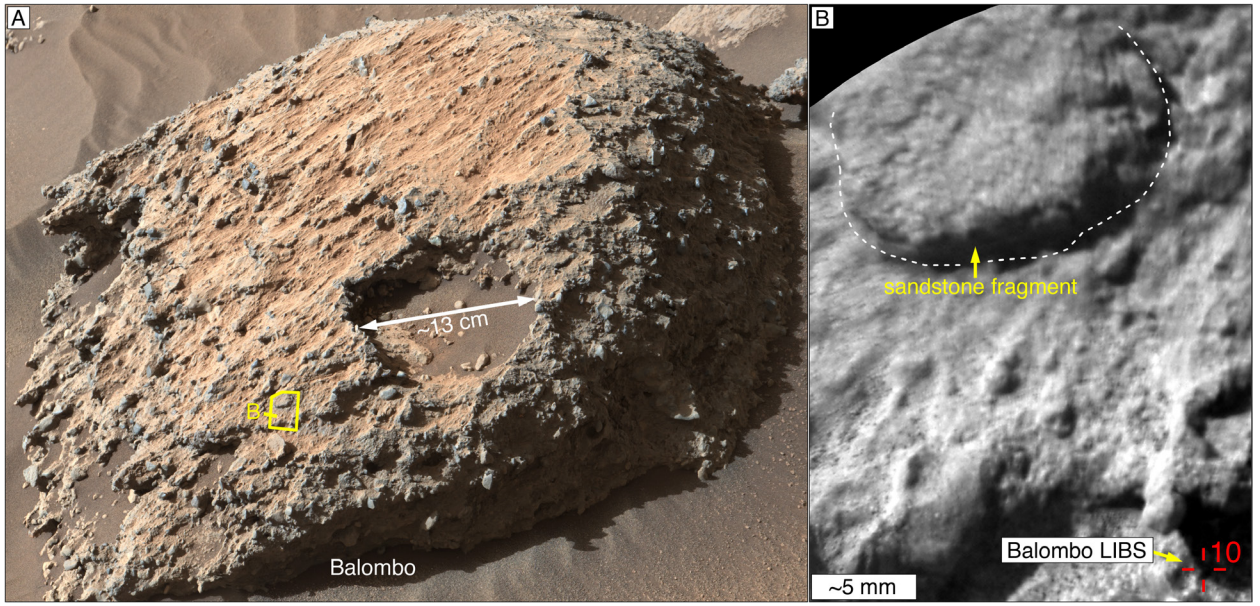

Figure 9. Sandstone fragment in conglomeratic boulder named Balombo. (A) Balombo boulder; outline indicates location of the ChemCam Remote Micro-Imager (RMI) view in B. (B) Sandstone pebble in the Balombo boulder, as viewed by ChemCam RMI. The location of the nearest ChemCam LIBS (laser-induced breakdown spectrometer) shot point, number 10, is indicated by red crosshairs. The LIBS spectroscopy results were published by Wiens et al. (2020).

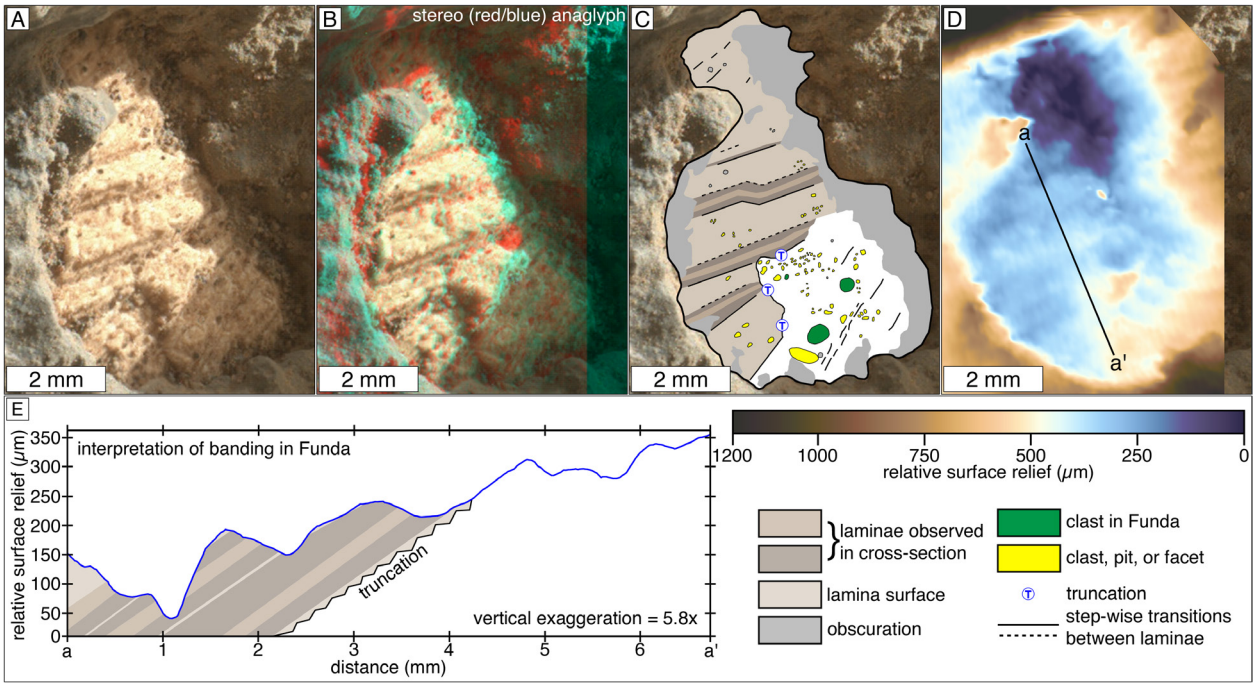

Figure 10. Close-up views of Funda. (A) White recessive feature named Funda, illuminated by sunlight from the top/upper right. (B) Stereo anaglyph view (please view using red/blue glasses). (C) Sketch of details evident in the Mars Hand Lens Imager (MAHLI) images of Funda, including rounded grains within Funda (green); features that could be clasts, crystals, pits, or facets (yellow); stepped, banded features (interpreted as fine laminae); and a truncation (interpreted as an unconformity in a layered sequence) between the banded, upper two thirds of Funda and the less-well-organized nature of the lower third. (D) Surface relief map determined using Structure-from-Motion (SfM) analysis (Garvin et al., 2017) of four overlapping Mars Hand Lens Imager (MAHLI) images; uncertainties are ±15%. The SfM point cloud product is in Supplement S6 (see text footnote 1). (E) Surface relief (±15% uncertainty) profile along line a–a′ in D, shown with interpreted lamination pattern and truncation surface.

Downloaded from http://pubs.geoscienceworld.org/gsa/geosphere/article-pdf/16/6/1508/5182958/1508.pdf
by California Inst of Technology user

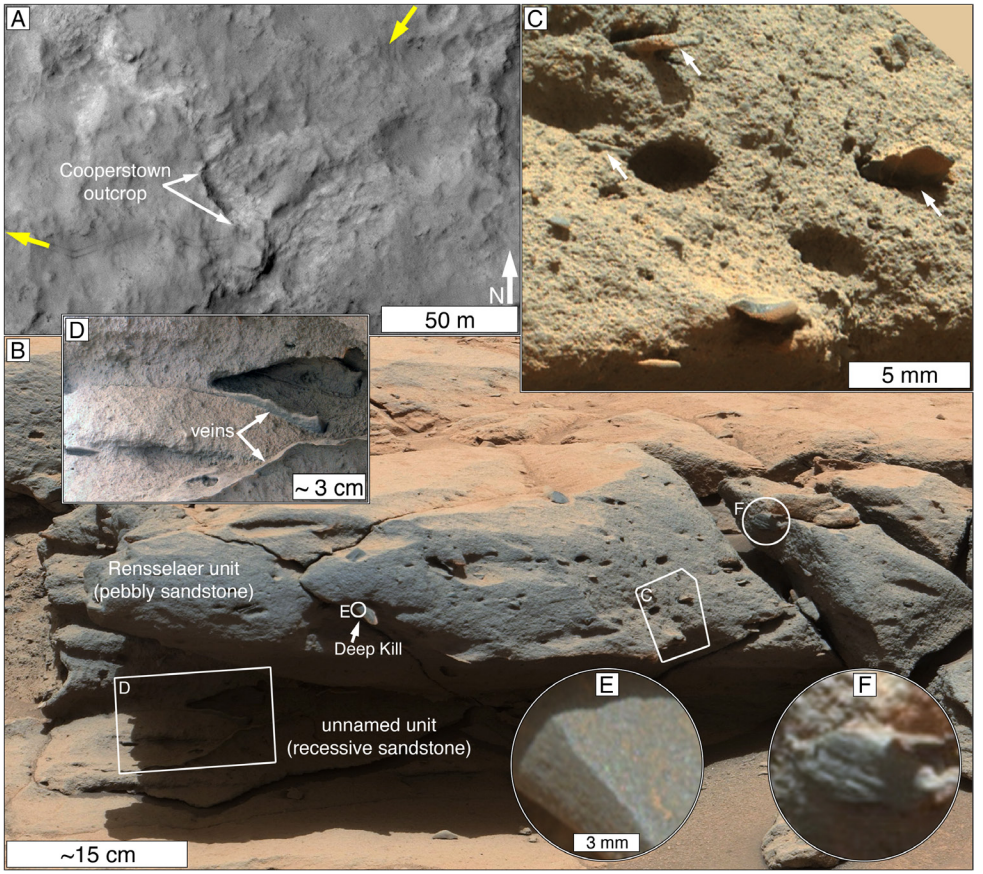

Figure 11. Sedimentary lithoclasts in sandstone at Cooperstown. (A) Regional view; tracks made by *Curiosity*'s wheels are visible; yellow arrows indicate rover drive direction. (B) Sandstones at Cooperstown; the dark, gray Rensselaer unit contains various angular granule- and pebble-sized clasts that protrude from the outcrop surface; also note sockets from which similar-sized clasts were removed. An unnamed, lighter-gray, recessive sandstone occurs beneath the Rensselaer unit. (C) Angular, platy granules and pebbles protruding from the Rensselaer unit sandstone (examples at arrows); also note empty sockets. (D) Mars Hand Lens Imager (MAHLI) view, under the overhanging Rensselaer unit, showing the recessive sandstone facies; it is crosscut by dark-toned, erosion-resistant veins. (E) Portion of dagger-shaped pebble, Deep Kill, which is too fine grained to distinguish whether it is igneous or sedimentary. (F) Example layered or fractured pebble in the Rensselaer unit.

Sedimentary Rock Fragments in Sandstone

The granules and pebbles protruding from the Rensselaer unit sandstone are angular to subangular (Figs. 11B and 11C; Supplement S7). Some exhibit internal banding or stratification (Fig. 11F; Supplement S7), and some are platy (Fig. 11C; Supplement S7). One clast, a dagger-shaped pebble named Deep Kill (Figs. 11B and 11E), was examined using ChemCam LIBS and found to have a mafic composition similar to that of the bulk Rensselaer unit (Le Deit et al., 2016). Imaged by MAHLI at ~100 µm/pixel, the Deep Kill pebble is finer grained than the sandstone in which it occurs (Fig. 11E). The same can be inferred for all of the pebble clasts examined using MAHLI and the Mastcams (Figs. 11C and 11F; Supplement S7). The pebbles are all about the same color as the sandstone.

The stratified pebbles are interpreted to be fragments of sedimentary rock. In addition, the platy clasts might also be sedimentary lithoclasts, or they could be pieces of the dark, gray vein material that occurs in the underlying recessive sandstone (Fig. 11D). The protrusive nature of the pebbles suggests that they are more resistant to weathering (e.g., eolian abrasion in the modern environment) than the well-cemented sandstone in which they occur. Grain sizes within the pebbles are not known, but the erosion resistance of the pebbles suggests that they might be coarser grained and more well cemented than typical Martian mudstones, and they are likely to be finer grained than the coarse to very coarse sand of the Rensselaer unit in which they occur. Thus, these pebble-sized sedimentary lithoclasts might consist of very fine to medium sand sandstones. We are uncertain as to whether the dagger-shaped pebble named Deep Kill (Figs. 11B and 11E) should be counted among the sedimentary lithoclasts in the Rensselaer unit. It is not stratified, and MAHLI and RMI images of it (e.g., Fig. 11E) do not have sufficient spatial resolution to distinguish whether it is a very fine– or fine-grained sandstone, a siltstone, or an aphanitic igneous or impact melt rock.

Vasavada et al. (2014) suggested that the pebbles in the Rensselaer unit are intraclasts. Their distinct erosional expression—and the possibility that some of the platy clasts could have come from dark-gray veins in the underlying, recessive rock unit—suggests that these pebble-sized clasts are less likely to be intraclasts than extraformational sedimentary rock (and possibly vein mineral) fragments. Whether an erosional unconformity occurs between the Rensselaer unit and the immediately subjacent, recessive sandstone is unknown, but if some of the platy, pebble-sized clasts in the Rensselaer unit were derived from the underlying gray veins (Fig. 11D),

Downloaded from http://pubs.geoscienceworld.org/gsa/geosphere/article-pdf/16/6/1508/5182958/1508.pdf
by California Inst of Technology user

then an eroded rock surface—like that present at Marias Pass before the Stimson formation sands were emplaced—would be required.

Dingo Gap

Bradbury group (Fig. 2D) rocks exposed on the south wall of a valley named Dingo Gap (Fig. 12A) include a weakly stratified, poorly sorted conglomerate deposited in an incision into an underlying, cross-stratified sandstone (Figs. 12B and 12C; Edgar et al., 2016). Unlike the Marias Pass and Cooperstown sites, these rock units have not been named. The conglomerate is interpreted to be a distinct fluvial channel body that formed by rapid deposition from a high-energy flow (Edgar et al., 2016).

Stratified Sandstone Cobbles in Conglomerate

The conglomerate (Fig. 12B) includes clasts that are angular, cobble sized, and well stratified (Figs. 12D–12F; Edgar et al., 2016). Some clasts exhibit alternating protrusive and recessive strata, with laminae thicknesses of ~1 mm. One clast exhibits possible cross-stratification (Fig. 12F). The clasts were not imaged by *Curiosity*'s close-up cameras; thus, their grain sizes are unknown, but they must be smaller than the lamination thickness.

The alternation of protrusive and recessive laminae closely resembles some sandstones, rather than any of the mudstones, encountered elsewhere in Gale crater (cf. Edgar et al., 2018, 2020). Thus, the stratified clasts are interpreted to be sandstone fragments. Their size and angularity suggest minimal transport. Edgar et al. (2016) considered them to be derived from the immediately subjacent sandstone (Fig. 12C) cut by the channel in which the conglomerate-forming gravels were deposited. To survive even minimal transport in the interpreted high-energy fluvial system, the sandstone from

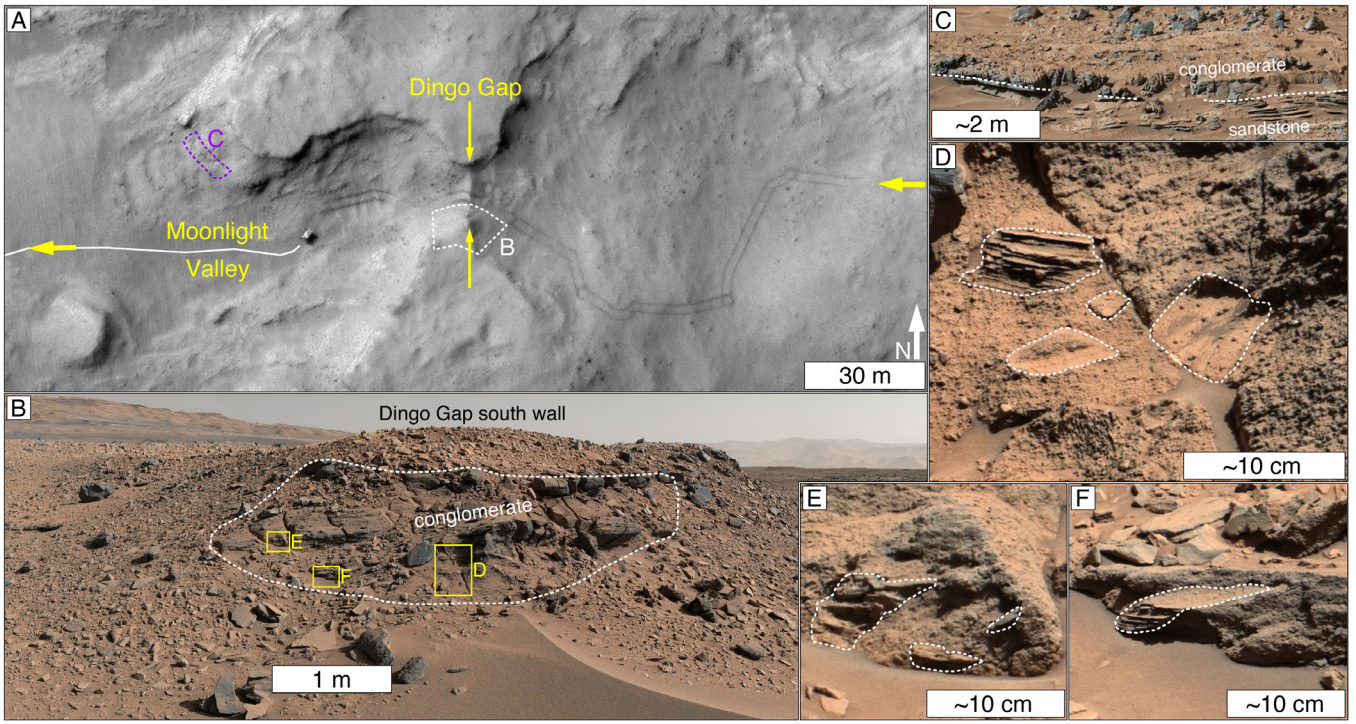

Figure 12. Sedimentary rock fragments in a conglomerate at Dingo Gap. (A) Regional view, including the *Curiosity* rover (left of center) and its dark-toned wheel tracks. Dashed polygons indicate the approximate locations of B and C; vertical yellow arrows indicate Dingo Gap; white trace indicates the subsequent rover path; yellow arrows at left and right indicate direction of rover travel. (B) Panoramic view of the south wall of Dingo Gap. The dashed outline approximately indicates the top and bottom of a conglomeratic channel body overlain by a thin, laminated facies (Edgar et al., 2016). (C) Outcrop on the north side of Moonlight Valley, showing contact (dashed white trace) between conglomerate and cross-bedded sandstone facies. (D–F) Examples of cobble-sized sedimentary lithoclasts in the conglomeratic facies, outlined in white.

Downloaded from http://pubs.geoscienceworld.org/gsa/geosphere/article-pdf/16/6/1508/5182958/1508.pdf
by California Inst of Technology user

which the cobbles were derived would have already been lithified. This means that these sandstone fragments are likely extraformational and that the channel incision was cut through preexisting rock. Although the depositional settings differed, the situation is similar to that which occurs at Marias Pass—fragments of an immediately subjacent sedimentary rock unit occur in younger sedimentary rock just above an erosional unconformity. We note, however, that cobble-sized sandstone fragments are reported to occur as intraformational rip-up clasts in some cases on Earth, particularly in submarine fans (Mendoza-Rosales et al., 2010). While Dingo Gap records a different depositional environment, it is possible, although less likely, that these sandstone clasts could be interpreted as rip-up clasts.

Lithified Sediment Fan

The observations at Marias Pass (and probably Dingo Gap) demonstrate the relations between extraformational sediment recycling and erosional unconformities cutting through older sedimentary rock occurring inside Gale crater. With that evidence in mind, we found that orbiter images of Aeolis Mons offer additional examples of deposits containing extraformational recycled sediment. In particular, several canyons cut Aeolis Mons strata and terminate in a sediment fan (Anderson and Bell, 2010; Le Deit et al., 2013; Fairén et al., 2014; Milliken et al., 2014; Palucis et al., 2016). Those fans should consist of rock fragments and individual liberated clasts derived from the sedimentary strata incised by the streams that cut the canyons. If lithified, then these fans would be directly analogous to the extraformational sediment recycling examples at Marias Pass. Sediment in the channel and terminal ridge at Gediz Vallis (Fig. 2C) might also be lithified, recycled sediment (Malin and Edgett, 2000; Palucis et al., 2016).

Figure 13 shows a representative example in the form of a stubby, fan-shaped landform at the terminus of a canyon that occurs on the lower west side of Aeolis Mons. The fan-forming material is stratified, holds steep slopes, is fractured, and produces boulders as it degrades. In addition, a circular depression occurs on the fan. The circular feature is interpreted to be the eroded remains of an impact structure. The fan is an eroded remnant of a formerly more extensive delta or alluvial fan composed of sediment eroded from Aeolis Mons. The sediment is considered to be lithified because it is competent enough to fracture, hold steep slopes, produce boulders upon weathering, and retain an impact structure. Because the stubby fan has to be composed of material eroded from Aeolis Mons (i.e., sedimentary rock), and because the fan is lithified, it must consist of recycled, extraformational sediment.

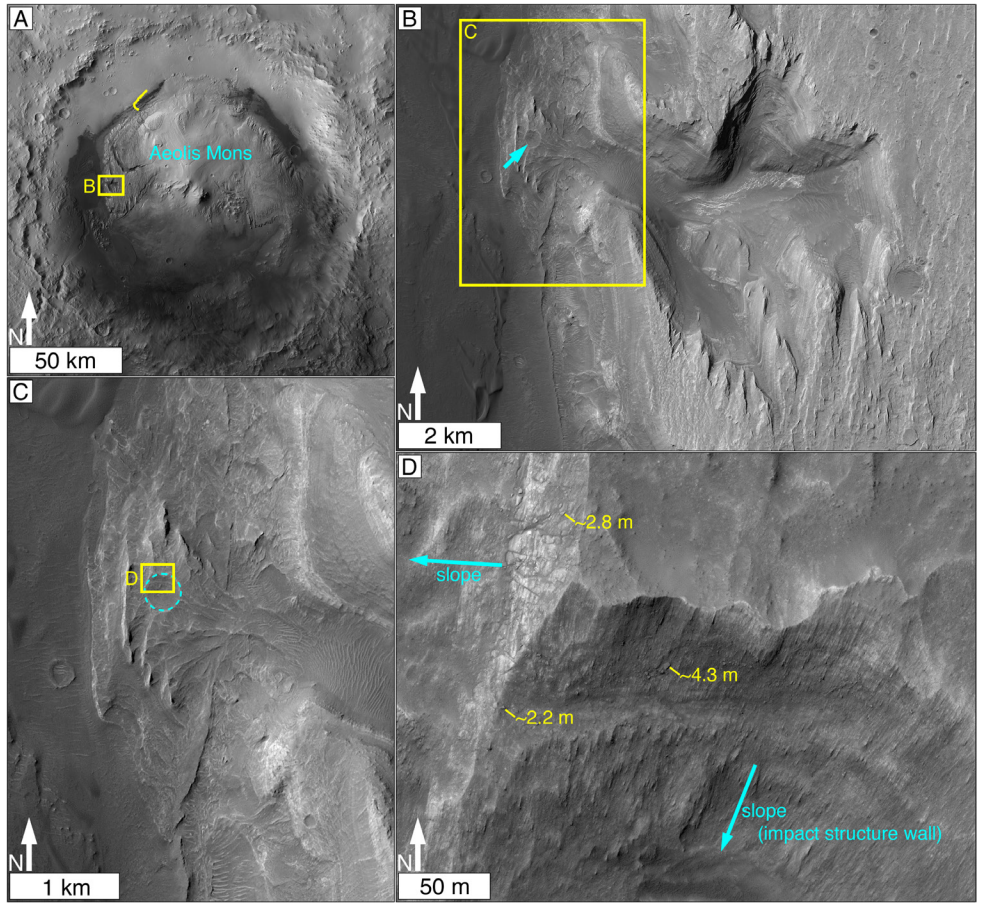

Figure 13. Remnant lithified sediment fan at terminus of a canyon on the west side of Aeolis Mons. (A) Gale crater with location of fan indicated. Yellow trace indicates the *Curiosity* rover traverse. (B) Remnant canyon and lithified fan; location of C is indicated; blue arrow indicates eroded impact structure superimposed on the fan. (C) Remnant lithified fan; location of D is indicated; blue, dashed circle indicates the impact structure. (D) Close-up view of two slopes (arrows), one of which is the wall of the remnant impact structure, cut into the lithified fan. The sizes of three large boulders, produced by erosion of the lithified fan sediment, are indicated.

Downloaded from http://pubs.geoscienceworld.org/gsa/geosphere/article-pdf/16/6/1508/5182958/1508.pdf
by California Inst of Technology user

DISCUSSION

Extraformational Recycled Sediment in Gale Crater

The two conglomeratic boulders at Bimbe (Figs. 6–9) definitively contain recycled, extraformational sedimentary lithoclasts. Indeed, the sedimentary rock fragments in the Tumba-Funda boulder came from three different sources, one a fractured (with vein) sandstone (Figs. 7A and 7C), the second a stratified, apparently intraclast-bearing calcium sulfate–rich rock (Figs. 8C and 10; Supplement S3 [footnote 1]); and the third a gray, layered rock (Fig. 7D). At least three sedimentary cycles are recorded at Bimbe (Fig. 14A). Using the Tumba pebble to illustrate, during the first known cycle (1 in Fig. 14A), the sands that compose Tumba were created, transported, deposited, and lithified. The sandstone was then fractured, and minerals were deposited in that fracture, creating a vein. At the start of the second cycle (2 in Fig. 14A), the sandstone was exposed, weathered, and eroded. The pebble named Tumba was created during erosion of, or transport away from, the sandstone outcrop, and it was eventually deposited with other sands and pebbles that were later lithified to form

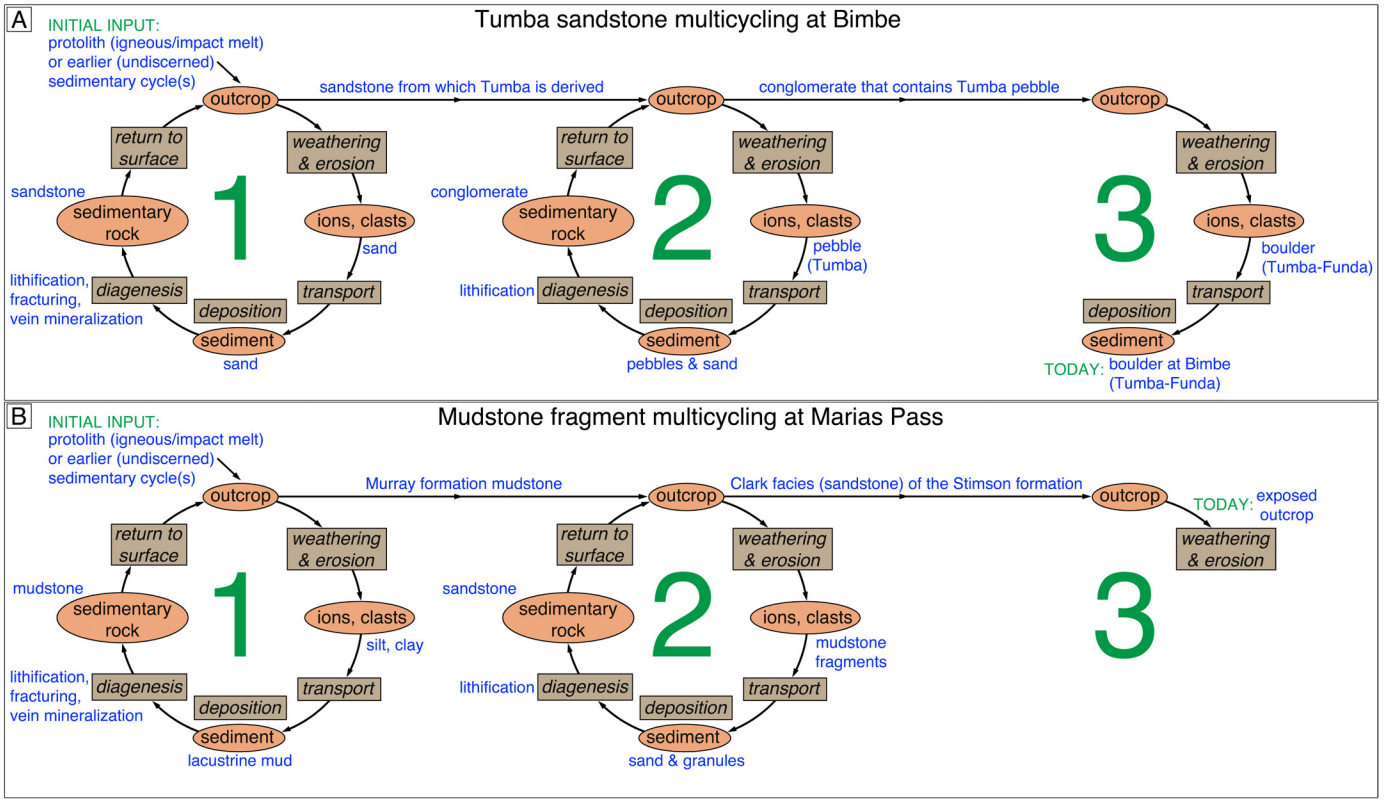

Figure 14. Extraformational multicycling of sediment in Gale crater, Mars. (A) Known cycles to which the sand grains inside the sandstone pebble Tumba were subjected. During the first known cycle, the sands were created, transported, deposited, lithified, and fractured (in which formed a vein), and then the resulting sandstone body became exposed at the Martian surface. The second cycle involved erosion of that sandstone, production, transport, and deposition of the Tumba pebble, followed by lithification within a conglomerate. The third cycle began with exposure of the conglomerate, followed by its weathering and erosion, which produced the Tumba-Funda boulder, deposited with the other boulders and cobbles at Bimbe. (B) Known cycles to which the tiny grains within the mudstone fragments in the Clark facies of the Stimson formation sandstone were subjected. The first known cycle involved clast creation, deposition, and diagenesis of the mud. The second cycle involved deep erosion of Aeolis Mons strata in Gale crater, forming the moat between the north wall of Gale crater and the north-facing slope of Aeolis Mons; exposure of the mudstone to erosion; transport and deposition of mudstone fragments with other sands; and lithification within a sandstone. The third cycle has more recently begun, with exposure and ongoing weathering of the sandstone at Marias Pass.

Downloaded from http://pubs.geoscienceworld.org/gsa/geosphere/article-pdf/16/6/1508/5182958/1508.pdf
by California Inst of Technology user

a conglomerate. The third cycle (3 in Fig. 14A) began with exposure of the conglomerate to the surface weathering and erosion environment; this led to the production, transport, and deposition of the Tumba-Funda boulder where we see it at Bimbe today.

The sandstone of the Clark facies (Stimson formation) at Marias Pass contains recycled, extraformational mudstone fragments (Fig. 4) and pieces of white vein minerals formed in fractures in older sedimentary rock (Figs. 4E, 5D, and 5E). At least two full sedimentary cycles, plus the start of a third, are recorded (Fig. 14B). The fine-grained muds and sands of the Murray formation (e.g., Rivera-Hernández et al., 2020) were deposited during the first known cycle (1 in Fig. 14B). These sediments include the light-gray, relatively high-silica mudstones of the upper Pahrump Hills member of the Murray formation (Morris et al., 2016) exposed at Marias Pass (Czarnecki et al., 2020). During the first cycle, all of the Murray formation sediments were deposited, buried beneath the ~4.5 km of strata that overlie these rocks in Aeolis Mons, lithified, and fractured. Vein-forming minerals precipitated in the fractures as fluids passed through them (Nachon et al., 2017; Kronyak et al., 2019b).

The second sedimentary cycle at Marias Pass (2 in Fig. 14B) began with a period of considerable erosion and removal of sediment from Gale crater (per Supplement 1), creating Aeolis Mons and the moat that separates it from the crater walls. The basal Siccar Point unconformity records the erosional surface formed during this major episode of sediment removal. At Marias Pass, ~25 km from the northern wall of the crater, this unconformity separates the Murray and Stimson formations (Watkins et al., 2016). Newsom et al. (2018) found that the Murray formation rock beneath the unconformity at Marias Pass was not chemically weathered before the Stimson formation sands were emplaced, nor are any paleosols present. Considering the stratigraphy and sedimentary structures of the Stimson formation above the unconformity, Banham et al. (2018a) concluded that these sands were deposited in a dry setting; eolian erosion would have removed any regolith or weathering rinds that might have previously developed at and near the erosional surface. Taken together, the sands, mudstone fragments, and vein mineral fragments incorporated into the Clark facies, just above the unconformity, are also interpreted to have been deposited in an arid setting in which eolian sedimentation was dominant (Newsom et al., 2018). Clark facies (Stimson formation) sediments were buried, lithified, and fractured in the subsurface (2 in Fig. 14B) before being, eventually, exposed at the surface by erosion (3 in Fig. 14B). For the detrital sediment within the mudstone fragments in the Clark facies, their exposure and weathering at the outcrop in Marias Pass (Fig. 4) signal that a third sedimentary cycle has begun (3 in Fig. 14B).

Sources of Extraformational Sedimentary Lithoclasts in Gale Crater

There are three potential sources for extraformational sedimentary lithoclasts—and individual clasts liberated from previous sedimentary rocks—in sedimentary rocks inside Gale crater: older sedimentary rocks formed inside Gale crater, Gale impactor target rock, and rock exposed in the terrain outside of Gale crater. Any one of these, or a combination, could have been a source for clastic sediment deposited in Gale crater at any point in its history, although the first could only occur after some sediment was deposited, lithified, re-exposed, and eroded inside the crater.

Older Sedimentary Rocks Formed Inside Gale Crater

The mudstone fragments in Stimson formation (Clark facies) rocks at Marias Pass (Fig. 4) definitively came from the erosion of older sedimentary rocks (the Murray formation) previously deposited inside Gale crater. A similar story likely applies to the sandstone cobbles in the conglomerate at Dingo Gap (Fig. 12) and definitively applies to the lithified sedimentary fans at the termini of canyons that incise Aeolis Mons (e.g., Fig. 13). In addition, based on geochemical observations, Bedford et al. (2020) offered sediment recycling—perhaps from erosion of Bradbury group (Fig. 2D) rocks—as at least a minor source of some of the eolian sands of the Stimson formation as a whole. These observations demonstrate that sufficient time and environmental conditions were available for extraformational recycling of sediment deposited in Gale crater to occur, completely inside the crater.

A less certain concern is whether the extraformational sedimentary lithoclasts in the conglomeratic boulders at Bimbe, and in the sandstone at Cooperstown, consist of fragments of rock previously deposited inside Gale crater. For Bimbe, there are two complicating factors. The first is that no intact rock outcrops quite like Tumba and Funda have been encountered by the *Curiosity* rover; however, there is an ~4.5 km section of Aeolis Mons stratigraphy *above* the area explored. The second is that the conglomerates are not intact rock outcrops; we can only make broad inferences regarding where they came from, and we cannot be certain of their relation to the basic stratigraphy (Fig. 2D) of the area. Although we cannot resolve where the sedimentary lithoclasts in the two boulders at Bimbe came from, the uncertainties allow discussion of alternative sources for sedimentary lithoclasts deposited in Gale crater: the impactor target rock and rock exposed or previously exposed in terrain outside of Gale crater.

Gale Impactor Target Rock

The impact event that created Gale crater excavated to a depth of 10–15 km (Schwenzer et al., 2012). Target rock would have been exposed in the crater walls and central uplift. The ejecta blanket would consist of fragments of target rock, and some of the ejecta would have been present at the crater rim and could have been eroded from there and redeposited inside the crater. At the time the Gale impact event occurred, 500–900 m.y. of geological history—minus episodes of nondeposition and losses at major unconformities—had already been recorded in the impactor target rock.

The rock exposed in the walls of Gale crater is usually assumed to be igneous because of the apparent plethora of igneous textures in pebbles observed in the conglomerates encountered along

Downloaded from http://pubs.geoscienceworld.org/gsa/geosphere/article-pdf/16/6/1508/5182958/1508.pdf
by California Inst of Technology user

Curiosity's traverse through Bradbury group rocks (Sautter et al., 2014, 2015; Mangold et al., 2016). The sandstones and mudstones deposited in Gale crater are also interpreted as having igneous protoliths (Vaniman et al., 2014; Treiman et al., 2016; Morris et al., 2016; Yen et al., 2017; Rampe et al., 2017; Mangold et al., 2017). However, to assume that all of the Gale impactor target rock was igneous would be an error. Some of the rock could have consisted of impact melts, and some could have been clastic sedimentary rock derived from igneous and impact melt protoliths. The problem is, no unambiguous igneous, impact melt, or sedimentary rock outcrops have been identified in orbiter or rover images to occur in the walls of Gale crater (e.g., Ehlmann and Buz, 2015; Buz et al., 2017).

The landscape outside of Gale crater offers clues as to the nature of the uppermost kilometers of the target rock. Figure 15 illustrates what is known about the regional surface just before the impactor struck. Gale ejecta overlies, and secondary craters damaged, impact structures that predate Gale crater (Thomson et al., 2011). Further, there was at least one fluvial valley that ran north-northeastward across the impactor target zone; it was partly covered by ejecta and partly destroyed (Fig. 15B) during the impact event (Irwin et al., 2005). The target zone also included scarps, mesas, and troughs (fretted terrain; sensu Sharp, 1973) of the geomorphic dichotomy boundary that divides the northern lowlands from the heavily cratered southern highlands (Figs. 2A and 15B). The fluvial system of Irwin et al. (2005) would have intersected this fretted terrain (Palucis et al., 2016). Because it is not traceable northward into the lowlands, the fluvial system could have terminated at the fretted terrain boundary and deposited a sedimentary fan or delta (Fig. 15B); such deposits are common at valley termini at the dichotomy boundary elsewhere in the region (Di Achille and Hynek, 2010; Rivera-Hernández and Palucis, 2019). We found no unequivocal pre–Gale crater volcanic landforms observable in the vicinity of the target area—no flows, edifices, or exposed dikes—although we note that Churchill (2018) proposed that one landform, located immediately northwest of Gale crater (brown in Fig. 15B), could be a volcanic edifice that predates the Gale crater–forming event.

The upper crust of the heavily cratered terrain of Mars is a three-dimensional patchwork of interbedded impact structures, impact melt, ejecta, sediment, regolith, and igneous materials (Supplement S1 [footnote 1]). The impact structures and fluvial landforms that predate the Gale crater–forming impact event provide evidence that some sedimentary deposits, whether lithified or not, could have been present in the impacted terrain. Eolian sediments were also likely present at the surface, and impact structures destroyed by the Gale crater–forming event might have been partly filled, filled, or buried by sediment. Although the exact lithologies in the 10–15-km-deep portion of the upper Martian crust that was disrupted and

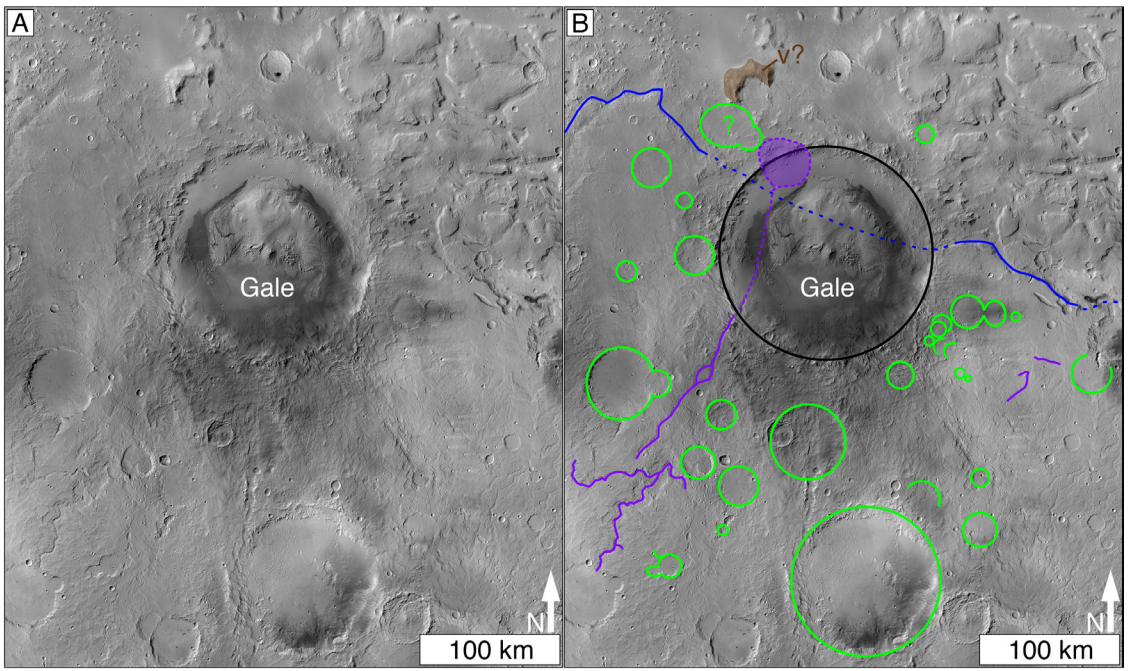

Figure 15. Gale crater target rock. Heavily cratered terrain, filled and partly filled impact structures, ejecta deposits, and eolian, fluvial, and alluvial sediments all likely occurred in the area obliterated by the Gale crater–forming impactor. (A) Present-day configuration of the terrain in and around Gale crater. (B) Sketch showing current knowledge of terrain features present immediately before the Gale crater–forming impact occurred. Larger impact structures interpreted to have been superposed by Gale ejecta (including secondary craters) are indicated in green, valleys are in purple, and the north-south dichotomy boundary is in blue. Dashed valley trace and delta (purple) are inferred to have existed as a logical northeastward extension of the valley covered by Gale ejecta described by Irwin et al. (2005). The brown feature (v?) was proposed by Churchill (2018) to be a remnant volcanic edifice that might have predated the Gale crater–forming impact. For simplicity, the buttes and mesas immediately north of the dichotomy boundary (visible in A) are not sketched; some of these are also superposed by Gale ejecta.

Downloaded from http://pubs.geoscienceworld.org/gsa/geosphere/article-pdf/16/6/1508/5182958/1508.pdf
by California Inst of Technology user

ejected during the impact event are unknown, sediments and sedimentary rocks were likely part of this ancient stratigraphy at the time of impact. If exposed in the crater walls or in the ejecta on the crater rim, sedimentary rocks would have contributed recycled, extraformational clasts to the sediments deposited inside Gale crater.

Rock Exposed in the Terrain Outside of Gale Crater

Another source for recycled sediment deposited in Gale crater is the terrain that occurs outside the crater, beyond its ejecta blanket. This can include rock exposed at the Martian surface today, rock that was exposed but later was (and remains) buried, and rock that no longer exists because it was eroded away or destroyed by a later impact event. If these included sedimentary rocks, then fragments of those rocks could have reached Gale crater. Even very distant sources could have provided recycled, extraformational sediment to Gale—not of the size of pebbles like Tumba, but in the form of eolian dust that settled in Gale crater during waning dust storms. Importation of clastic sediment from outside of Gale crater is practically required to explain how the crater was filled, or nearly filled, with sediment (Supplement 1). Even if the crater was not filled, but instead Aeolis Mons was built up as a mound (Niles and Michalski, 2012; Kite et al., 2013), sediment arriving from outside of Gale crater would have been incorporated into the stratigraphy.

Record of Second Cycle Weathering and Diagenesis in Gale Crater

The recycled extraformational sediments inside Gale crater offer insight into the nature of the weathering and diagenetic conditions of the second known sedimentary cycle to which the recycled lithoclasts were subjected. One consequence of extraformational, siliciclastic sediment recycling on Earth is compositional maturation, which results from the integration of multiple cycles of weathering and diagenesis (e.g., Cox and Lowe, 1995a, 1995b). Compositional maturity should not be confused with textural maturity, as the two are distinct and result from differing processes (Dott, 1964). Compositional maturity describes the extent to which sediment has been reduced to residual minerals though chemical reactions. Sorting can segregate clasts by grain size and density, but that, alone, is not maturation. Likewise, mechanical comminution does not mature sediments (Nesbitt and Young, 1996), although some mineral grains and rock fragments are less susceptible to kinetic destruction than others (e.g., Cornwall et al., 2015). On Earth, the major residual phases representative of compositionally mature sediments are quartz/chert (e.g., sandstones and siltstones) and kaolinite, which commonly transforms into illite during diagenesis (e.g., mudstones).

Hydrolysis of rocks and minerals occurs during weathering and diagenesis. Initial phase mineralogy, time, temperature, fluid chemistry, porosity, and permeability are all important variables. Weathering occurs in the source region, and potentially during temporary storage while sediment is in transit to its depositional basin. Intense weathering regimes and extended periods of storage can lead to maturation of first cycle sediments before clasts arrive at their ultimate depositional site (Johnsson et al., 1988; Akhtar and Ahmad, 1991; Nesbitt et al., 2009). Chemical reactions can occur during sediment diagenesis that operate like weathering to remove or segregate labile mineral grains and rock fragments (e.g., Land et al., 1987).

The mineralogy of compositionally mature sediment is highly dependent on source lithology. A basalt source will never mature into quartz sand. Crystal size in source rock (and tephra) is a vital factor. If, for example, quartz grains in a parent igneous or metamorphic rock are not as coarse or coarser than sand size, then quartz sand will not be produced in abundance. The same is true for rocks on Mars. For example, if an igneous extrusive rock has no plagioclase phenocrysts of sand size or larger, then a sand produced from weathering that rock will not contain monomineralic plagioclase grains (Fedo et al., 2015). With the predominantly basaltic crust of Mars (McSween et al., 2009), major constituents will be altered by weathering and diagenesis in the typical order, glass >> olivine > plagioclase >> pyroxene > metal oxides (Eggleton et al., 1987; Nesbitt and Wilson, 1992), ultimately leaving a residuum of kaolinite and iron oxides (e.g., Nesbitt and Wilson, 1992; Babechuk et al., 2014).

For cold, dry, Amazonian Mars (the last ~3.3 b.y.; Tanaka et al., 2014), chemical weathering has been minor (McSween et al., 2009), but buried sediments in the diagenetic window could have had—as interpreted for a mudstone in Gale crater (Martin et al., 2017)—prolonged contact with subsurface aqueous fluids. Given the substantive evidence for liquid water on Mars during the Noachian and Hesperian Periods, however, it is possible that chemical weathering might have been more pronounced during those times (e.g., Carter et al., 2015; Mangold et al., 2019).

The first (known) and second (known) cycle sediments in Gale crater (e.g., Fig. 14) were subjected to Hesperian environments. The conglomerate boulders at Bimbe and the sandstone of the Clark facies at Marias Pass, for example, are compositionally immature because they contain rock fragments. The sedimentary lithoclasts survived second cycle weathering, transport, deposition, and diagenesis and have, thus far, survived the start of a third sedimentary cycle. The third weathering cycle is still occurring in the modern, cold, hyperarid, Amazonian environment; this is a setting in which mechanical weathering dominates over chemical weathering. The immature nature of the Hesperian second cycle sediments that contain first cycle lithoclasts indicates that physical weathering processes, which do not impose compositional change, also dominated this sedimentary cycle.

Fate of Sediment Exported from Gale Crater

Some of the most recent sediment derived from the weathering and erosion of sedimentary rocks inside Gale crater likely constitutes the dark wind streak that emanates from the south side of the crater (Anderson and Bell, 2010; Day and Kocurek, 2016). The pyroxene-bearing (Anderson and Bell, 2010) streak stretches southward ~400 km across heavily cratered terrain (Fig. 16A). When the southern rim of Gale crater is viewed at ~25 cm/pixel,

Downloaded from http://pubs.geoscienceworld.org/gsa/geosphere/article-pdf/16/6/1508/5182958/1508.pdf
by California Inst of Technology user

the streak is seen to consist of material that is smooth-textured (at that scale) in some areas and rippled in others, and it obscures the impact crater rim morphology at decameter scales (Fig. 16B). These observations suggest that the wind streak is composed of sediment that mantles the underlying erosional remnants of the otherwise rugged crater rim and ejecta deposit.

Based on analogy with the wind streaks associated with craters in western Arabia Terra (Edgett, 2002), the streak emanating from southern Gale crater might consist of silt- to fine sand–sized sediment that came from the erosion of rocks inside the crater. The wind streak covers ~45,000 km^2. If its thickness were to average 1 m, then its volume would be 45 km^3; if it is an average of 10 m thick, it would be 450 km^3. These volumes of sediment are quite small relative to the tens of thousands of cubic kilometers of sediment proposed (Malin and Edgett, 2000; Grotzinger and Milliken, 2012; Day et al., 2016; Bennett and Bell, 2016) to have been removed from Gale crater (cf. Day and Catling, 2020) to create the moat that separates Aeolis Mons from the crater walls (Supplement 1 [footnote 1]). Much of this erosion and removal (at least in northern Gale crater) had to have occurred during the Hesperian, before exposure of the surface recorded by the unconformity at Marias Pass (Fig. 4). The majority of sediment exported from Gale crater is not in the modern wind streak (Fig. 16) but was long ago redeposited elsewhere.

Incorporation of sedimentary lithoclasts derived from lower Aeolis Mons strata (Murray formation mudstones) into the rocks just above the unconformity at Marias Pass (Figs. 4 and 5) also demonstrates that sediments derived from sedimentary rocks that formed earlier inside Gale crater could also be recycled to become part of new sedimentary rocks. Sedimentary rock that previously occupied the moat that lies between the crater walls and Aeolis Mons was exported from Gale crater before the Clark facies of the Stimson formation was deposited. Inside Gale crater, after the Stimson formation eolian sands were in place, conditions on Hesperian Mars were such that the sands were preserved in the sedimentary record. To be retained, they were wetted (Kronyak et al., 2019a), buried, and lithified.

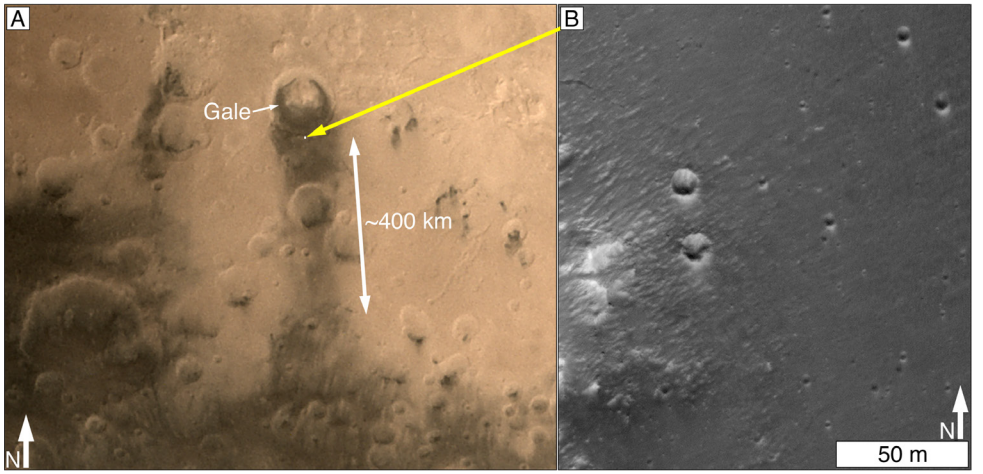

Figure 16. Dark-toned wind streak emanating from the south side of Gale crater. (A) Regional view from *Mangalyaan* shows that the streak extends ~400 km southward from Gale crater. (B) Close-up view of a portion of the southern rim of Gale, showing the dark-toned sediment that composes the wind streak. This material obscures much of the rugged topography normally found on the raised rim of an impact crater.

The fate of recycled sediment eroded from Aeolis Mons strata and incorporated into the Clark facies (Fig. 4) signals the fate of sediment exported from Gale crater during the Hesperian as well. At that time, surface and subsurface (the realm of diagenesis) environments prevailed on Mars in which sediments could be deposited, retained, buried, and lithified. Sediment removed from Gale crater would have been very fine grained and transported out of the basin by wind. Coarser fine sediments (very fine sand and silt) might have been initially stored in a wind streak like we see today (Fig. 16). Finer sediments would have left the vicinity altogether. Ultimately, most of these fine clasts would have been redeposited and, as the Clark facies observations indicate, could have become lithified somewhere else on Hesperian Mars.

APPLICATION

The observations and results presented here can be applied to the study of other regions on Mars. Most of Mars has not been explored using rovers and landers. However, since 1999, more than 99.9% (as of 1 July 2020) of the planet's surface has been imaged from orbit at very high spatial resolution (0.25–6.0 m/pixel). Such images can be used to identify at least a few sites of likely extraformational, recycled sedimentary rock on Mars. The observations from rover and orbiter images of Gale crater show that two important indicators are: proximity to erosional unconformities in sedimentary rock sections; and lithified fluvial, alluvial, or deltaic sediment deposited after transport through valleys that incised preexisting sedimentary rock (e.g., Fig. 13). In this section, we draw attention to an additional case: very large sedimentary rock fragments (megaclasts) occurring in a younger sedimentary rock unit. We also consider the potential for extraformational recycled sediments at the planned field sites for the upcoming *Perseverance* and *Rosalind Franklin* rover missions. Given the possibility that much of the sedimentary rock broken down and removed from Gale crater to form Aeolis Mons might have been recycled into new sedimentary rock, none of these examples captures the full extent of the recycling that might have actually occurred on Mars.

Downloaded from http://pubs.geoscienceworld.org/gsa/geosphere/article-pdf/16/6/1508/5182958/1508.pdf
by California Inst of Technology user

Lithified Deposit Containing Sedimentary Rock Megaclasts

It is evident from our investigations in Gale crater that images acquired by cameras aboard *Curiosity* have sufficient spatial resolution to permit identification of extraformational sedimentary lithoclasts as small as coarse sand (Figs. 3D and 4) in sediments and sedimentary rocks. Pictures acquired from orbiting and aerial platforms (e.g., MSL Mars Descent Imager, MARDI—Malin et al., 2017; NASA helicopter *Ingenuity*, planned for 2021—Balaram et al., 2018) could also be used for such identifications if the sedimentary rock fragment size is large enough relative to the spatial resolution of the images obtained. Figure 17 shows an example in the form of a mesa in a vast sedimentary rock exposure (Mangold et al., 2008; Murchie et al., 2009; Okubo, 2010) in western Candor Chasma of the Valles Marineris. The mesa top displays angular megaclasts of tens to hundreds of meters across. They have a variety of orientations, and, depending on orientation, some exhibit internal stratification. None of the large clasts straddles the cliff tops or has fallen from the mesa to accumulate below, suggesting that the deposit is not a loose accumulation. Instead, these large clasts are apparently cemented in place, forming an erosion-resistant megabreccia rock unit that protects underlying, finer-grained strata from erosion. If this interpretation is correct, then the materials in Figure 17 provide an example of extraformational sedimentary rock recycling visible from orbit.

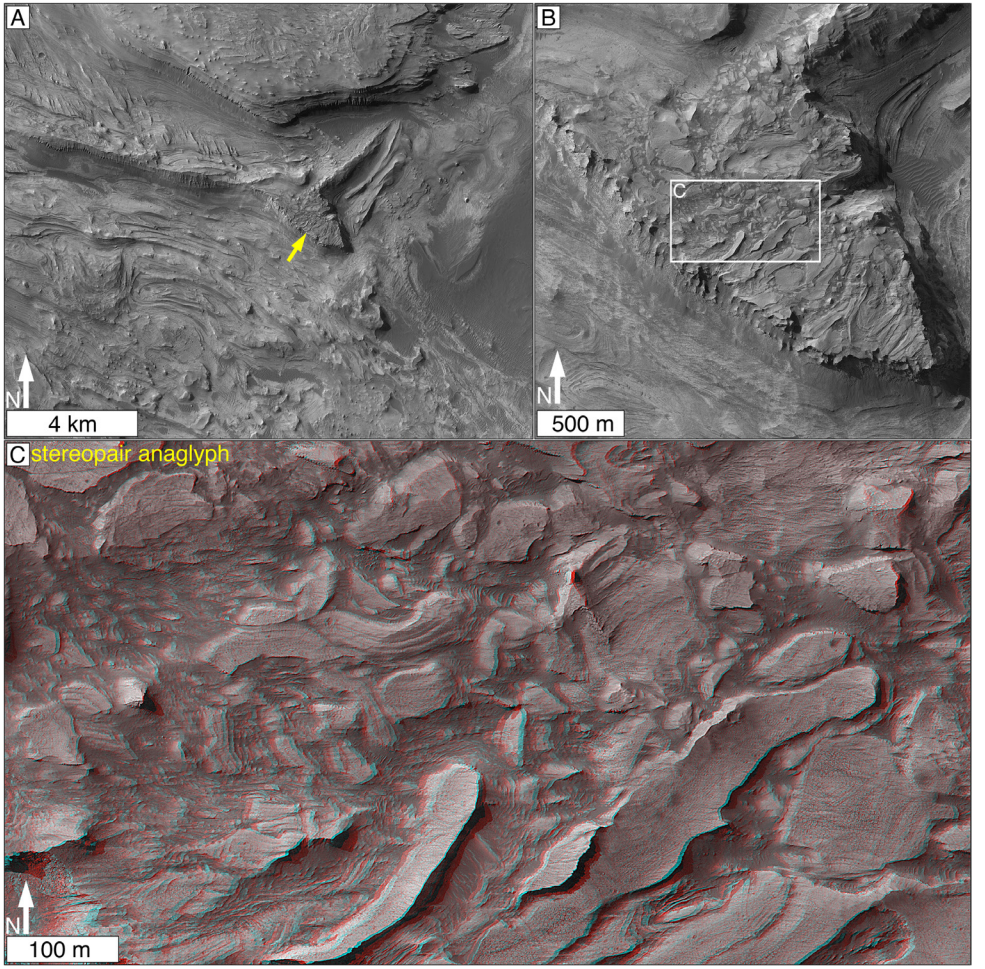

Figure 17. Mesa-capping rock composed of megaclastic sediment in western Candor Chasma, located at 6.58°S, 75.40°W (6.51°S, 284.69°E). (A) Mesa (arrow) in context, surrounded by outcrops of light- and intermediate-toned, stratified bedrock. (B) Megaclastic nature of the capping material, with the location of C indicated. (C) Stereo anaglyph view of the angular, stratified megaclasts (please examine wearing red-left-eye, blue-right-eye three-dimensional glasses).

Field Sites of the *Perseverance* and *Rosalind Franklin* Rovers

The lithified sediment deposited at the terminus of a fluvial valley that cuts through sedimentary strata in Gale crater (Fig. 13) establishes relations that can be directly applied to two of the three Mars rover landing sites planned for the early 2020s, the European Space Agency (ESA)/Roscosmos ExoMars *Rosalind Franklin* rover site at Oxia Planum, and the NASA Mars 2020 *Perseverance* rover site at Jezero crater. The third site, for China's rover landing in 2021, is currently anticipated to be in Utopia Planitia at a location to be selected after *Tianwen-1* orbiter reconnaissance (Wan et al., 2020). As with any future interplanetary mission, it should be understood that critical mission events can lead to an inability to obtain the anticipated science data from these rovers.

Oxia Planum/Coogoon Vallis Deltaic Sediment

The *Rosalind Franklin* mission is focused on the search for evidence of life (Vago et al., 2017). The 2023 landing site on Oxia Planum (Fig. 18; Quantin-Nataf et al., 2019) offers an opportunity

Downloaded from http://pubs.geoscienceworld.org/gsa/geosphere/article-pdf/16/6/1508/5182958/1508.pdf
by California Inst of Technology user

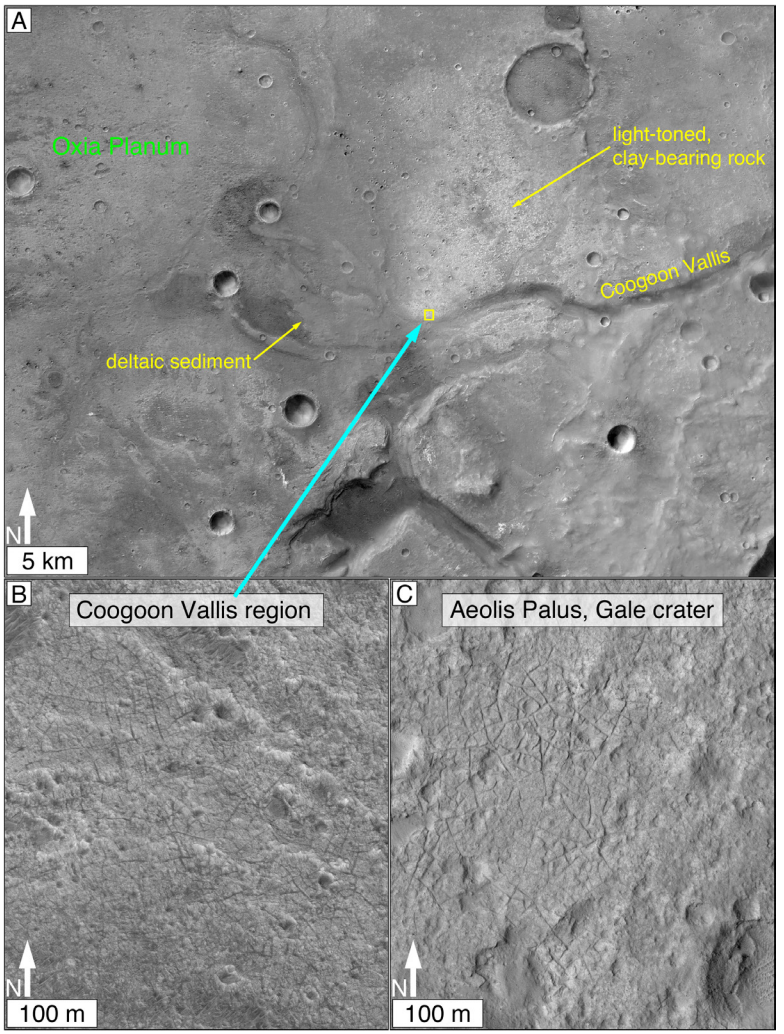

Figure 18. Potential for extraformational, recycled sediment at the planned *Rosalind Franklin* rover field site in Oxia Planum. (A) Regional view of the Coogoon Vallis terminus and lithified deltaic sediment at Oxia Planum, near 18.1°N, 23.9°W (also 17.9°N, 336.2°E). Location of B is indicated by the blue arrow. (B) Light-toned, clay-bearing rock, interpreted as sedimentary (Quantin-Nataf et al., 2019), cut by Coogoon Vallis near the valley terminus. Compare the scale and pattern of fractures in the bedrock with image in C. (C) Example of sedimentary rock exposure in northern Gale crater (near but not visited by the *Curiosity* rover), shown at the same scale as the image in B; note the similar fracture pattern and impact structure retention.

to explore a record that includes deltaic sediment deposited at the terminus of the Coogoon Vallis fluvial system (Molina et al., 2017; Fawdon et al., 2019; Ivanov et al., 2020). These sediments might or might not be accessed by the rover, depending on exactly where it lands, where the science team decides to drive the rover, and how much time is available for exploration of the area.

The Coogoon Vallis deltaic sediments overlie clay-bearing bedrock (Carter et al., 2016) that Quantin-Nataf et al. (2019) and Parkes Bowen et al. (2019) interpreted as sedimentary. More importantly, just before it terminates at the delta, Coogoon Vallis was cut through rock that is also interpreted to be sedimentary (Quantin-Nataf et al., 2019). This rock has a light tone (Figs. 18A, 18B) and a polygonally fractured geomorphic expression (Fig. 18B; Parkes Bowen et al., 2019; Ivanov et al., 2020), and it contains clay minerals (Carter et al., 2016; Molina et al., 2017). The fracture pattern, the scale of the fracture pattern, and the crater retention properties of this rock (Fig. 18B) are similar to that of sedimentary rocks—likely sandstones—exposed in northern Gale crater (Fig. 18C). Additional sedimentary rocks might also occur further up the slope along the course of Coogoon Vallis (Molina et al., 2017). If these interpretations are correct, then the deltaic sediment at Oxia Planum is likely to include extraformational clay-bearing sedimentary lithoclasts and individual grains liberated from older clastic rocks.

Jezero Crater Deltaic Sediment

The *Perseverance* rover and experimental *Ingenuity* helicopter are scheduled to land in western Jezero crater (Fig. 19A) in February 2021. The rover will be used to search for biosignatures, explore lithified deltaic sediment (Fig. 19B; Goudge et al., 2017), study proposed lacustrine carbonates (Horgan et al., 2020), and collect samples for later retrieval and shipment to Earth (Williford et al., 2018). Two fluvially incised valleys, Neretva and Sava, intersect Jezero crater on its north and west sides (Fig. 19A). The eroded remains of lithified deltaic sediments occur at the termini of these valleys (Fassett and

Downloaded from http://pubs.geoscienceworld.org/gsa/geosphere/article-pdf/16/6/1508/5182958/1508.pdf
by California Inst of Technology user

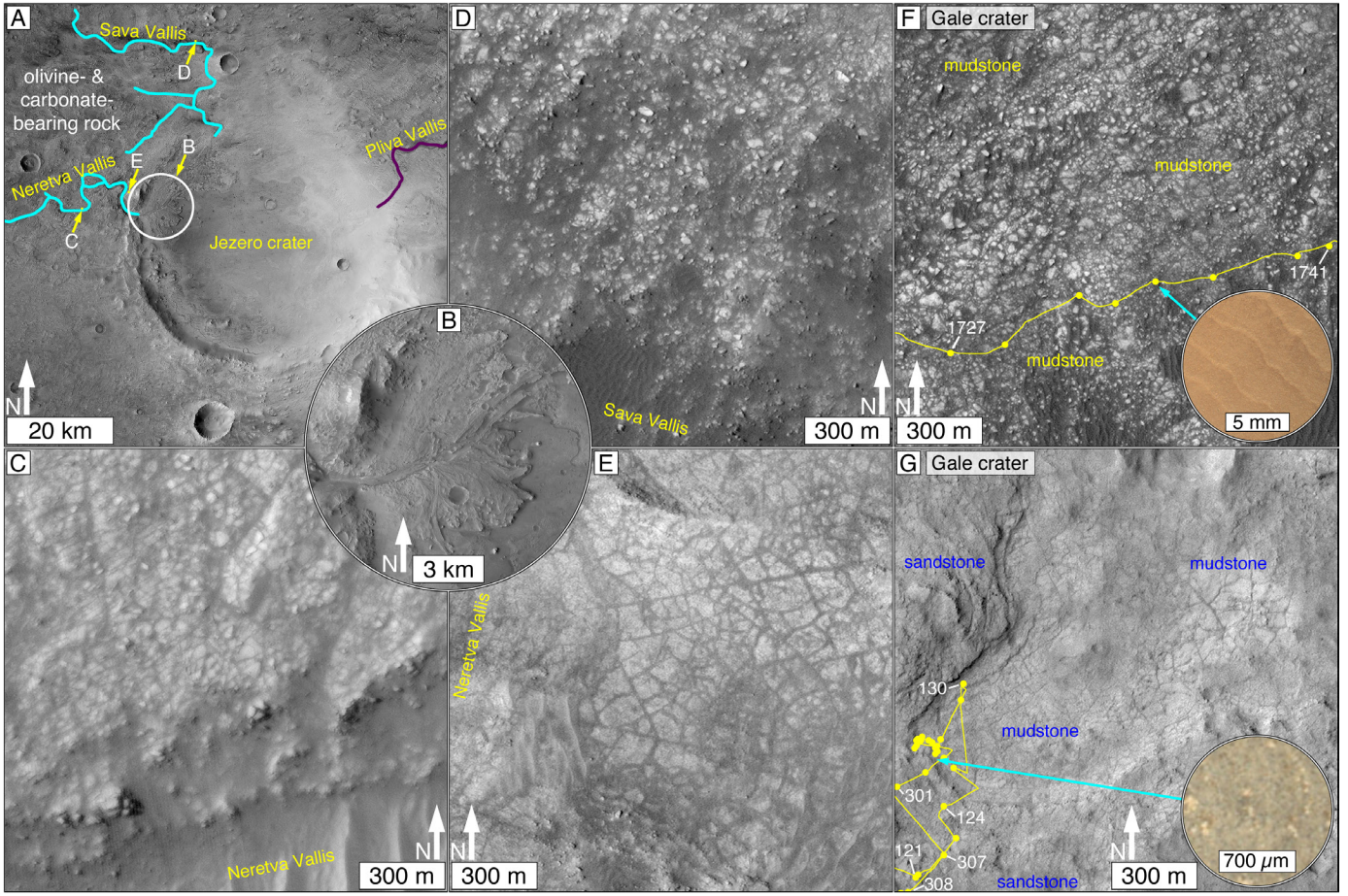

Figure 19. Potential for extraformational, recycled sediment at the planned *Perseverance* rover site in Jezero crater, located at 18.6°N, 282.4°W (18.4°N, 77.7°E). C–G are presented at the same scale. (A) Jezero crater and local context. The locations of B–E are indicated. Blue traces indicate inlet valleys (Neretva and Sava); purple trace indicates an outlet valley (Pliva). West of Jezero crater, olivine- and carbonate-bearing rock is cut by Neretva Vallis and Sava Vallis (Goudge et al., 2015). (B) Lithified, deltaic sediment of the "western delta" in Jezero crater. (C) Detailed view of the geomorphic expression of rock cut by Neretva Vallis. (D) Detailed view of the geomorphic expression of rock cut by Sava Vallis. (E) Detailed view of the geomorphic expression of rock cut by Neretva Vallis. (F) Compare with D; detailed view of an outcrop of the fine-grained (largely mudstone) Murray formation in Gale crater; dark-toned materials are windblown sands, and lighter-toned features are blocks of mudstone slightly displaced in outcrop expression. Yellow trace indicates the *Curiosity* rover traverse; yellow dots indicate locations where the rover parked after each drive; white numbers indicate the sols that bracketed this portion of the traverse. Color inset from Mars Hand Lens Imager (MAHLI) shows a dust-coated mudstone surface investigated along this traverse (arrow); the bands are a stair-stepped expression of fine laminae. (G) Compare with E; detailed view of a dust-coated outcrop of the Sheepbed (mudstone) member of the Yellowknife Bay formation in Gale crater (see Schieber et al., 2017). Yellow trace and dots indicate rover traverse through the area between sols 121 and 309. Color inset from MAHLI shows the very fine–grained nature of the mudstone; the larger, lighter-toned objects are dust clumps stirred by the rover's wire brush tool; the finer, speckled surface illustrates silt-sized grains.

Downloaded from http://pubs.geoscienceworld.org/gsa/geosphere/article-pdf/16/6/1508/5182958/1508.pdf
by California Inst of Technology user

Head, 2005; Goudge et al., 2017). The bedrock cut by the valleys outside of Jezero crater is olivine- and carbonate-bearing bedrock (Goudge et al., 2015; Salvatore et al., 2018). Figure 19 shows that the erosional expressions of—and fracture patterns in—this bedrock are similar in scale and pattern to those of mudstone outcrops explored using *Curiosity* in Gale crater. These observations suggest that the olivine- and carbonate-bearing rock could have physical properties similar to those of some of the mudstones in Gale crater (e.g., finely laminated, fine grained, perhaps crosscut by veins). Based on paleotopographic draping stratigraphic relations, these rocks have been interpreted as consisting of weathered, olivine-bearing tephra (Kremer et al., 2019; Mandon et al., 2020). The draping stratigraphy could also be consistent with interpretations that the material is loessite, duststone (sensu Bridges and Muhs, 2012), or even subaqueous mud.

The delta to be explored by the *Perseverance* rover team will contain debris eroded from the olivine- and carbonate-bearing bedrock that occurs to the west of the crater (Goudge et al., 2015). If some of those rocks are sedimentary (or if any of the rocks cut by Neretva Vallis are sedimentary), then the delta will contain recycled, extraformational sediment. The deltaic sediments could include sand-, granule-, and pebble-sized rock fragments as well as individual grains liberated from the older rock. Whether sedimentary rock or primary tephra (tuff) fragments, or both, their presence will extend the geographic and stratigraphic range accessible to the rover and its associated astrobiological investigations.

CONCLUSIONS

Gale crater is considered to have formed near the start of the Hesperian Period, sometime between 500 and 900 m.y. after Mars obtained a solid crust. By that time, the planet would have already developed a substantial sedimentary record. After the Gale crater–forming impact occurred, the new crater was, naturally, a site of net sediment deposition. The impact structure might have been completely filled, as the preserved sedimentary record includes solid rock at the 5-km-high summit of the stratified mountain, Aeolis Mons, inside Gale crater. Sometime during the Hesperian, conditions changed, and Gale crater became a net source of sediment as some of the material that had filled the crater was weathered and eroded away, creating the moat that surrounds Aeolis Mons. Even after much of the volume of rock that once occurred between Aeolis Mons and the crater walls had left the crater, however, new deposition and lithification occurred inside Gale crater (creating, for example, Siccar Point group rocks such as the Stimson formation).

Curiosity rover images of sedimentary lithoclasts in younger sedimentary rocks inside Gale crater demonstrate that sedimentation on Mars is not always a single cycle journey from igneous protolith or impact melt to sedimentary rock. The observations of sedimentary lithoclasts in younger sedimentary rock inside Gale crater are definitive evidence that extraformational sediment recycling has occurred on Mars. Also, in Gale crater, lithified sediment fans deposited at the termini of canyons that cut across the sedimentary rock strata of Aeolis Mons must consist of recycled, extraformational sediment. Most of the observed recycled sediments are clastic; this means that individual grains liberated from clastic rocks would also have been recycled. Stratified, white, extraformational lithoclasts in a boulder at Bimbe (e.g., Funda) might be fragments derived from an intraclast-bearing chemical sediment, something not yet observed in intact stratigraphy using Mars rover instrumentation.

The possible sources for recycled extraformational sediment observed in rocks in Gale crater are: (1) previous sedimentary rocks formed inside Gale crater; (2) sedimentary rocks exposed in the wall, deposited as ejecta on the rim, or exposed in the central uplift of the Gale impact structure; and (3) sedimentary rocks that occur or occurred (and were later eroded away) outside of Gale crater. The mudstone fragments in sandstone at Marias Pass, the sandstone fragments in the conglomerate at Dingo Gap, and the sediments that compose the lithified fans at the termini of canyons that cut Aeolis Mons were sourced from previous sedimentary rocks that formed inside Gale crater. The recycled, extraformational sediments that occur in conglomeratic boulders at Bimbe, and in sandstone at Cooperstown, could also have come from strata previously deposited inside Gale crater, or they could have come from sediments exposed in Gale's crater walls or central uplift, or they could have come from outside the crater.

The sedimentary rocks that contain recycled, extraformational sediment observed using *Curiosity*'s cameras are compositionally immature. This observation indicates that the generation of second cycle sediments in Gale crater during the Hesperian was dominated by physical weathering processes, which do not involve changes to the composition of detrital components. The mudstone fragments incorporated into a sandstone immediately above a major erosional unconformity on the lower slopes of Aeolis Mons at Marias Pass offer a vital clue as to the fate of any sediment that might have been removed from Gale crater to form Aeolis Mons and the moat that surrounds Aeolis Mons. If Gale crater was filled (or nearly filled) with sediment, and Aeolis Mons formed by exportation of some of that sediment, then the processes of disaggregation and removal of most of the sediment that left Gale crater occurred before the erosional surface at the unconformity at Marias Pass was created. Because sediments above that unconformity became lithified, it is reasonable to assume that the sediments exported from Gale crater before that time could also have been subjected to deposition, burial, and lithification in some other sedimentary sink on Hesperian Mars.

The observations presented here—particularly that (1) extraformational sediment recycling has occurred on Mars and (2) fluvial sedimentary deposits derived from channels that cut through sedimentary rock can contain extraformational recycled sediment—can be used as tools to make predictions about sediments observed elsewhere on Mars. For example, recycled, extraformational sediment might occur within the lithified deltas at the planned *Perseverance* rover field site in Jezero crater and at the terminus of Coogoon Vallis in Oxia Planum, the planned field site for the *Rosalind Franklin* rover.

ACKNOWLEDGMENTS

We thank Gwénaël Caravaca (Mars Science Laboratory [MSL] Science Team), Colin Dundas (U.S. Geological Survey internal reviewer), two peer reviewers (Tim Goudge and anonymous),

Downloaded from http://pubs.geoscienceworld.org/gsa/geosphere/article-pdf/16/6/1508/5182958/1508.pdf
by California Inst of Technology user

the Associate Editor (Lesli Wood), and the Editor (Shanaka de Silva) for comments and suggestions that helped us to improve our manuscript. We thank The Planetary Society for sharing with the public two years' worth of images from India's Mars Color Camera. This research was supported by NASA through the MSL Project managed by the Jet Propulsion Laboratory of the California Institute of Technology. Fairén was supported by the Project "MarsFirstWater," European Research Council Consolidator Grant 818602. MSL is a monumental undertaking that involved thousands of individuals spanning nearly two decades and dozens of nations from mission conception to the present. Everyone connected to this project is heartily thanked for their contributions. In addition, Mars-orbiting spacecraft and their science and engineering operations teams, along with NASA's Deep Space Network, were vital for relaying data from *Curiosity* to Earth and in supporting surface operations through data acquisitions of landforms and minerals in Gale crater and its regional context; we thank them for their strong and sustained efforts. During the August 2012–January 2020 study period, the following orbiters and their operations personnel performed data relays from *Curiosity*: *Mars Reconnaissance Orbiter*, *Mars Odyssey*, *Mars Express*, Mars Atmosphere and Volatile Evolution (*MAVEN*), and the ExoMars *Trace Gas Orbiter*.

REFERENCES CITED

Abramov, O., and Mojzsis, S.J., 2016, Thermal effects of impact bombardments on Noachian Mars: Earth and Planetary Science Letters, v. 442, p. 108–120, https://doi.org/10.1016/j.epsl.2016.02.035.

Akhtar, K., and Ahmad, A.H.M., 1991, Single-cycle cratonic quartzarenites produced by tropical weathering: The Nimar sandstone (Lower Cretaceous), Narmada basin, India: Sedimentary Geology, v. 71, p. 23–32, https://doi.org/10.1016/0037-0738(91)90004-W.

Anderson, R.B., and Bell, J.F., III, 2010, Geologic mapping and characterization of Gale crater and implications for its potential as a Mars Science Laboratory landing site: Mars: The International Journal of Mars Science and Exploration, v. 5, p. 76–128, https://doi.org/10.1555/mars.2010.0004.

Anderson, R.B., Edgar, L.A., Rubin, D.M., Lewis, K.W., and Newman, C., 2018, Complex bedding geometry in the upper portion of Aeolis Mons, Gale crater, Mars: Icarus, v. 314, p. 246–264, https://doi.org/10.1016/j.icarus.2018.06.009.

Ansan, V., Loizeau, D., Mangold, N., Le Mouélic, S., Carter, J., Poulet, F., Dromart, G., Lucas, A., Bibring, J.-P., Gendrin, A., Gondet, B., Langevin, Y., Masson, Ph., Murchie, S., Mustard, J.F., and Neukum, G., 2011, Stratigraphy, mineralogy, and origin of layered deposits inside Terby crater, Mars: Icarus, v. 211, p. 273–304, https://doi.org/10.1016/j.icarus.2010.09.011.

Arya, A.S., Sarkar, S.S., Srinivas, A.R., Moorthi, S.M., Patel, V.D., Singh, R.B., Rajasekhar, R.P., Roy, S., Misra, I., Sukamal Kr., P., Shah, D., Patel, K., Gambhir, R.K., Rao, U.S.H., Patel, A., Desai, J., Dev, R., Prashar, A.K., Rambhia, H., Parnami, R., Seth, H., Murali, K.R., Kaushik, R., Patidar, D., Soni, N., Chauhan, P., Samudraiah, D.R.M., and Kiran, A.S., 2015, Mars Colour Camera: The payload characterization/calibration and data analysis from Earth imaging phase: Current Science, v. 109, p. 1076–1086.

Babechuk, M.G., Widdowson, M., and Kamber, B.S., 2014, Quantifying chemical weathering intensity and trace element release from two contrasting basalt profiles, Deccan Traps, India: Chemical Geology, v. 363, p. 56–75, https://doi.org/10.1016/j.chemgeo.2013.10.027.

Balaram, B., Canham, T., Duncan, C., Grip, H.F., Johnson, W., Maki, J., Quon, A., Stern, R., and Zhu, D., 2018, Mars helicopter technology demonstrator, *in* American Institute of Aeronautics and Astronautics (AIAA) Atmospheric Flight Mechanics Conference: Reston, Virginia, American Institute of Aeronautics and Astronautics, paper AIAA 2018–0023, https://doi.org/10.2514/6.2018-0023.

Banham, S.G., Gupta, S., Rubin, D.M., Watkins, J.A., Sumner, D.Y., Edgett, K.S., Grotzinger, J.P., Lewis, K.W., Edgar, L.A., Stack-Morgan, K.M., Barnes, R., Bell, J.F., III, Day, M.D., Ewing, R.C., Lapôtre, M.G.A., Stein, N.T., Rivera-Hernández, F., and Vasavada, A.R., 2018a, Ancient Martian aeolian processes and palaeomorphology reconstructed from the Stimson formation on the lower slope of Aeolis Mons, Gale crater, Mars: Sedimentology, v. 65, p. 993–1042, https://doi.org/10.1111/sed.12469.

Banham, S.G., Gupta, S., Rubin, D.M., Edgett, K.S., Van Beek, J., Watkins, J.A., Edgar, L.A., Fedo, C., and Vasavada, A., 2018b, A journey to the centre of an ancient extraterrestrial aeolian erg, *in* 57th British Sedimentary Research Group Annual General Meeting Abstract Book, p. 17–18, http://lyellcentre.ac.uk/docs/57thBSRGAbstract.pdf (accessed July 2020).

Banham, S.G., Gupta, S., Bryk, A.B., Rubin, D.M., Edgett, K.S., Dietrich, W.E., Fedo, C.M., Edgar, L.A., and Vasavada, A.R., 2020, Does the Greenheugh pediment capping unit represent a continuation of the Stimson formation?: Houston, Texas, Lunar and Planetary Institute Contribution 2326, Lunar and Planetary Science Conference 51, abstract 2337, https://www.hou.usra.edu/meetings/lpsc2020/pdf/2337.pdf (accessed July 2020).

Bedford, C.C., Schwenzer, S.P., Bridges, J.C., Banham, S., Wiens, R.C., Gasnault, O., Rampe, E.B., Frydenvang, J., and Gasda, P.J., 2020, Geochemical variation in the Stimson formation of Gale crater: Provenance, mineral sorting, and a comparison with modern Martian dunes: Icarus, v. 341, 113622, https://doi.org/10.1016/j.icarus.2020.113622.

Bennett, K.A., and Bell, J.F., III, 2016, A global survey of Martian central mounds: Central mounds as remnants of previously more extensive large-scale sedimentary deposits: Icarus, v. 264, p. 331–341, https://doi.org/10.1016/j.icarus.2015.09.041.

Blatt, H., 1967, Provenance determinations and recycling of sediments: Journal of Sedimentary Research, v. 37, p. 1031–1044, https://doi.org/10.1306/74D71825-2B21-11D7-8648000102C1865D.

Bouvier, L.C., Costa, M.M., Connelly, J.N., Jensen, N.K., Wielandt, D., Storey, M., Nemchin, A.A., Whitehouse, M.J., Snape, J.F., Bellucci, J.J., Moynier, F., Agranier, A., Gueguen, B., Schönbächler, M., and Bizzarro, M., 2018, Evidence for extremely rapid magma ocean crystallization and crust formation on Mars: Nature, v. 558, p. 586–589, https://doi.org/10.1038/s41586-018-0222-z.

Bridges, N.T., and Muhs, D.R., 2012, Duststones on Mars: Source, transport, deposition, and erosion, *in* Grotzinger, J.P., and Milliken, R.E., eds., Sedimentary Geology of Mars: Society for Sedimentary Geology (SEPM) Special Publication 102, p. 169–182, https://doi.org/10.2110/pec.12.102.0169.

Bryk, A.B., Dietrich, W.E., Lamb, M.P., Grotzinger, J.P., Vasavada, A.R., Stack, K.M., Arvidson, R., Fedo, C.M., Fox, V.K., Gupta, S., Wiens, R.C., Williams, R.M.E., Kronyak, R.E., Lewis, K.W., Rubin, D.M., Rapin, W.N., Le Deit, L., Le Mouélic, S., Edgett, K.S., Fraeman, A.A., Banham, S.G., Hughes, M.N., and Kah, L.C., 2019, What was the original extent of the Greenheugh pediment and Gediz Vallis ridge deposits in Gale crater, Mars?: Houston, Texas, Lunar and Planetary Institute Contribution 2089, 9th International Conference on Mars, abstract 6296, https://www.hou.usra.edu/meetings/ninthmars2019/pdf/6296.pdf (accessed July 2020).

Buz, J., Ehlmann, B.L., Pan, L., and Grotzinger, J.P., 2017, Mineralogy and stratigraphy of the Gale crater rim, wall, and floor units: Journal of Geophysical Research–Planets, v. 122, p. 1090–1118, https://doi.org/10.1002/2016JE005163.

Cabrol, N.A., Grin, E.A., Newsom, H.E., Landheim, R., and McKay, C.P., 1999, Geologic evolution of Gale crater and its relevance to the exobiological exploration of Mars: Icarus, v. 139, p. 235–245, https://doi.org/10.1006/icar.1999.6099.

Carr, M.H., Baum, W.A., Briggs, G.A., Masursky, H., Wise, D.W., and Montgomery, D.R., 1972, Imaging experiment: The *Viking* Mars orbiter: Icarus, v. 16, p. 17–33, https://doi.org/10.1016/0019-1035(72)90134-0.

Carter, J., Loizeau, D., Mangold, N., Poulet, F., and Bibring, J.-P., 2015, Widespread surface weathering on early Mars: A case for a warmer and wetter climate: Icarus, v. 248, p. 373–382, https://doi.org/10.1016/j.icarus.2014.11.011.

Carter, J., Quantin, C., Thollot, P., Loizeau, D., Ody, A., and Lozach, L., 2016, Oxia Planum, a clay-laden landing site proposed for the ExoMars rover mission: Aqueous mineralogy and alteration scenarios: Houston, Texas, Lunar and Planetary Institute Contribution 1964, Lunar and Planetary Science Conference 47, abstract 2064, https://www.hou.usra.edu/meetings/lpsc2016/pdf/2064.pdf (accessed July 2020).

Caswell, T.E., and Milliken, R.E., 2017, Evidence for hydraulic fracturing at Gale crater, Mars: Implications for burial depth of the Yellowknife Bay formation: Earth and Planetary Science Letters, v. 468, p. 72–84, https://doi.org/10.1016/j.epsl.2017.03.033.

Chojnacki, M., Burr, D.M., Moersch, J.E., and Wray, J.J., 2014, Valles Marineris, dune sediment provenance and pathways: Icarus, v. 232, p. 187–219, https://doi.org/10.1016/j.icarus.2014.01.011.

Christensen, P.R., Jakosky, B.M., Kieffer, H.H., Malin, M.C., McSween, H.Y., Jr., Nealson, K., Mehall, G.L., Silverman, S.H., Ferry, S., Caplinger, M., and Ravine, M., 2004a, The Thermal Emission Imaging System (THEMIS) for the Mars 2001 *Odyssey* Mission: Space Science Reviews, v. 110, p. 85–130, https://doi.org/10.1023/B:SPAC.0000021008.16305.94.

Christensen, P.R., Wyatt, M.B., Glotch, T.D., Rogers, A.D., Anwar, S., Arvidson, R.E., Bandfield, J.L., Blaney, D.L., Budney, C., Calvin, W.M., Fallacaro, A., Fergason, R.L., Gorelick, N., Graff, T.G., Hamilton, V.E., Hayes, A.G., Johnson, J.R., Knudson, A.T., McSween, H.Y., Jr., Mehall, G.L., Mehall, L.K., Moersch, J.E., Morris, R.V., Smith, M.D., Squyres, S.W., Ruff, S.W., and Wolff, M.J., 2004b, Mineralogy at Meridiani Planum from the Mini-TES experiment on the *Opportunity* rover: Science, v. 306, p. 1733–1739, https://doi.org/10.1126/science.1104909.

Churchill, J., 2018, North Gale Landform and the Volcanic Sources of Sediment in Gale Crater, Mars [M.S. thesis]: St. Catharines, Ontario, Canada, Brock University, 165 p., https://dr.library.brocku.ca/handle/10464/14110 (accessed July 2020).

Downloaded from http://pubs.geoscienceworld.org/gsa/geosphere/article-pdf/16/6/1508/5182958/1508.pdf
by California Inst of Technology user

Condie, K.C., 2019, Earth's oldest rocks and minerals, *in* Van Kranendonk, M.J., Bennett, V., and Hoffmann, J.E., eds., Earth's Oldest Rocks (2nd ed.): Amsterdam, Netherlands, Elsevier, p. 239–253, https://doi.org/10.1016/B978-0-444-63901-1.00011-3.

Cornwall, C., Bandfield, J.L., Titus, T.N., Schreiber, B.C., and Montgomery, D.R., 2015, Physical abrasion of mafic minerals and basalt grains: Application to Martian aeolian deposits: Icarus, v. 256, p. 13–21, https://doi.org/10.1016/j.icarus.2015.04.020.

Cousin, A., Sautter, V., Payré, V., Forni, O., Mangold, N., Gasnault, O., Le Deit, L., Johnson, J., Maurice, S., Salvatore, M., Wiens, R.C., Gasda, P., and Rapin, W., 2017, Classification of igneous rocks analyzed by ChemCam at Gale crater, Mars: Icarus, v. 288, p. 265–283, https://doi.org/10.1016/j.icarus.2017.01.014.

Cox, R., and Lowe, D.R., 1995a, Compositional evolution of coarse clastic sediments in the southwestern United States from 1.8 to 0.2 Ga and implications for relationships between development of crustal blocks and their sediment cover: Journal of Sedimentary Research, v. 65, p. 477–494, https://doi.org/10.2110/jsr.65.477.

Cox, R., and Lowe, D.R., 1995b, A conceptual review of regional-scale controls on the composition of clastic sediment and the co-evolution of continental blocks and their sediment cover: Journal of Sedimentary Research, v. 65, p. 1–12, https://doi.org/10.1306/D4268009-2B26-11D7-8648000102C1865D.

Czarnecki, S., Hardgrove, C., Gasda, P.J., Gabriel, T.S.J., Starr, M., Rice, M., Frydenvang, J., Wiens, R.C., Rapin, W., Nikiforov, S., Lisov, D., Litvak, M., Calef, F., Gengl, H., Newsom, H., Thompson, L., and Nowicki, S., 2020, Identification and description of a silicic volcaniclastic layer in Gale crater, Mars, using an active neutron interrogation: Journal of Geophysical Research–Planets, v. 125, e2019JE006180, https://doi.org/10.1029/2019JE006180.

Davis, J.M., Gupta, S., Balme, M., Grindrod, P.M., Fawdon, P., Dickeson, Z.I., and Williams, R.M.E., 2019, A diverse array of fluvial depositional systems in Arabia Terra: Evidence for mid-Noachian to early Hesperian rivers on Mars: Journal of Geophysical Research–Planets, v. 124, p. 1913–1934, https://doi.org/10.1029/2019JE005976.

Day, M., and Kocurek, G., 2016, Observations of an aeolian landscape: From surface to orbit in Gale crater: Icarus, v. 280, p. 37–71, https://doi.org/10.1016/j.icarus.2015.09.042.

Day, M., Anderson, W., Kocurek, G., and Mohrig, D., 2016, Carving intracrater layered deposits with wind on Mars: Geophysical Research Letters, v. 43, p. 2473–2479, https://doi.org/10.1002/2016GL068011.

Day, M.D., and Catling, D.C., 2020, Potential aeolian deposition of intra-crater layering: A case study of Henry crater, Mars: Geological Society of America Bulletin, v. 132, p. 608–616, https://doi.org/10.1130/B35230.1.

De Hon, R.A., 1987, Ring furrows: Inversion of topography in Martian highland terrains: Icarus, v. 71, p. 287–297, https://doi.org/10.1016/0019-1035(87)90153-9.

Di Achille, G., and Hynek, B.M., 2010, Ancient ocean on Mars supported by global distribution of deltas and valleys: Nature Geoscience, v. 3, p. 459–463, https://doi.org/10.1038/ngeo891.

DiBiase, R.A., Limaye, A.B., Scheingross, J.S., Fischer, W.W., and Lamb, M.P., 2013, Deltaic deposits at Aeolis Dorsa: Sedimentary evidence for a standing body of water on the northern plains of Mars: Journal of Geophysical Research–Planets, v. 118, p. 1285–1302, https://doi.org/10.1002/jgre.20100.

Dickinson, W.R., and Gehrels, G.E., 2010, Insights into North American paleogeography and paleotectonics from U-Pb ages of detrital zircons in Mesozoic strata of the Colorado Plateau, USA: International Journal of Earth Sciences, v. 99, p. 1247–1265, https://doi.org/10.1007/s00531-009-0462-0.

Dott, R.H., Jr., 1964, Wacke, graywacke and matrix—What approach to immature sandstone classification?: Journal of Sedimentary Petrology, v. 34, p. 625–632, https://doi.org/10.1306/74D71109-2B21-11D7-8648000102C1865D.

Dott, R.H., Jr., 2003, The importance of eolian abrasion in supermature quartz sandstones and the paradox of weathering on vegetation-free landscapes: The Journal of Geology, v. 111, p. 387–405, https://doi.org/10.1086/375286.

Dromart, G., Le Deit, L., Rapin, W., Anderson, R.B., Gasnault, O., Le Mouélic, S., Mangold, N., Maurice, S., and Wiens, R.C., 2018, The light-toned yardang unit, Mount Sharp, Gale crater, Mars, spotted by the long distance Remote Micro-Imager on ChemCam (MSL mission): Houston, Texas, Lunar and Planetary Institute Contribution 2083, Lunar and Planetary Science Conference 49, abstract 1222, https://www.hou.usra.edu/meetings/lpsc2018/pdf/1222.pdf (accessed July 2020).

Dunne, T., Mertes, L.A.K., Meade, R.H., Richey, J.E., and Forsberg, B.R., 1998, Exchanges of sediment between the flood plain and channel of the Amazon River in Brazil: Geological Society of America Bulletin, v. 110, p. 450–467, https://doi.org/10.1130/0016-7606(1998)110<0450:EOSBTF>2.3.CO;2.

East, A.E., Clift, P.D., Carter, A., Alizai, A., and VanLaningham, S., 2015, Fluvial-eolian interactions in sediment routing and sedimentary signal buffering: An example from the Indus Basin and Thar Desert: Journal of Sedimentary Research, v. 85, p. 715–728, https://doi.org/10.2110/jsr.2015.42.

Edgar, L.A., Gupta, S., Rubin, D.M., Schieber, J., Stack, K., and Lewis, K.W., 2016, Environmental transitions recorded by fluvial fan stratigraphy at Dingo Gap and Moonlight Valley, Gale crater, Mars: San Francisco, California, American Geophysical Union, 2016 fall meeting supplement, abstract P21D–02, https://ui.adsabs.harvard.edu/abs/2016AGUFM.P21D..02E/abstract (accessed July 2020).

Edgar, L.A., Gupta, S., Rubin, D.M., Lewis, K.W., Kocurek, G.A., Anderson, R.B., Bell, J.F., III, Dromart, G., Edgett, K.S., Grotzinger, J.P., Hardgrove, C., Kah, L.C., Leveille, R., Malin, M.C., Mangold, N., Milliken, R.E., Minitti, M., Palucis, M., Rice, M., Rowland, S.K., Schieber, J., Stack, K.M., Sumner, D.Y., Wiens, R.C., Williams, R.M.E., and Williams, A.J., 2018, Shaler: In situ analysis of a fluvial sedimentary deposit on Mars: Sedimentology, v. 65, p. 96–122, https://doi.org/10.1111/sed.12370.

Edgar, L.A., Fedo, C.M., Gupta, S., Banham, S.G., Fraeman, A.A., Grotzinger, J.P., Stack, K.M., Stein, N.T., Bennett, K.A., Rivera-Hernández, F., Sun, V.Z., Edgett, K.S., Rubin, D.M., House, C., and Van Beek, J., 2020, A lacustrine paleoenvironment recorded at Vera Rubin ridge, Gale crater: Overview of the sedimentology and stratigraphy observed by the Mars Science Laboratory *Curiosity* rover: Journal of Geophysical Research–Planets, v. 125, e2019JE006307, https://doi.org/10.1029/2019JE006307.

Edgett, K.S., 2002, Low albedo surfaces and eolian sediment: Mars Orbiter Camera views of western Arabia Terra craters and wind streaks: Journal of Geophysical Research–Planets, v. 107, 5038, https://doi.org/10.1029/2001JE001587.

Edgett, K.S., 2016, The other sedimentary rocks of early Mars: Houston, Texas, Lunar and Planetary Institute Contribution 1903, Lunar and Planetary Science Conference 47, abstract 1379, https://www.hou.usra.edu/meetings/lpsc2016/pdf/1379.pdf (accessed July 2020).

Edgett, K.S., Yingst, R.A., Ravine, M.A., Caplinger, M.A., Maki, J.N., Ghaemi, F.T., Schaffner, J.A., Bell, J.F., III, Edwards, L.J., Herkenhoff, K.E., Heydari, E., Kah, L.C., Lemmon, M.T., Minitti, M.E., Olson, T.S., Parker, T.J., Rowland, S.K., Schieber, J., Sullivan, R.J., Sumner, D.Y., Thomas, P.C., Jensen, E.H., Simmonds, J.J., Sengstacken, A.J., Willson, R.G., and Goetz, W., 2012, *Curiosity*'s Mars Hand Lens Imager (MAHLI) investigation: Space Science Reviews, v. 170, p. 259–317, https://doi.org/10.1007/s11214-012-9910-4.

Eggleton, R.A., Foudoulis, C., and Varkevisser, D., 1987, Weathering of basalt: Changes in rock chemistry and mineralogy: Clays and Clay Minerals, v. 35, p. 161–169, https://doi.org/10.1346/CCMN.1987.0350301.

Ehlmann, B.L., and Buz, J., 2015, Mineralogy and fluvial history of the watersheds of Gale, Knobel, and Sharp craters: A regional context for the Mars Science Laboratory *Curiosity*'s exploration: Geophysical Research Letters, v. 42, p. 264–273, https://doi.org/10.1002/2014GL062553.

Fairén, A.G., Stokes, C.R., Davies, N.S., Schulze-Makuch, D., Rodríguez, J.A.P., Davila, A.F., Uceda, E.R., Dohm, J.M., Baker, V.R., Clifford, S.M., McKay, C.P., and Squyres, S.W., 2014, A cold hydrological system in Gale crater, Mars: Planetary and Space Science, v. 93–94, p. 101–118, https://doi.org/10.1016/j.pss.2014.03.002.

Fassett, C.I., and Head, J.W., III, 2005, Fluvial sedimentary deposits on Mars: Ancient deltas in a crater lake in the Nili Fossae region: Geophysical Research Letters, v. 32, L14201, https://doi.org/10.1029/2005GL023456.

Fawdon, P., Balme, M.R., Bridges, J., Davis, J.M., Gupta, S., and Quantin-Nataf, C., 2019, The ancient fluvial catchment of Oxia Planum: The ExoMars 2020 rover landing site: Houston, Texas, Lunar and Planetary Institute Contribution 2132, Lunar and Planetary Science Conference 50, abstract 2356, https://www.hou.usra.edu/meetings/lpsc2019/pdf/2356.pdf (accessed July 2020).

Fedo, C.M., McGlynn, I.O., and McSween, H.Y., Jr., 2015, Grain size and hydrodynamic sorting controls on the composition of basaltic sediments: Implications for interpreting Martian soils: Earth and Planetary Science Letters, v. 423, p. 67–77, https://doi.org/10.1016/j.epsl.2015.03.052.

Flahaut, J., Mustard, J.F., Quantin, C., Clenet, H., Allemand, P., and Thomas, P., 2011, Dikes of distinct composition intruded into Noachian-aged crust exposed in the walls of Valles Marineris: Geophysical Research Letters, v. 38, L15202, https://doi.org/10.1029/2011GL048109.

Folk, R.L., 1959, Practical petrographic classification of limestones: American Association of Petroleum Geologists Bulletin, v. 43, p. 1–38, https://doi.org/10.1306/0BDA5C36-16BD-11D7-8645000102C1865D.

Fonstad, M.A., and Zettler-Mann, A., 2020, The camera and the geomorphologist: Geomorphology, v. 366, 107181, https://doi.org/10.1016/j.geomorph.2020.107181.

Fraeman, A.A., Ehlmann, B.L., Arvidson, R.E., Edwards, C.S., Grotzinger, J.P., Milliken, R.E., Quinn, D.P., and Rice, M.S.,

Downloaded from http://pubs.geoscienceworld.org/gsa/geosphere/article-pdf/16/6/1508/5182958/1508.pdf
by California Inst of Technology user

2016, The stratigraphy and evolution of lower Mount Sharp from spectral, morphological, and thermophysical orbital data sets: Journal of Geophysical Research–Planets, v. 121, p. 1713–1736, https://doi.org/10.1002/2016JE005095.

Frydenvang, J., Gasda, P.J., Hurowitz, J.A., Grotzinger, J.P., Wiens, R.C., Newsom, H.E., Edgett, K.S., Watkins, J., Bridges, J.C., Maurice, S., Fisk, M.R., Johnson, J.R., Rapin, W., Stein, N.T., Clegg, S.M., Schwenzer, S.P., Bedford, C.C., Edwards, P., Mangold, N., Cousin, A., Anderson, R.B., Payré, V., Vaniman, D., Blake, D.F., Lanza, N.L., Gupta, S., Van Beek, J., Sautter, V., Meslin, P.-Y., Rice, M., Milliken, R., Gellert, R., Thompson, L., Clark, B.C., Sumner, D.Y., Fraeman, A.A., Kinch, K.M., Madsen, M.B., Mitrofanov, I.G., Jun, I., Calef, F., and Vasavada, A.R., 2017, Diagenetic silica enrichment and late-stage groundwater activity in Gale crater, Mars: Geophysical Research Letters, v. 44, p. 4716–4724, https://doi.org/10.1002/2017GL073323.

Garrels, R.M., and MacKenzie, F.T., 1972, A quantitative model for the sedimentary rock cycle: Marine Chemistry, v. 1, p. 27–41, https://doi.org/10.1016/0304-4203(72)90004-7.

Garvin, J.B., Edgett, K.S., Dotson, R., Fey, D.M., Herkenhoff, K.E., Hallet, B.J., and Kennedy, M.R., 2017, Quantitative relief models of rock surfaces on Mars at sub-millimeter scales from Mars *Curiosity* rover Mars Hand Lens Imager (MAHLI) observations: Geologic implications: Microscopy and Microanalysis, v. 23, supplement S1, p. 2146–2147, https://doi.org/10.1017/S1431927617011394.

Gellert, R., Clark, B.C., III, and the MSL and MER Science Teams, 2015, In situ compositional measurements of rocks and soils with the Alpha Particle X-Ray Spectrometer on NASA's Mars rovers: Elements, v. 11, p. 39–44, https://doi.org/10.2113/gselements.11.1.39.

Goudge, T.A., Mustard, J.F., Head, J.W., Fassett, C.I., and Wiseman, S.M., 2015, Assessing the mineralogy of the watershed and fan deposits of the Jezero crater paleolake system, Mars: Journal of Geophysical Research–Planets, v. 120, p. 775–808, https://doi.org/10.1002/2014JE004782.

Goudge, T.A., Milliken, R.E., Head, J.W., Mustard, J.F., and Fassett, C.I., 2017, Sedimentological evidence for a deltaic origin of the western fan deposit in Jezero crater, Mars, and implications for future exploration: Earth and Planetary Science Letters, v. 458, p. 357–365, https://doi.org/10.1016/j.epsl.2016.10.056.

Grant, J.A., Arvidson, R.E., Crumpler, L.S., Golombek, M.P., Hahn, B., Haldemann, A.F.C., Li, R., Soderblom, L.A., Squyres, S.W., Wright, S.P., and Watters, W.A., 2006, Crater gradation in Gusev crater and Meridiani Planum, Mars: Journal of Geophysical Research–Planets, v. 111, E02S08, https://doi.org/10.1029/2005JE002465.

Grant, J.A., Wilson, S.A., Mangold, N., Calef, F., III, and Grotzinger, J.P., 2014, The timing of alluvial activity in Gale crater, Mars: Geophysical Research Letters, v. 41, p. 1142–1149, https://doi.org/10.1002/2013GL058909.

Grotzinger, J.P., and Milliken, R.E., 2012, The sedimentary rock record of Mars: Distribution, origins, and global stratigraphy, *in* Grotzinger, J.P., and Milliken, R.E., eds., Sedimentary Geology of Mars: Society for Sedimentary Geology (SEPM) Special Publication 102, p. 1–48, https://doi.org/10.2110/pec.12.102.0001.

Grotzinger, J.P., Arvidson, R.E., Bell, J.F., III, Calvin, W., Clark, B.C., Fike, D.A., Golombek, M., Greeley, R., Haldemann, A., Herkenhoff, K.E., Jolliff, B.L., Knoll, A.H., Malin, M., McLennan, S.M., Parker, T., Soderblom, L., Sohl-Dickstein, J.N., Squyres, S.W., Tosca, N.J., and Watters, W.A., 2005, Stratigraphy and sedimentology of a dry to wet eolian depositional system, Burns formation, Meridiani Planum, Mars: Earth and Planetary Science Letters, v. 240, p. 11–72, https://doi.org/10.1016/j.epsl.2005.09.039.

Grotzinger, J.P., Beaty, D., Dromart, G., Griffes, J., Gupta, S., Harris, P., Hurowitz, J., Kocurek, G., McLennan, S., Milliken, R., Ori, G.G., and Sumner, D., 2011, The sedimentary record of Mars: The Sedimentary Record, v. 9, no. 2, p. 4–8, https://doi.org/10.2110/sedred.2011.2.4.

Grotzinger, J.P., Sumner, D.Y., Kah, L.C., Stack, K., Gupta, S., Edgar, L., Rubin, D., Lewis, K., Schieber, J., Mangold, N., Milliken, R., Conrad, P.G., DesMarais, D., Farmer, J., Siebach, K., Calef, F., III, Hurowitz, J., McLennan, S.M., Ming, D., Vaniman, D., Crisp, J., Vasavada, A., Edgett, K.S., Malin, M., Blake, D., Gellert, R., Mahaffy, P., Wiens, R.C., Maurice, S., Grant, J.A., Wilson, S., Anderson, R.C., Beegle, L., Arvidson, R., Hallet, B., Sletten, R.S., Rice, M., Bell, J., III, Griffes, J., Ehlmann, B., Anderson, R.B., Bristow, T.F., Dietrich, W.E., Dromart, G., Eigenbrode, J., Fraeman, A., Hardgrove, C., Herkenhoff, K., Jandura, L., Kocurek, G., Lee, S., Leshin, L.A., Leveille, R., Limonadi, D., Maki, J., McCloskey, S., Meyer, M., Minitti, M., Newsom, H., Oehler, D., Okon, A., Palucis, M., Parker, T., Rowland, S., Schmidt, M., Squyres, S., Steele, A., Stolper, E., Summons, R., Treiman, A., Williams, R., Yingst, A., and the MSL Science Team, 2014, A habitable fluvio-lacustrine environment at Yellowknife Bay, Gale crater, Mars: Science, v. 343, 1242777, https://doi.org/10.1126/science.1242777.

Grotzinger, J.P., Gupta, S., Malin, M.C., Rubin, D.M., Schieber, J., Siebach, K., Sumner, D.Y., Stack, K.M., Vasavada, A.R., Arvidson, R.E., Calef, F., III, Edgar, L., Fischer, W.F., Grant, J.A., Griffes, J., Kah, L.C., Lamb, M.P., Lewis, K.W., Mangold, N., Minitti, M.E., Palucis, M., Rice, M., Williams, R.M.E., Yingst, R.A., Blake, D., Blaney, D., Conrad, P., Crisp, J., Dietrich, W.E., Dromart, G., Edgett, K.S., Ewing, R.C., Gellert, R., Hurowitz, J.A., Kocurek, G., Mahaffy, P., McBride, M.J., McLennan, S.M., Mischna, M., Ming, D., Milliken, R., Newsom, H., Oehler, D., Parker, T.J., Vaniman, D., Wiens, R.C., and Wilson, S.A., 2015, Deposition, exhumation, and paleoclimate of an ancient lake deposit, Gale crater, Mars: Science, v. 350, aac7575, https://doi.org/10.1126/science.aac7575.

Gwizd, S., Fedo, C., Grotzinger, J., Edgett, K.S., Rivera-Hernández, F., Gupta, S., Stack, K.M., Banham, S., Edgar, L.A., Sumner, D., and Stein, N., 2020, Transition from a lacustrine margin to a lacustrine basin in Gale crater, Mars: The Hartmann's Valley and Karasburg members of the Murray formation: Houston, Texas, Lunar and Planetary Institute Contribution 2326, Lunar and Planetary Science Conference 51, abstract 2719, https://www.hou.usra.edu/meetings/lpsc2020/pdf/2719.pdf (accessed July 2020).

Horgan, B.H.N., Anderson, R.B., Dromart, G., Amador, E.S., and Rice, M.S., 2020, The mineral diversity of Jezero crater: Evidence for possible lacustrine carbonates on Mars: Icarus, v. 339, 113526, https://doi.org/10.1016/j.icarus.2019.113526.

Hynek, B.M., and Phillips, R.J., 2001, Evidence for extensive denudation of the Martian highlands: Geology, v. 29, p. 407–410, https://doi.org/10.1130/0091-7613(2001)029<0407:EFEDOT>2.0.CO;2.

Irwin, R.P., III, Howard, A.D., Craddock, R.A., and Moore, J.M., 2005, An intense terminal epoch of widespread fluvial activity on early Mars: 2. Increased runoff and paleolake development: Journal of Geophysical Research–Planets, v. 110, E12S15, https://doi.org/10.1029/2005JE002460.

Ivanov, M.A., Slyuta, E.N., Grishakina, E.A., and Dmitrovskii, A.A., 2020, Geomorphological analysis of ExoMars candidate landing site Oxia Planum: Solar System Research, v. 54, p. 1–14, https://doi.org/10.1134/S0038094620010050.

Jacob, S., 2015, Characteristics and Origin of an Erosionally Resistant Unit in the Mars Science Laboratory Landing Ellipse (Gale Crater, Mars), Based on Analyses of Surface Data and Orbital Images [M.S. thesis]: Honolulu, Hawai'i, University of Hawai'i at Mānoa, 101 p., https://hdl.handle.net/10125/50930 (accessed July 2020).

Johnsson, M.J., Stallard, R.F., and Meade, R.H., 1988, First-cycle quartz arenites in the Orinoco River basin, Venezuela and Colombia: The Journal of Geology, v. 96, p. 263–277, https://doi.org/10.1086/629219.

Kite, E.S., Lewis, K.W., Lamb, M.P., Newman, C.E., and Richardson, M.I., 2013, Growth and form of the mound in Gale crater, Mars: Slope wind enhanced erosion and transport: Geology, v. 41, p. 543–546, https://doi.org/10.1130/G33909.1.

Kremer, C.H., Mustard, J.F., and Bramble, M.S., 2019, A widespread olivine-rich ash deposit on Mars: Geology, v. 47, p. 677–681, https://doi.org/10.1130/G45563.1.

Kronyak, R.E., Kah, L.C., Miklusicak, N.B., Edgett, K.S., Sun, V.Z., Bryk, A.B., and Williams, R.M.E., 2019a, Extensive polygonal fracture network in Siccar Point group strata: Fracture mechanisms and implications for fluid circulation in Gale crater, Mars: Journal of Geophysical Research–Planets, v. 124, p. 2613–2634, https://doi.org/10.1029/2019JE006125.

Kronyak, R.E., Kah, L.C., Edgett, K.S., VanBommel, S.J., Thompson, L.M., Wiens, R.C., Sun, V.Z., and Nachon, M., 2019b, Mineral-filled fractures as indicators of multigenerational fluid flow in the Pahrump Hills member of the Murray formation, Gale crater, Mars: Earth and Space Science, v. 6, p. 238–265, https://doi.org/10.1029/2018EA000482.

Lakdawalla, E., 2017, ISRO Mars Orbiter Mission Colour Camera Data: Pasadena, California, The Planetary Society, https://planetary.s3.amazonaws.com/data/mom/mom_mcc.html (accessed July 2020).

Land, L.S., Milliken, K.L., and McBride, E.F., 1987, Diagenetic evolution of Cenozoic sandstones, Gulf of Mexico sedimentary basin: Sedimentary Geology, v. 50, p. 195–225, https://doi.org/10.1016/0037-0738(87)90033-9.

Le Deit, L., Hauber, E., Fueten, F., Pondrelli, M., Rossi, A.P., and Jaumann, R., 2013, Sequence of infilling events in Gale crater, Mars: Results from morphology, stratigraphy, and mineralogy: Journal of Geophysical Research–Planets, v. 118, p. 2439–2473, https://doi.org/10.1002/2012JE004322.

Le Deit, L., Mangold, N., Forni, O., Cousin, A., Lasue, J., Schröder, S., Wiens, R.C., Sumner, D., Fabre, C., Stack, K.M., Anderson, R.B., Blaney, D., Clegg, S., Dromart, G., Fisk, M., Gasnault, O., Grotzinger, J.P., Gupta, S., Lanza, N., Le Mouélic, S., Maurice, S., McLennan, S.M., Meslin, P.-Y., Nachon, M., Newsom, H., Payré, V., Rapin, W., Rice, M., Sautter, V., and Treiman, A.H., 2016, The potassic sedimentary rocks in Gale crater, Mars, as seen by ChemCam on board *Curiosity*: Journal of Geophysical Research–Planets, v. 121, p. 784–804, https://doi.org/10.1002/2015JE004987.

Le Mouélic, S., Gasnault, O., Herkenhoff, K.E., Bridges, N.T., Langevin, Y., Mangold, N., Maurice, S., Wiens, R.C., Pinet, P.,

Downloaded from http://pubs.geoscienceworld.org/gsa/geosphere/article-pdf/16/6/1508/5182958/1508.pdf
by California Inst of Technology user

Newsom, H.E., Deen, R.G., Bell, J.F., III, Johnson, J.R., Rapin, W., Barraclough, B., Blaney, D.L., Deflores, L., Maki, J., Malin, M.C., Pérez, R., and Saccoccio, M., 2015, The ChemCam Remote Micro-Imager at Gale crater: Review of the first year of operations on Mars: Icarus, v. 249, p. 93–107, https://doi.org/10.1016/j.icarus.2014.05.030.

Lewis, K.W., and Aharonson, O., 2014, Occurrence and origin of rhythmic sedimentary rocks on Mars: Journal of Geophysical Research–Planets, v. 119, p. 1432–1457, https://doi.org/10.1002/2013JE004404.

Lewis, K.W., and Turner, M.L., 2019, Geologic structure of the Vera Rubin ridge, Gale crater, Mars: Houston, Texas, Lunar and Planetary Institute Contribution 2132, Lunar and Planetary Science Conference 50, abstract 2216, https://www.hou.usra.edu/meetings/lpsc2019/pdf/2216.pdf (accessed July 2020).

L'Haridon, J., 2018, Diagenetic Processes on Mars: Analysis by the ChemCam Instrument on the Curiosity Rover [Ph.D. thesis]: Nantes, France, Université de Nantes, 184 p., https://www.theses.fr/2018NANT4087 (accessed July 2020).

L'Haridon, J., Mangold, N., Meslin, P.-Y., Johnson, J., Rapin, W., Forni, O., Cousin, A., Payré, V., Dehouck, E., Nachon, M., Le Deit, L., Gasnault, O., Maurice, S., and Wiens, R.C., 2018, Chemical variability in mineralized veins observed by ChemCam on the lower slopes of Mount Sharp in Gale crater, Mars: Icarus, v. 311, p. 69–86, https://doi.org/10.1016/j.icarus.2018.01.028.

Licht, A., Pullen, A., Kapp, P., Abell, J., and Geisler, N., 2016, Eolian cannibalism: Reworked loess and fluvial sediment as the main sources of the Chinese Loess Plateau: Geological Society of America Bulletin, v. 128, p. 944–956, https://doi.org/10.1130/B31375.1.

Maki, J., Thiessen, D., Pourangi, A., Kobzeff, P., Litwin, T., Scherr, L., Elliott, S., Dingizian, A., and Maimone, M., 2012, The Mars Science Laboratory engineering cameras: Space Science Reviews, v. 170, p. 77–93, https://doi.org/10.1007/s11214-012-9882-4.

Malin, M.C., and Edgett, K.S., 2000, Sedimentary rocks of early Mars: Science, v. 290, p. 1927–1937, https://doi.org/10.1126/science.290.5498.1927.

Malin, M.C., and Edgett, K.S., 2001, Mars Global Surveyor Mars Orbiter Camera: Interplanetary cruise through primary mission: Journal of Geophysical Research–Planets, v. 106, p. 23429–23570, https://doi.org/10.1029/2000JE001455.

Malin, M.C., Bell, J.F., III, Cantor, B.A., Caplinger, M.A., Calvin, W.M., Clancy, R.T., Edgett, K.S., Edwards, L., Haberle, R.M., James, P.B., Lee, S.W., Ravine, M.A., Thomas, P.C., and Wolff, M.J., 2007, Context Camera investigation on board the *Mars Reconnaissance Orbiter*: Journal of Geophysical Research–Planets, v. 112, E05S04, https://doi.org/10.1029/2006JE002808.

Malin, M.C., Edgett, K.S., Cantor, B.A., Caplinger, M.A., Danielson, G.E., Jensen, E.H., Ravine, M.A., Sandoval, J.L., and Supulver, K.D., 2010, An overview of the 1985–2006 Mars Orbiter Camera science investigation: Mars: The International Journal of Mars Science and Exploration, v. 5, p. 1–60, https://doi.org/10.1555/mars.2010.0001.

Malin, M.C., Ravine, M.A., Caplinger, M.A., Ghaemi, F.T., Schaffner, J.A., Maki, J.N., Bell, J.F., III, Cameron, J.F., Dietrich, W.E., Edgett, K.S., Edwards, L.J., Garvin, J.B., Hallet, B., Herkenhoff, K.E., Heydari, E., Kah, L.C., Lemmon, M.T., Minitti, M.E., Olson, T.S., Parker, T.J., Rowland, S.K., Schieber, J., Sletten, R., Sullivan, R.J., Sumner, D.Y., Yingst, R.A., Duston, B.M., McNair, S., and Jensen, E.H., 2017, The Mars Science Laboratory (MSL) mast cameras and descent imager: Investigation and instrument descriptions: Earth and Space Science, v. 4, p. 506–539, https://doi.org/10.1002/2016EA000252.

Mandon, L., Quantin-Nataf, C., Thollot, P., Mangold, N., Lozac'h, L., Dromart, G., Beck, P., Dehouck, E., Breton, S., Millot, C., and Volat, M., 2020, Refining the age, emplacement and alteration scenarios of the olivine-rich unit in the Nili Fossae region, Mars: Icarus, v. 336, 113436, https://doi.org/10.1016/j.icarus.2019.113436.

Mangold, N., Gendrin, A., Gondet, B., Le Mouélic, S., Quantin, C., Ansan, V., Bibring, J.-P., Langevin, Y., Masson, P., and Neukum, G., 2008, Spectral and geological study of the sulfate-rich region of west Candor Chasma, Mars: Icarus, v. 194, p. 519–543, https://doi.org/10.1016/j.icarus.2007.10.021.

Mangold, N., Thompson, L.M., Forni, O., Williams, A.J., Fabre, C., Le Deit, L., Wiens, R.C., Williams, R., Anderson, R.B., Blaney, D.L., Calef, F., Cousin, A., Clegg, S.M., Dromart, G., Dietrich, W.E., Edgett, K.S., Fisk, M.R., Gasnault, O., Gellert, R., Grotzinger, J.P., Kah, L., Le Mouélic, S., McLennan, S.M., Maurice, S., Meslin, P.-Y., Newsom, H.E., Palucis, M.C., Rapin, W., Sautter, V., Siebach, K.L., Stack, K., Sumner, D., and Yingst, A., 2016, Composition of conglomerates analyzed by the *Curiosity* rover: Implications for Gale crater crust and sediment sources: Journal of Geophysical Research–Planets, v. 121, p. 353–387, https://doi.org/10.1002/2015JE004977.

Mangold, N., Schmidt, M.E., Fisk, M.R., Forni, O., McLennan, S.M., Ming, D.W., Sautter, V., Sumner, D., Williams, A.J., Clegg, S.M., Cousin, A., Gasnault, O., Gellert, R., Grotzinger, J.P., and Wiens, R.C., 2017, Classification scheme for sedimentary and igneous rocks in Gale crater, Mars: Icarus, v. 284, p. 1–17, https://doi.org/10.1016/j.icarus.2016.11.005.

Mangold, N., Dehouck, E., Fedo, C., Forni, O., Achilles, C., Bristow, T., Downs, R.T., Frydenvang, J., Gasnault, O., L'Haridon, J., Le Deit, L., Maurice, S., McLennan, S.M., Meslin, P.-Y., Morrison, S., Newsom, H.E., Rampe, E., Rapin, W., Rivera-Hernandez, F., Salvatore, M., and Wiens, R.C., 2019, Chemical alteration of fine-grained sedimentary rocks at Gale crater: Icarus, v. 321, p. 619–631, https://doi.org/10.1016/j.icarus.2018.11.004.

Marriott, S.B., and Wright, V.P., 1996, Sediment recycling on Silurо-Devonian floodplains: Journal of the Geological Society [London], v. 153, p. 661–664, https://doi.org/10.1144/gsjgs.153.5.0661.

Martin, P.E., Farley, K.A., Baker, M.B., Malespin, C.A., Schwenzer, S.P., Cohen, B.A., Mahaffy, P.R., McAdam, A.C., Ming, D.W., Vasconcelos, P.M., and Navarro-González, R., 2017, A two-step K-Ar experiment on Mars: Dating the diagenetic formation of jarosite from Amazonian groundwaters: Journal of Geophysical Research–Planets, v. 122, p. 2803–2818, https://doi.org/10.1002/2017JE005445.

McEwen, A.S., Eliason, E.M., Bergstrom, J.W., Bridges, N.T., Hansen, C.J., Delamere, W.A., Grant, J.A., Gulick, V.C., Herkenhoff, K.E., Keszthelyi, L., Kirk, R.L., Mellon, M.T., Squyres, S.W., Thomas, N., and Weitz, C.M., 2007, Mars Reconnaissance Orbiter's High Resolution Imaging Science Experiment (HiRISE): Journal of Geophysical Research–Planets, v. 112, E05S02, https://doi.org/10.1029/2005JE002605.

McLennan, S.M., and Grotzinger, J.P., 2008, The sedimentary rock cycle of Mars, *in* Bell, J.F., III, ed., The Martian Surface: Composition, Mineralogy, and Physical Properties: New York, Cambridge University Press, p. 541–577, https://doi.org/10.1017/CBO9780511536076.025.

McSween, H.Y., Jr., 2015, Petrology on Mars: The American Mineralogist, v. 100, p. 2380–2395, https://doi.org/10.2138/am-2015-5257.

McSween, H.Y., Jr., Taylor, G.J., and Wyatt, M.B., 2009, Elemental composition of the Martian crust: Science, v. 324, p. 736–739, https://doi.org/10.1126/science.1165871.

McSween, H.Y., Jr., Labotka, T.C., and Viviano-Beck, C.E., 2015, Metamorphism in the Martian crust: Meteoritics & Planetary Science, v. 50, p. 590–603, https://doi.org/10.1111/maps.12330.

Mendoza-Rosales, C.C., Centeno-García, E., Silva-Romo, G., Campos-Madrigal, E., and Bernal, J.P., 2010, Barremian rift-related turbidites and alkaline volcanism in southern Mexico and their role in the opening of the Gulf of Mexico: Earth and Planetary Science Letters, v. 295, p. 419–434, https://doi.org/10.1016/j.epsl.2010.04.020.

Milliken, R.E., Grotzinger, J.P., and Thomson, B.J., 2010, Paleoclimate of Mars as captured by the stratigraphic record in Gale crater: Geophysical Research Letters, v. 37, L04201, https://doi.org/10.1029/2009GL041870.

Milliken, R.E., Ewing, R.C., Fischer, W.W., and Hurowitz, J., 2014, Wind-blown sandstones cemented by sulfate and clay minerals in Gale crater, Mars: Geophysical Research Letters, v. 41, p. 1149–1154, https://doi.org/10.1002/2013GL059097.

Moecher, D.P., Kelly, E.A., Hietpas, J., and Samson, S.D., 2019, Proof of recycling in clastic sedimentary systems from textural analysis and geochronology of detrital monazite: Implications for detrital mineral provenance analysis: Geological Society of America Bulletin, v. 131, p. 1115–1132, https://doi.org/10.1130/B31947.1.

Molina, A., López, I., Prieto-Ballesteros, O., Fernández-Remolar, D., de Pablo, M.A., and Gómez, F., 2017, Coogoon Valles, western Arabia Terra: Hydrological evolution of a complex Martian channel system: Icarus, v. 293, p. 27–44, https://doi.org/10.1016/j.icarus.2017.04.002.

Morris, R.V., Vaniman, D.T., Blake, D.F., Gellert, R., Chipera, S.J., Rampe, E.B., Ming, D.W., Morrison, S.M., Downs, R.T., Treiman, A.H., Yen, A.S., Grotzinger, J.P., Achilles, C.N., Bristow, T.F., Crisp, J.A., Des Marais, D.J., Farmer, J.D., Fendrich, K.V., Frydenvang, J., Graff, T.G., Morookian, J.M., Stolper, E.M., and Schwenzer, S.P., 2016, Silicic volcanism on Mars evidenced by tridymite in high-SiO_2 sedimentary rock at Gale crater: Proceedings of the National Academy of Sciences of the United States of America, v. 113, p. 7071–7076, https://doi.org/10.1073/pnas.1607098113.

Murchie, S., Roach, L., Seelos, F., Milliken, R., Mustard, J., Arvidson, R., Wiseman, S., Lichtenberg, K., Andrews-Hanna, J., Bishop, J., Bibring, J.-P., Parente, M., and Morris, R., 2009, Evidence for the origin of layered deposits in Candor Chasma, Mars, from mineral composition and hydrologic modeling: Journal of Geophysical Research–Planets, v. 114, E00D05, https://doi.org/10.1029/2009JE003343.

Mutch, T.A., Arvidson, R.E., Head, J.W., III, Jones, K.L., and Saunders, R.S., 1976, Physiographic provinces, *in* The Geology of Mars: Princeton, New Jersey, Princeton University Press, p. 56–91.

Nachon, M., Clegg, S.M., Mangold, N., Schröder, S., Kah, L.C., Dromart, G., Ollila, A., Johnson, J.R., Oehler, D.Z., Bridges,

Downloaded from http://pubs.geoscienceworld.org/gsa/geosphere/article-pdf/16/6/1508/5182958/1508.pdf
by California Inst of Technology user

J.C., Le Mouélic, S., Forni, O., Wiens, R.C., Anderson, R.B., Blaney, D.L., Bell, J.F., III, Clark, B., Cousin, A., Dyar, M.D., Ehlmann, B., Fabre, C., Gasnault, O., Grotzinger, J., Lasue, J., Lewin, E., Léveillé, R., McLennan, S., Maurice, S., Meslin, P.-Y., Rapin, W., Rice, M., Squyres, S.W., Stack, K., Sumner, D.Y., Vaniman, D., and Wellington, D., 2014, Calcium sulfate veins characterized by ChemCam/*Curiosity* at Gale crater, Mars: Journal of Geophysical Research–Planets, v. 119, p. 1991–2016, https://doi.org/10.1002/2013JE004588.

Nachon, M., Mangold, N., Forni, O., Kah, L.C., Cousin, A., Wiens, R.C., Anderson, R., Blaney, D., Blank, J.G., Calef, F., Clegg, S.M., Fabre, C., Fisk, M.R., Gasnault, O., Grotzinger, J.P., Kronyak, R., Lanza, N.L., Lasue, J., Le Deit, L., Le Mouélic, S., Maurice, S., Meslin, P.-Y., Oehler, D.Z., Payré, V., Rapin, W., Schröder, S., Stack, K., and Sumner, D., 2017, Chemistry of diagenetic features analyzed by ChemCam at Pahrump Hills, Gale crater, Mars: Icarus, v. 281, p. 121–136, https://doi.org/10.1016/j.icarus.2016.08.026.

National Aeronautics and Space Administration Planetary Data System (NASA PDS), 2020, National Aeronautics and Space Administration Planetary Data System: https://pds.nasa.gov/ (accessed July 2020).

Nesbitt, H.W., and Wilson, R.E., 1992, Recent chemical weathering of basalts: American Journal of Science, v. 292, p. 740–777, https://doi.org/10.2475/ajs.292.10.740.

Nesbitt, H.W., and Young, G.M., 1996, Petrogenesis of sediments in the absence of chemical weathering: Effects of abrasion and sorting on bulk composition and mineralogy: Sedimentology, v. 43, p. 341–358, https://doi.org/10.1046/j.1365-3091.1996.d01-12.x.

Nesbitt, H.W., Young, G.M., and Bosman, S.A., 2009, Major and trace element geochemistry and genesis of supracrustal rocks of the North Spirit Lake Greenstone belt, NW Ontario, Canada: Precambrian Research, v. 174, p. 16–34, https://doi.org/10.1016/j.precamres.2009.06.006.

Newsom, H.E., Edgett, K.S., Fey, D.M., Wiens, R.C., Frydenvang, J., Banham, S.G., Gupta, S., Williams, A.J., Grotzinger, J.P., Mangold, N., Schieber, J., Rivera-Hernández, F., and Belgacem, I., 2018, A buried aeolian lag deposit at an unconformity between the Murray and Stimson formation at Marias Pass, Gale crater, Mars: Houston, Texas, Lunar and Planetary Institute Contribution 2083, Lunar and Planetary Science Conference 49, abstract 2263, https://www.hou.usra.edu/meetings/lpsc2018/pdf/2263.pdf (accessed July 2020).

Niles, P.B., and Michalski, J., 2012, Origin and evolution of sediments in Gale crater through ice-hosted processes: Houston, Texas, Lunar and Planetary Institute Contribution 1659, Lunar and Planetary Science Conference 43, abstract 2575, https://www.lpi.usra.edu/meetings/lpsc2012/pdf/2575.pdf (accessed July 2020).

Okubo, C.H., 2010, Structural geology of Amazonian-aged layered sedimentary deposits in southwest Candor Chasma, Mars: Icarus, v. 207, p. 210–225, https://doi.org/10.1016/j.icarus.2009.11.012.

Pain, C.F., Clarke, J.D.A., and Thomas, M., 2007, Inversion of relief on Mars: Icarus, v. 190, p. 478–491, https://doi.org/10.1016/j.icarus.2007.03.017.

Palucis, M.C., Dietrich, W.E., Williams, R.M.E., Hayes, A.G., Parker, T., Sumner, D.Y., Mangold, N., Lewis, K., and Newsom, H., 2016, Sequence and relative timing of large lakes in Gale crater (Mars) after the formation of Mount Sharp: Journal of Geophysical Research–Planets, v. 121, p. 472–496, https://doi.org/10.1002/2015JE004905.

Parker, T., and Calef, F.J., III, 2016, MSL Gale Merged Digital Elevation Model (1 Meter per Pixel Scale): U.S. Geological Survey NASA Planetary Data System (PDS) Annex, https://bit.ly/MSL_DEM (accessed July 2020).

Parkes Bowen, A., Bridges, J.C., Page, J., El-Maary, M.R., Thomas, N., Cremonese, G., Pajola, M., and Tornabene, L., 2019, Fracture mapping and CaSSIS imaging of the ExoMars 2020 landing site Oxia Planum: Characterising clay-rich sediments: Houston, Texas, Lunar and Planetary Institute Contribution 2132, Lunar and Planetary Science Conference 50, abstract 1952, https://www.hou.usra.edu/meetings/lpsc2019/pdf/1952.pdf (accessed July 2020).

Pelkey, S.M., Jakosky, B.M., and Christensen, P.R., 2004, Surficial properties of Gale crater, Mars, from *Mars Odyssey* THEMIS data: Icarus, v. 167, p. 244–270, https://doi.org/10.1016/j.icarus.2003.09.013.

Quantin-Nataf, C., Carter, J., Mandon, L., Balme, M., Fawdon, P., Davis, J., Thollot, P., Dehouck, E., Pan, L., Volat, M., Millot, C., Breton, S., Loizeau, D., and Vago, J.L., 2019, ExoMars at Oxia Planum, probing the aqueous-related Noachian environments: Houston, Texas, Lunar and Planetary Institute Contribution 2089, 9th International Conference on Mars, abstract 6317, https://www.hou.usra.edu/meetings/ninthmars2019/pdf/6317.pdf (accessed July 2020).

Rampe, E.B., Ming, D.W., Blake, D.F., Bristow, T.F., Chipera, S.J., Grotzinger, J.P., Morris, R.V., Morrison, S.M., Vaniman, D.T., Yen, A.S., Achilles, C.N., Craig, P.I., DesMarais, D.J., Downs, R.T., Farmer, J.D., Fendrich, K.V., Gellert, R., Hazen, R.M., Kah, L.C., Morookian, J.M., Peretyazhko, T.S., Sarrazin, P., Treiman, A.H., Berger, J.A., Eigenbrode, J., Fairén, A.G., Forni, O., Gupta, S., Hurowitz, J.A., Lanza, N.L., Schmidt, M.E., Siebach, K., Sutter, B., and Thompson, L.M., 2017, Mineralogy of an ancient lacustrine mudstone succession from the Murray formation, Gale crater, Mars: Earth and Planetary Science Letters, v. 471, p. 172–185, https://doi.org/10.1016/j.epsl.2017.04.021.

Rapin, W., Dromart, G., Rubin, D., Le Deit, L., Mangold, N., Fox, V., Gasnaut, O., Herkenhoff, K., Le Mouélic, S., Dickson, J.L., Ehlmann, B.L., Maurice, S., Wiens, R.C., Edgar, L.A., and Anderson, R.B., 2020, Predicting changes in depositional environments up Mount Sharp stratigraphy: Houston, Texas, Lunar and Planetary Institute Contribution 2326, Lunar and Planetary Science Conference 51, abstract 3006, https://www.hou.usra.edu/meetings/lpsc2020/pdf/3006.pdf (accessed July 2020).

Ray, R.G., 1960, Aerial Photographs in Geologic Interpretation and Mapping: U.S. Geological Survey Professional Paper 373, 230 p., https://doi.org/10.3133/pp373.

Rivera-Hernández, F., and Palucis, M.C., 2019, Do deltas along the crustal dichotomy boundary of Mars in the Gale crater region record a northern ocean?: Geophysical Research Letters, v. 46, p. 8689–8699, https://doi.org/10.1029/2019GL083046.

Rivera-Hernández, F., Sumner, D.Y., Mangold, N., Banham, S.G., Edgett, K.S., Fedo, C.M., Gupta, S., Gwizd, S., Heydari, E., Maurice, S., Nachon, M., Newsom, H., Schieber, J., Stack-Morgan, K., Stein, N., and Wiens, R.C., 2020, Grain size variations in the Murray formation: Stratigraphic evidence for changing depositional environments in Gale crater, Mars: Journal of Geophysical Research–Planets, v. 125, e2019JE006230, https://doi.org/10.1029/2019JE006230.

Robinson, M., Collins, C., Leger, P., Carsten, J., Tompkins, V., Hartman, F., and Yen, J., 2013, In-situ operations and planning for the Mars Science Laboratory robotic arm: The first 200 sols, *in* Proceedings of the 8th IEEE International Conference on System of Systems Engineering: Institute of Electrical and Electronics Engineers, Piscataway, New Jersey, p. 153–158, https://doi.org/10.1109/SYSoSE.2013.6575259.

Salvatore, M.R., Goudge, T.A., Bramble, M.S., Edwards, C.S., Bandfield, J.L., Amador, E.S., Mustard, J.F., and Christensen, P.R., 2018, Bulk mineralogy of the NE Syrtis and Jezero crater regions of Mars derived through thermal infrared spectral analyses: Icarus, v. 301, p. 76–96, https://doi.org/10.1016/j.icarus.2017.09.019.

Sautter, V., Fabre, C., Forni, O., Toplis, M.J., Cousin, A., Ollila, A.M., Meslin, P.-Y., Maurice, S., Wiens, R.C., Baratoux, D., Mangold, N., Le Mouélic, S., Gasnault, O., Berger, G., Lasue, J., Anderson, R.A., Lewin, E., Schmidt, M., Dyar, D., Ehlmann, B.L., Bridges, J., Clark, B., and Pinet, P., 2014, Igneous mineralogy at Bradbury rise: The first ChemCam campaign at Gale crater: Journal of Geophysical Research–Planets, v. 119, p. 30–46, https://doi.org/10.1002/2013JE004472.

Sautter, V., Toplis, M.J., Wiens, R.C., Cousin, A., Fabre, C., Gasnault, O., Maurice, S., Forni, O., Lasue, J., Ollila, A., Bridges, J.C., Mangold, N., Le Mouélic, S., Fisk, M., Meslin, P.-Y., Beck, P., Pinet, P., Le Deit, L., Rapin, W., Stolper, E.M., Newsom, H., Dyar, D., Lanza, N., Vaniman, D., Clegg, S., and Wray, J.J., 2015, In situ evidence for continental crust on early Mars: Nature Geoscience, v. 8, p. 605–609, https://doi.org/10.1038/ngeo2474.

Schieber, J., Bish, D., Coleman, M., Reed, M., Hausrath, E.M., Cosgrove, J., Gupta, S., Minitti, M.E., Edgett, K.S., and Malin, M., 2017, Encounters with an unearthly mudstone: Understanding the first mudstone found on Mars: Sedimentology, v. 64, p. 311–358, https://doi.org/10.1111/sed.12318.

Schwenzer, S.P., Abramov, O., Allen, C.C., Bridges, J.C., Clifford, S.M., Filiberto, J., Kring, D.A., Lasue, J., McGovern, P.J., Newsom, H.J., Treiman, A.H., Vaniman, D.T., Wiens, R.C., and Wittmann, A., 2012, Gale crater: Formation and post-impact hydrous environments: Planetary and Space Science, v. 70, p. 84–95, https://doi.org/10.1016/j.pss.2012.05.014.

Sharp, R.P., 1973, Fretted and chaotic terrains: Journal of Geophysical Research, v. 78, p. 4073–4083, https://doi.org/10.1029/JB078i020p04073.

Siebach, K.L., 2016, Causes of geochemical diversity in three different Gale crater sedimentary rock formations, *in* Formation and Diagenesis of Sedimentary Rocks in Gale Crater, Mars [Ph.D. thesis]: Pasadena, California, California Institute of Technology, p. 107–148, https://doi.org/10.7907/Z97D2S4K.

Smith, D.E., Zuber, M.T., Frey, H.V., Garvin, J.B., Head, J.W., Muhleman, D.O., Pettengill, G.H., Phillips, R.J., Solomon, S.C., Zwally, H.J., Banerdt, W.B., Duxbury, T.C., Golombek, M.P., Lemoine, F.G., Neumann, G.A., Rowlands, D.D., Aharonson, O., Ford, P.G., Ivanov, I.B., Johnson, C.L., McGovern, P.J., Abshire, J.B., Afzal, R.S., and Sun, X., 2001, Mars Orbiter Laser Altimeter: Experiment summary and the first year of global mapping of Mars: Journal of Geophysical Research–Planets, v. 106, p. 23689–23722, https://doi.org/10.1029/2000JE001364.

Spray, J.G., Elliot, B.E., and Thompson, L.M., 2013, The Gale impact structure, Mars: Original shape and formation age:

Downloaded from http://pubs.geoscienceworld.org/gsa/geosphere/article-pdf/16/6/1508/5182958/1508.pdf
by California Inst of Technology user

Houston, Texas, Lunar and Planetary Institute Contribution 1719, Lunar and Planetary Science Conference 44, abstract 2959, https://www.lpi.usra.edu/meetings/lpsc2013/pdf/2959.pdf (accessed July 2020).

Stack, K.M., Grotzinger, J.P., Kah, L.C., Schmidt, M.E., Mangold, N., Edgett, K.S., Sumner, D.Y., Siebach, K.L., Nachon, M., Lee, R., Blaney, D.L., Deflores, L.P., Edgar, L.A., Fairén, A.G., Leshin, L.A., Maurice, S., Oehler, D.Z., Rice, M.S., and Wiens, R.C., 2014, Diagenetic origin of nodules in the Sheepbed member, Yellowknife Bay formation, Gale crater, Mars: Journal of Geophysical Research–Planets, v. 119, p. 1637–1664, https://doi.org/10.1002/2014JE004617.

Stack, K.M., Edwards, C.S., Grotzinger, J.P., Gupta, S., Sumner, D.Y., Calef, F.J., III, Edgar, L.A., Edgett, K.S., Fraeman, A.A., Jacob, S.R., Le Deit, L., Lewis, K.W., Rice, M.S., Rubin, D., Williams, R.M.E., and Williford, K.H., 2016, Comparing orbiter and rover image-based mapping of an ancient sedimentary environment, Aeolis Palus, Gale crater, Mars: Icarus, v. 280, p. 3–21, https://doi.org/10.1016/j.icarus.2016.02.024.

Stack, K.M., Grotzinger, J.P., Lamb, M.P., Gupta, S., Rubin, D.M., Kah, L.C., Edgar, L.A., Fey, D.M., Hurowitz, J.A., McBride, M., Rivera-Hernández, F., Sumner, D.Y., Van Beek, J.K., Williams, R.M.E., and Yingst, R.A., 2019, Evidence for plunging river plume deposits in the Pahrump Hills member of the Murray formation, Gale crater, Mars: Sedimentology, v. 66, p. 1768–1802, https://doi.org/10.1111/sed.12558.

Stein, N.T., Quinn, D.P., Grotzinger, J.P., Fedo, C., Ehlmann, B.L., Stack, K.M., Edgar, L.A., Fraeman, A.A., and Deen, R., 2020, Regional structural orientation of the Mount Sharp group revealed by in situ dip measurements and stratigraphic correlations on the Vera Rubin ridge: Journal of Geophysical Research–Planets, v. 125, e2019JE006298, https://doi.org/10.1029/2019JE006298.

Tanaka, K.L., Skinner, J.A., Jr., Dohm, J.M., Irwin, R.P., III, Kolb, E.J., Fortezzo, C.M., Platz, T., Michael, G.G., and Hare, T.M., 2014, Pamphlet to Accompany Geologic Map of Mars: U.S. Geological Survey Scientific Investigations Map 3292, scale 1:20,000,000, https://doi.org/10.3133/sim3292.

Thomas, M.F., McEwen, A.S., and Dundas, C.M., 2020, Present-day mass wasting in sulfate-rich sediments in the equatorial regions of Mars: Icarus, v. 342, 113566, https://doi.org/10.1016/j.icarus.2019.113566.

Thomson, B.J., Bridges, N.T., Milliken, R., Baldridge, A., Hook, S.J., Crowley, J.K., Marion, G.M., de Souza Filho, C.R., Brown, A.J., and Weitz, C.M., 2011, Constraints on the origin and evolution of the layered mound in Gale crater, Mars, using *Mars Reconnaissance Orbiter* data: Icarus, v. 214, p. 413–432, https://doi.org/10.1016/j.icarus.2011.05.002.

Treiman, A.H., Bish, D.L., Vaniman, D.T., Chipera, S.J., Blake, D.F., Ming, D.W., Morris, R.V., Bristow, T.F., Morrison, S.M., Baker, M.B., Rampe, E.B., Downs, R.T., Filiberto, J., Glazner, A.F., Gellert, R., Thompson, L.M., Schmidt, M.E., Le Deit, L., Wiens, R.C., McAdam, A.C., Achilles, C.N., Edgett, K.S., Farmer, J.D., Fendrich, K.V., Grotzinger, J.P., Gupta, S., Morookian, J.M., Newcombe, M.E., Rice, M.S., Spray, J.G., Stolper, E.M., Sumner, D.Y., Vasavada, A.R., and Yen, A.S., 2016, Mineralogy, provenance, and diagenesis of a potassic basaltic sandstone on Mars: CheMin X-Ray diffraction of the Windjana sample (Kimberley area, Gale crater): Journal of Geophysical Research–Planets, v. 121, p. 75–106, https://doi.org/10.1002/2015JE004932.

Vago, J.L., Westall, F., Pasteur Instrument Teams, Landing Site Selection Working Group, and Other Contributors, 2017, Habitability on early Mars and the search for biosignatures with the ExoMars rover: Astrobiology, v. 17, p. 471–510, https://doi.org/10.1089/ast.2016.1533.

VanBommel, S.J., Gellert, R., Berger, J.A., Thompson, L.M., Edgett, K.S., McBride, M.J., Minitti, M.E., Boyd, N.I., and Campbell, J.L., 2017, Modeling and mitigation of sample relief effects applied to chemistry measurements by the Mars Science Laboratory Alpha Particle X-ray Spectrometer: X-Ray Spectrometry, v. 46, p. 229–236, https://doi.org/10.1002/xrs.2755.

Vaniman, D.T., Bish, D.L., Ming, D.W., Bristow, T.F., Morris, R.V., Blake, D.F., Chipera, S.J., Morrison, S.M., Treiman, A.H., Rampe, E.B., Rice, M., Achilles, C.N., Grotzinger, J., McLennan, S.M., Williams, J., Bell, J., III, Newsom, H., Downs, R.T., Maurice, S., Sarrazin, P., Yen, A.S., Morookian, J.M., Farmer, J.D., Stack, K., Milliken, R.E., Ehlmann, B., Sumner, D.Y., Berger, G., Crisp, J.A., Hurowitz, J.A., Anderson, R., DesMarais, D., Stolper, E.M., Edgett, K.S., Gupta, S., Spanovich, N., and the MSL Science Team, 2014, Mineralogy of a mudstone at Yellowknife Bay, Gale crater, Mars: Science, v. 343, 1243480, https://doi.org/10.1126/science.1243480.

Vaniman, D.T., Martínez, G.M., Rampe, E.B., Bristow, T.F., Blake, D.F., Yen, A.S., Ming, D.W., Rapin, W., Meslin, P.-Y., Morookian, J.M., Downs, R.T., Chipera, S.J., Morris, R.V., Morrison, S.M., Treiman, A.H., Achilles, C.N., Robertson, K., Grotzinger, J.P., Hazen, R.M., Wiens, R.C., and Sumner, D.Y., 2018, Gypsum, bassanite, and anhydrite at Gale crater, Mars: The American Mineralogist, v. 103, p. 1011–1020, https://doi.org/10.2138/am-2018-6346.

Vasavada, A.R., Grotzinger, J.P., Arvidson, R.E., Calef, F.J., Crisp, J.A., Gupta, S., Hurowitz, J., Mangold, N., Maurice, S., Schmidt, M.E., Wiens, R.C., Williams, R.M.E., and Yingst, R.A., 2014, Overview of the Mars Science Laboratory mission: Bradbury Landing to Yellowknife Bay and beyond: Journal of Geophysical Research–Planets, v. 119, p. 1134–1161, https://doi.org/10.1002/2014JE004622.

Veizer, J., and Jansen, S.L., 1979, Basement and sedimentary recycling and continental evolution: The Journal of Geology, v. 87, p. 341–370, https://doi.org/10.1086/628425.

Wan, W.X., Wang, C., Li, C.L., and Wei, Y., 2020, China's first mission to Mars: Nature Astronomy, v. 4, p. 721, https://doi.org/10.1038/s41550-020-1148-6.

Warner, N., Silverman, M., Samuels, J., DeFlores, L., Sengstacken, A., Maki, J., Scodary, A., Peters, S., Litwin, T., and Metz, B., 2016, The Mars Science Laboratory Remote Sensing Mast, *in* Proceedings of the 2016 IEEE Aerospace Conference: Piscataway, New Jersey, Institute of Electrical and Electronics Engineers, p. 564–571, https://doi.org/10.1109/AERO.2016.7500554.

Watkins, J., Grotzinger, J., Stein, N., Banham, S.G., Gupta, S., Rubin, D., Stack, K.M., and Edgett, K.S., 2016, Paleotopography of erosional unconformity, base of Stimson formation, Gale crater, Mars: Houston, Texas, Lunar and Planetary Institute Contribution 1903, Lunar and Planetary Science Conference 47, abstract 2939, https://www.hou.usra.edu/meetings/lpsc2016/pdf/2939.pdf (accessed July 2020).

Werner, S.C., 2019, In situ calibration of the Martian cratering chronology: Meteoritics & Planetary Science, v. 54, p. 1182–1193, https://doi.org/10.1111/maps.13263.

Wiens, R.C., Edgett, K.S., Stack, K.M., Dietrich, W.E., Bryk, A.B., Mangold, N., Bedford, C., Gasda, P., Fairén, A., Thompson, L., Johnson, J., Gasnault, O., Clegg, S., Cousin, A., Forni, O., Frydenvang, J., Lanza, N., Maurice, S., Newsom, H., Ollila, A., Payré, V., Rivera-Hernández, F., and Vasavada, A., 2020, Origin and composition of three heterolithic boulder- and cobble-bearing deposits overlying the Murray and Stimson formations, Gale crater, Mars: Icarus, v. 350, 113897, https://doi.org/10.1016/j.icarus.2020.113897.

Williams, R.M.E., Grotzinger, J.P., Dietrich, W.E., Gupta, S., Sumner, D.Y., Wiens, R.C., Mangold, N., Malin, M.C., Edgett, K.S., Maurice, S., Forni, O., Gasnault, O., Ollila, A., Newsom, H.E., Dromart, G., Palucis, M.C., Yingst, R.A., Anderson, R.B., Herkenhoff, K.E., Le Mouélic, S., Goetz, W., Madsen, M.B., Koefoed, A., Jensen, J.K., Bridges, J.C., Schwenzer, S.P., Lewis, K.W., Stack, K.M., Rubin, D., Kah, L.C., Bell, J.F., III, Farmer, J.D., Sullivan, R., Van Beek, T., Blaney, D.L., Pariser, O., Deen, R.G., and the MSL Science Team, 2013, Martian fluvial conglomerates at Gale crater: Science, v. 340, p. 1068–1072, https://doi.org/10.1126/science.1237317.

Williford, K.H., Farley, K.A., Stack, K.M., Allwood, A.C., Beaty, D., Beegle, L.W., Bhartia, R., Brown, A.J., de la Torre Juarez, M., Hamran, S.-E., Hecht, M.H., Hurowitz, J.A., Rodriguez-Manfredi, J.A., Maurice, S., Milkovich, S., and Wiens, R.C., 2018, The NASA Mars 2020 rover mission and the search for extraterrestrial life, *in* Cabrol, N.A., and Grin, E.A., eds., From Habitability to Life on Mars: Amsterdam, Netherlands, Elsevier, p. 275–308, https://doi.org/10.1016/B978-0-12-809935-3.00010-4.

Wilson, R.C., Picard, M.D., and Harp, E.L., 1974, Geologic cycle of Mars: A comparison with Earth and Moon: Geology, v. 2, p. 121–124, https://doi.org/10.1130/0091-7613(1974)2<121:GCOMAC>2.0.CO;2.

Yen, A.S., Ming, D.W., Vaniman, D.T., Gellert, R., Blake, D.F., Morris, R.V., Morrison, S.M., Bristow, T.F., Chipera, S.J., Edgett, K.S., Treiman, A.H., Clark, B.C., Downs, R.T., Farmer, J.D., Grotzinger, J.P., Rampe, E.B., Schmidt, M.E., Sutter, B., Thompson, L.M., and the MSL Science Team, 2017, Multiple stages of aqueous alteration along fractures in mudstone and sandstone strata in Gale crater, Mars: Earth and Planetary Science Letters, v. 471, p. 186–198, https://doi.org/10.1016/j.epsl.2017.04.033.

Zabrusky, K., Andrews-Hanna, J.C., and Wiseman, S.M., 2012, Reconstructing the distribution and depositional history of the sedimentary deposits of Arabia Terra, Mars: Icarus, v. 220, p. 311–330, https://doi.org/10.1016/j.icarus.2012.05.007.

Zhang, S., and O'Neill, C., 2016, The early geodynamic evolution of Mars-type planets: Icarus, v. 265, p. 187–208, https://doi.org/10.1016/j.icarus.2015.10.019.

Zuffa, G.G., 1987, Unravelling hinterland and offshore palaeogeography from deep-water arenites, *in* Leggett, J.K., and Zuffa, G.G., eds., Marine Clastic Sedimentology: Dordrecht, Netherlands, Springer, p. 39–61, https://doi.org/10.1007/978-94-009-3241-8_2.

Downloaded from http://pubs.geoscienceworld.org/gsa/geosphere/article-pdf/16/6/1508/5182958/1508.pdf
by California Inst of Technology user